

## INFORMATION TO USERS

This manuscript has been reproduced from the microfilm master. UMI films the text directly from the original or copy submitted. Thus, some thesis and dissertation copies are in typewriter face, while others may be from any type of computer printer.

The quality of this reproduction is dependent upon the quality of the copy submitted. Broken or indistinct print, colored or poor quality illustrations and photographs, print bleedthrough, substandard margins, and improper alignment can adversely affect reproduction.

In the unlikely event that the author did not send UMI a complete manuscript and there are missing pages, these will be noted. Also, if unauthorized copyright material had to be removed, a note will indicate the deletion.

Oversize materials (e.g., maps, drawings, charts) are reproduced by sectioning the original, beginning at the upper left-hand corner and continuing from left to right in equal sections with small overlaps.

ProQuest Information and Learning  
300 North Zeeb Road, Ann Arbor, MI 48106-1346 USA  
800-521-0600

**UMI**<sup>®</sup>



**University of Alberta**

**Turbulence-Enhanced Burning Velocity of Methane-Air/EGR/RG  
Mixtures**

by

**Guofang Jiang**



**A thesis submitted to the Faculty of Graduate Studies and Research in partial  
fulfillment of the**

**requirements for the degree of Master of Science**

**Department of Mechanical Engineering**

**Edmonton, Alberta  
Fall 2005**



Library and  
Archives Canada

Published Heritage  
Branch

395 Wellington Street  
Ottawa ON K1A 0N4  
Canada

Bibliothèque et  
Archives Canada

Direction du  
Patrimoine de l'édition

395, rue Wellington  
Ottawa ON K1A 0N4  
Canada

0-494-09197-5

*Your file* *Votre référence*

*ISBN:*

*Our file* *Notre référence*

*ISBN:*

#### NOTICE:

The author has granted a non-exclusive license allowing Library and Archives Canada to reproduce, publish, archive, preserve, conserve, communicate to the public by telecommunication or on the Internet, loan, distribute and sell theses worldwide, for commercial or non-commercial purposes, in microform, paper, electronic and/or any other formats.

The author retains copyright ownership and moral rights in this thesis. Neither the thesis nor substantial extracts from it may be printed or otherwise reproduced without the author's permission.

---

In compliance with the Canadian Privacy Act some supporting forms may have been removed from this thesis.

While these forms may be included in the document page count, their removal does not represent any loss of content from the thesis.

#### AVIS:

L'auteur a accordé une licence non exclusive permettant à la Bibliothèque et Archives Canada de reproduire, publier, archiver, sauvegarder, conserver, transmettre au public par télécommunication ou par l'Internet, prêter, distribuer et vendre des thèses partout dans le monde, à des fins commerciales ou autres, sur support microforme, papier, électronique et/ou autres formats.

L'auteur conserve la propriété du droit d'auteur et des droits moraux qui protègent cette thèse. Ni la thèse ni des extraits substantiels de celle-ci ne doivent être imprimés ou autrement reproduits sans son autorisation.

---

Conformément à la loi canadienne sur la protection de la vie privée, quelques formulaires secondaires ont été enlevés de cette thèse.

Bien que ces formulaires aient inclus dans la pagination, il n'y aura aucun contenu manquant.

  
**Canada**

## ABSTRACT

An experimental investigation was conducted on effects of exhaust gas recirculation (EGR) and reformer gas (RG) on the turbulent burning velocity of stoichiometric methane-air by using a spherical bomb technique. The mixtures were ignited at 276 K and 1 atm. Experiments were performed within the wrinkled laminar flamelet turbulent regime with Reynolds number over a range of 100 to 1300. Measurements showed that even without fuel enrichment by reformer gas, the reduced burning velocity caused by EGR dilution could effectively be restored by turbulence enhancement. Also, turbulence appeared to be more effective for low Markstein number mixtures diluted by EGR. When adding reformer gas, the turbulent flame tended to be more stable due to increasing Markstein number. The turbulent burning velocity normalized by laminar burning velocity was linearly dependent on the turbulent intensity and the effectiveness of turbulence on burning velocity increased as the flame developed.

## ACKNOWLEDGMENTS

I would like to thank the following friends and colleagues for spending time to help solve problems and provide information and advices for this thesis:

Panfeng Han, Jayson Loewen, Senthil Ponnusamy Travis Manchur, Glen Thomas, Chengye Fan, Raul Munoz, Vahid Hosseini, Paitoon Kongsereeparp.

The quality of this experiment was greatly enhanced by the gracious assistance of Terry Nord and Bernie Faulkner. I also appreciate their rapid feedback to technical problems and help for teaching to use electrical apparatus. Thanks also to Ian Buttar, Roger Marchand, Curt Stout, and Dirk Kelm for their technical assistance.

The thesis would not have been possible without the kind support, probing questions, valuable comments, and remarkable patience of my thesis supervisor: Dr. M. D. Checkel.

This project was financially supported by Auto21 National Centre of Excellence.

Finally, I would like to express my appreciation to my family for their understanding, encouragement and support throughout this research.

# TABLE OF CONTENTS

## CHAPTER

<b>1 INTRODUCTION</b>	<b>1</b>
1.1 Background .....	1
1.2 Previous Investigations in This Laboratory .....	2
1.3 About This Study.....	2
<b>2 THEORY AND BACKGROUND STUDIES</b>	<b>3</b>
2.1 The Structure of Turbulence.....	3
2.2 Turbulent Scales.....	5
2.2.1 Length Scales.....	5
2.2.1.1 The Case of Two Eddy Theory.....	7
2.2.1.2 The Case of Kido's Model.....	7
2.2.2 Time scales .....	8
2.2.3 Dimensionless Scales.....	9
2.3 Definitions of Laminar Flame Thickness.....	11
2.4 Premixed Turbulent Combustion Regimes.....	13
2.5 Laminar Flamelet Theory.....	15
2.6 Measurement of the Wrinkled Flame Surface.....	20
2.6.1 Fractal Geometry Application .....	20
2.6.2 Flame Surface Density.....	22
2.7 Effects of Mixture Characteristics on Burning Velocity.....	24
2.7.1 Lewis Number.....	24

2.7.2	Markstein Number.....	28
2.7.3	Preferential Diffusion .....	32
2.7.4	Flame Instability .....	33
2.7.5	Flame Stretch Rate .....	34
2.8	Effect of EGR and RG.....	37
2.8.1	On Flame Chemistry.....	38
2.8.2	On Molecular Properties .....	39
2.9	Effect of Turbulence Parameters.....	39
2.9.1	Turbulent Intensity.....	40
2.9.2	Turbulent Length Scale .....	42
2.10	Measuring Turbulent Burning Velocity .....	43
2.10.1	Pressure Trace.....	43
2.10.2	Visualization Method .....	44
2.11	Concluding Remarks .....	45
<b>3</b>	<b>EXPERIMENTAL METHOD</b>	<b>47</b>
3.1	Combustion Chamber.....	47
3.2	Gas Filling Station.....	49
3.3	Turbulence Generation Mechanism.....	51
3.3.1	Plate Motion Mechanism.....	51
3.3.2	Plate Speed Measurement .....	51
3.4	Data Acquisition and Control System .....	53
3.4.1	Sensor Box.....	54
3.4.2	Virtual Instrument Channels .....	54



3.5	Experiment Control Procedure.....	55
3.6	Mixtures Investigated.....	56
<b>4</b>	<b>CALCULATION METHOD</b>	<b>63</b>
4.1	Calculation of Turbulent Burning Velocity.....	63
4.1.1	Multi-zone Thermodynamic Equilibrium Model .....	64
4.1.2	Multi-zone Thermodynamic Equilibrium Model for Turbulent Flames .....	66
4.1.3	Application of Instantaneous Burning Velocity.....	67
4.2	Estimation of Turbulent Intensity and Integral Length Scale.....	69
4.2.1	A Decay Model.....	70
4.2.1.1	Theoretical Background.....	70
4.2.1.2	Coefficients of Empirical Equations.....	72
4.2.2	A Rapid Distortion Model.....	72
4.3	Calculation of Lewis Number and Markstein Number.....	75
<b>5</b>	<b>RESULTS AND DISCUSSION</b>	<b>81</b>
5.1	Experimental Results.....	81
5.1.1	Combustion Duration .....	83
5.1.2	Rate of Burned Mass Fraction .....	87
5.2	Correlations of Turbulent Burning Velocity .....	90
5.2.1	With Turbulent Intensity .....	96
5.2.2	With Turbulent Strain Rate .....	106
5.2.3	With Combined Product of Strain Factor and Lewis Number .....	111
5.2.4	With Damköhler Number and Turbulent Karlovitz Number .....	115

5.3	Comparison with Peters's Model .....	118
5.4	Conclusions .....	121
<b>6</b>	<b>LIMITATIONS AND RECOMMENDATIONS</b>	<b>123</b>
6.1	Turbulence Parameters.....	123
6.2	Range of Turbulent Intensity.....	124
6.3	Simulated EGR.....	125
6.4	Estimation of Markstein Number.....	125
<b>REFERENCES .....</b>		<b>127</b>
<b>APPENDIX A</b>	<b>TURBULENT EXPERIMENT CONTROL PROGRAM..</b>	<b>136</b>
<b>APPENDIX B</b>	<b>MULTI-ZONE THERMODYNAMIC EQUILIBRIUM</b>	
	<b>MODEL PROGRAM PACKAGE .....</b>	<b>140</b>
<b>APPENDIX C</b>	<b>TURBULENCE      PARAMETERS      CALCULATION</b>	
	<b>PROGRAM .....</b>	<b>168</b>

## LIST OF TABLES

Table 2.1	Properties of Methane-Air (300 K, 1 atm).....	31
Table 2.2	Properties of Propane-Air (300 K, 1 atm).....	31
Table 2.3	Properties of Hydrogen-air (300 K, 1 atm).....	32
Table 3.1	VI Channel Inputs and Outputs.....	55
Table 3.2	Compositions of Tested Mixtures (volumetric fraction) .....	57
Table 4.1	Turbulent Coefficients .....	72
Table 4.2	Properties of Tested Mixtures .....	79
Table 4.3	Comparison of Ma and Le for Stoichiometric Methane-air .....	80
Table 5.1	Current Conditions and Burning Velocity of Quiescent Flames at r = 46 mm and 55 mm .....	82
Table 5.2	Summary of Experimental Results for Quiescent and Turbulent Combustion .....	84
Table 5.3	Turbulent Experimental Conditions and Results for Methane-air at r = 46 mm .....	92
Table 5.4	Turbulent Experimental Conditions and Results for Methane-Air/EGR5 at r = 46 mm .....	92
Table 5.5	Turbulent Experimental Conditions and Results for Methane- Air/EGR15 at r = 46 mm .....	93
Table 5.6	Turbulent Experimental Conditions and Results for Methane- Air/EGR5/RG11 at r = 46 mm .....	93
Table 5.7	Turbulent Experimental Conditions and Results for Methane-air	

	at r = 55 mm .....	94
Table 5.8	Turbulent Experimental Conditions and Results for Methane-Air/EGR5 at r = 55mm .....	95
Table 5.9	Turbulent Experimental Conditions and Results for Methane- Air/EGR15 at r = 55 mm .....	95
Table 5.10	Turbulent Experimental Conditions and Results for Methane- Air/EGR5/RG11 at r = 55 mm .....	96

## LIST OF FIGURES or ILLUSTRATIONS

Figure 2.1	Turbulent Combustion Regimes.....	14
Figure 2.2	Turbulent Flame Structure .....	16
Figure 3.1	Schematic Diagram of the Experimental Set Up.....	47
Figure 3.2	Combustion Chamber Configurations .....	48
Figure 3.3	Schematic Diagram of Gas Filling Station .....	50
Figure 3.4	Turbulence Generation Mechanism .....	52
Figure 3.5	Schematic Diagram of Data Acquisition and Control System .....	53
Figure 3.6	Circuits for Tooth, Flywheel, Spark and Gird in Sensor Box .....	58
Figure 3.7	Circuits for Solenoid Trigger and Magnet.....	59
Figure 3.8	Modified Circuits for Capacitance Discharge Ignition.....	60
Figure 3.9	Schematic Diagram of the Data Channel Connections.....	61
Figure 3.10	Typical Data Recorded (Pressure Rise and Plate Motion as a Function of Time) .....	62
Figure 4.1	Schematic of the MTEM .....	64
Figure 4.2	Spherical Propagation Flame.....	74
Figure 4.3	Schematic Coordinates of an Element .....	74
Figure 5.1	Comparisons of Pressure Trace.....	86
Figure 5.2	Comparison of Burned Mass Fraction .....	89
Figure 5.3	Turbulent Burning Velocity as a Function of Turbulent Intensity and Flame Radius $r$ for Methane-air .....	101
Figure 5.4	Turbulent Burning Velocity as a Function of Turbulent Intensity and	

	Flame Radius $r$ for Methane-air/EGR5 .....	102
Figure 5.5	Turbulent Burning Velocity as a Function of Turbulent Intensity and Flame Radius $r$ for Methane-air/EGR15.....	103
Figure 5.6	Turbulent Burning Velocity as a Function of Turbulent Intensity and Flame Radius for Methane-air/EGR5/RG11.....	104
Figure 5.7	Summary of Turbulent Burning Velocity as a Function of Turbulent Intensity and Flame Radius $r$ for all Mixtures.....	105
Figure 5.8	Turbulent Burning Velocity as a Function of Turbulent Strain Rate (flame radius $r = 46$ mm) .....	109
Figure 5.9	Turbulent Burning Velocity as a Function of Turbulent Strain Rate (flame radius $r = 55$ mm) .....	110
Figure 5.10	Correlation between $S_t/u'$ and $K_{as}Le$ (flame radius $r = 46$ mm) .....	113
Figure 5.11	Correlation between $S_t/u'$ and $K_{as}Le$ (flame radius $r = 55$ mm) .....	114
Figure 5.12	Correlation between $S_t/u'$ and $Da$ or $Ka$ (flame radius $r = 46$ mm) .....	116
Figure 5.13	Correlation between $S_t/u'$ and $Da$ or $Ka$ (flame radius $r = 55$ mm) .....	117
Figure 5.14	Comparison between Peters's Model Solution and Experimental Values at Flame Radius $r = 46$ mm and $r = 55$ mm.....	120
Figure A.1	Sequence Structure Frame 0 of Turbulent Experiment Control Program.....	136
Figure A.2	Sequence Structure Frame 1 of Turbulent Experiment Control Program.....	137
Figure A.3	Sequence Structure Frame 2 of Turbulent Experiment Control	

Program.....138

**Figure A.4 Sequence Structure Frame 3 of Turbulent Experiment Control**

Program.....139

## LIST OF SYMBOLS, NOMENCLATURE

$a_{1-14}$	coefficients
A	flame surface area
$A_{ex}$	excess flame surface area
$c_{1-4}$	coefficients (see Eqs.4.4 and 4.10)
C	coefficient of determination, R-squared
$C_p$	Specific heat at constant pressure
d	plate hole diameter
e	coefficient (see Eq.4.15)
D	mass diffusivity
$D_2$	2-dimensional fractal dimension
$D_3$	3-dimensional fractal dimension
$D_a$	turbulent Damköhler number
E	activation energy
f	fraction
EI	internal energy
g	constant (see Eq.2.36)
$I_0$	Stretch factor
K	flame stretch rate
k	thermal conductivity
$K_a$	turbulent Karlovitz number
$K_{as}$	Karlovitz stretch factor
L	integral length scale
$L_d$	integral length scale derived from decay model
$Le$	Lewis number
$L_y$	characteristic length scale of flame wrinkling (see Eq.2.36)
m	mass
$\dot{m}$	mass rate
Ma	Markstein number
P	pressure



Pr	Prandtl number
R	Gas constant
r	flame radius
$R_L$	turbulent Reynolds number
s	normal geometric strain
S	burning velocity
$S_{L0}$	laminar burning velocity at standard condition
$St_{,\infty}$	turbulent burning velocity at steady state
Sc	Schmidt number
T	Temperature
$T_a$	activation temperature
$T_{ad}$	adiabatic combustion temperature
t	time
$t_d$	delay time set by digital delay generator
u	fluctuation velocity
$u'$	r.m.s turbulence intensity
$u'_{\eta}$	r.m.s turbulence intensity in Kolmogorov structure
$u'_{rd}$	r.m.s turbulent intensity on the basis of a rapid distortion model
$u'_d$	r.m.s turbulent intensity on the basis of a normal decay
$u'_k$	time dependent r.m.s turbulent intensity
v	volume
V	plate speed
$V_F$	flame speed
$\dot{w}$	mean rate of conversion of reactants into products
W	compression work
x	dummy variable
X	dimensionless distance; also X-axis coordinate in graphs
Y	Y-axis coordinate

### Subscripts

b	burned
i	inside
ig	at ignition time
ini	initial condition
L	laminar case
o	outer
t	turbulence case
u	unburned

### Greek Symbol

$\alpha$	thermal diffusivity
$\beta$	Zeldovich number (see Eq.4.20)
$\bar{c}$	Reynolds averaged reaction progress variable (see Eq.2.36 )
$\delta$	flame thickness
$\delta_d$	flame thickness derived from kinetic viscosity
$\delta_m$	flame thickness derived from mass diffusivity
$\delta_{th}$	flame thickness derived from thermal diffusivity
$\varepsilon$	turbulence energy dissipation rate
$\phi$	equivalence ratio
$\gamma$	reduced temperature
$\eta$	Kolmogorov length scale
$\iota$	outline length in fractal geometry
$\xi$	Markstein length
$\lambda$	Taylor microscale
$\mu$	dynamic viscosity
$\nu$	kinetic viscosity
$\Re$	autocorrelation coefficient
$\Re_E$	autocorrelation coefficient as $t = \tau_I$
$\rho$	mixture density

$\Sigma$	Flame surface density
$\sigma_t$	flame surface ratio of turbulent flame to laminar flame
$\sigma_y$	orientation factor(see Eq.2.36)
$\tau_c$	chemical time
$\tau_I$	integral time scale
$\tau_t$	turbulent turnover time
$\tau_{t-small}$	turbulent turnover time in small eddies
$\tau_{t-large}$	turbulent turnover time in large eddies
$\omega$	measurement scale in fractal geometry
$\zeta$	volumetric compression ratio
$\psi$	turbulence energy ratio

# CHAPTER 1: INTRODUCTION

## 1.1 Background

It is well known that the normal burning rate of any stationary fuel air mixture is not practically useful in high speed combustion engines due to the extremely short time available for each engine cycle. Rapid combustion is of importance for combustion engines so that self-ignition, knock and high oxides of nitrogen (NO<sub>x</sub>) emission can be avoided.

Another major concern for combustion engines is the emission of NO<sub>x</sub>, a highly undesirable pollutant. More and more stringent regulations for combustion engines have limited the allowable amount of NO<sub>x</sub> emission. An approach where exhaust gas is recycled (EGR) is widely applied because EGR can hold the combustion temperature down which is the main factor of the production of NO<sub>x</sub>. However, EGR has a negative effect on the burning rate.

Turbulence in the reaction zone can wrinkle the flame front, spreading the flame several times faster than the laminar flame. For this reason, turbulent combustion has drawn much attention of researchers for decades in the forum of experimental and theoretical studies. However, due to the complexity of turbulent combustion science, so far no model and theory has proven generally applicable for combustion application. It is necessary to explore the real world of turbulence using experimental methods, because not only do the measurement results provide qualitative guide and technical support for industrial applications, they can also be used to test the accuracy of the models.

## **1.2 Previous Investigations in This Laboratory**

The Combustion Laboratory at the University of Alberta has a twenty years history of turbulent combustion research. In particular, Ting [1992] has investigated the turbulence effect on burning velocity for lean methane-air and propane-air. It was found that a linear relationship between dimensionless turbulent burning velocity and turbulent intensity existed, as well as the turbulence strain rate effect on burning rate.

To compensate the reduced burning velocity caused by EGR (composed of carbon dioxide and nitrogen), Ponnusamy [2005] and Han [2005] used simulated reformer gas (RG), composed of hydrogen and carbon monoxide, added into the EGR-diluted methane-air mixtures. Their results showed that RG can efficiently restore the laminar burning rate to the normal level.

## **1.3 About This Study**

The objective of this study is to create a turbulent combustion database of methane-air mixtures diluted by simulated EGR and enriched by RG, and to investigate the effect of EGR and RG on turbulent flames. Chapter 2 presents the turbulent combustion theory and a survey of present and past studies. Chapter 3 details the experimental method including apparatus, control and data acquisition. Chapter 4 explains the calculation method for turbulent burning velocity, turbulent parameters and Markstein number and Lewis number. After exhibition and discussion of the experimental results, Chapter 5 examines the current investigations by comparing the empirical correlations with other database. Chapter 6 gives the directions and suggestions to improve the current study.

## CHAPTER 2: THEORY AND BACKGROUND STUDIES

This chapter presents the theoretical guidelines for the current research and reviews other researchers' results in the turbulence combustion field.

### 2.1 The Structure of Turbulence

In the turbulent combustion field, the fluctuating velocity of turbulence is generated by disturbing the mean flow. The turbulence energy is contained in the large eddies which are dependent upon the physical turbulence generation mechanism. As the large eddies are extracting energy from the mean flow, the process is always accompanied by a so-called vortex stretching process [Andrews et al. 1975]. This vortex stretching creates smaller scale eddies which are also called dissipative eddies because the viscous stress produced by the molecular motion dissipates the velocity fluctuations [Tennekes et al. 1972].

For uniform isotropic turbulence, the rate of turbulence energy fed by large eddies is equal to the rate of energy dissipation. This point makes it possible to correlate large eddies with small eddies. With increasing turbulence, smaller and smaller dissipative eddies are produced to enable large and small eddy structures to keep in a state of dynamic equilibrium.

On the other hand, the large eddies represent low frequency turbulence, whilst the small eddies are associated with the high frequency turbulence. Batchelor et al. [1949] found an interesting phenomenon that the high frequency turbulence was not continuous and exhibited intermittency. Based on this investigation, the intermittency factor, introduced

by Andrews et al. [1975], indicates the time fraction of turbulent flow and equivalently a volume fraction of the dissipative regions. The intermittency in small eddies led to several postulations responsible for the experimental investigation. Townsend [1951] assumed a turbulence structure where small scale eddies might be represented as a random tangle of vortex sheets (locally parallel vortex lines). Corrsin [1962] suggested that the vortex sheets had a thickness of the order of the Kolmogorov microscale and spacing of the order of integral scale. Tennekes [1968] postulated that the dissipative eddies concentrated in vortex tubes with a diameter of the order of Kolmogorov microscale and spacing of the order of the Taylor micro-scale. Abdel-Gayed et al. [1981] considered an equilibrium existing between large and small eddies, that the large eddies broke down into small eddies and the volumetric rate of formation of small eddies was equal to the rate of dissipation. However, the low frequency of turbulent fluctuation demonstrated continuous turbulence, thereby an intermittency factor of unity in large eddy structure.

Moving to the influence of turbulence upon combustion, it is commonly accepted that the fact of turbulence enhancing burning rate is associated with an increase of flame area in macro structure. This would lead to a wrinkled laminar flamelet theory which is described in latter section 2.4.

As an alternative, Chomiak [1979] proposed a mechanism for turbulent flame growth. Starting from the intermittent small scale structure of turbulence, he suggested that the flame would propagate rapidly along a vortex tube where the combustion produces a density gradient which causes the vortex to collapse. The postulated effect enables the flame to travel along the vortex tubes at a much higher turbulent flame velocity than

laminar flame velocity. As the flame propagation proceeds through the space between the vortex tubes, the flame speed restores the laminar flame velocity, and this intermittency is dependent upon the distance between the vortex tubes. Andrews et al. [1975] attributed the faster turbulent burning rate to the preferential combustion within the isotropic dissipative eddies which allow the flame to advance more rapidly than in the case of laminar flame.

Based on the turbulence structure, a well-known two-eddy theory developed by Abdel-Gayed et al. [1981], postulated that the burning proceeded within both large and small eddy turbulence structure. The analytical expression of burning rate in this theory was associated with both eddy decay and chemical reaction rates for the aforementioned two groups of eddy. For high levels of turbulence, this theory agreed well with the experimental results, but uncertainties remained in the small scale turbulent structure and the mode of combustion in these scales.

## **2.2 Turbulence Scales**

To characterize the turbulent flow, it is necessary to define the spatial and time scales of turbulence. Although the scales used in the turbulent combustion can be found in many literatures, the various expressions make it hard to follow all of them. This study employed these parameters to analyze and compare the present results with other studies; thereby it is of importance to clarify the definitions and the associated physical meanings.

### **2.2.1 Length Scales**



The integral length scale  $L$  is directly generated by the jet flow, hence it is the largest eddy size in turbulent flow field and can be measured during experiments using the autocorrelation coefficient technique outlined in section 4.2.1.1.

The Kolmogorov length  $\eta$  is derived from the Kolmogorov's universal equilibrium theory cited by Tennekes et al. [1972]. Due to the viscosity, the large size eddies continually break up into small scales, say  $\eta$ , that is generally considered as the magnitude of vortex tube size. It is supposed that the smallest size of eddy  $\eta$  is fed by the breakdown of larger size of eddy  $L$ . In an equilibrium situation the rate of energy supply by large eddies equals the rate of viscous dissipation.

The Taylor micro length scale  $\lambda$  is assumed as the distance between the vortex tubes.

For isotropic turbulence, the rate of energy dissipation can be expressed as

$$\varepsilon = 15\nu\left(\frac{\partial u}{\partial x}\right)^2 = 15\nu\left(\frac{u'}{\lambda}\right)^2 \quad [\text{Taylor 1935}]. \quad 2.1$$

The rate of production of turbulent energy can be taken to be proportional to  $\frac{u'^3}{L}$  [Andrews et al. 1975]. Then

$$\varepsilon = a_1 \frac{u'^3}{L}. \quad 2.2$$

Putting Eqs.2.1 and 2.2 together yields

$$\frac{\lambda^2}{L} = \frac{15 \nu}{a_1 u'} \quad 2.3$$

$$\lambda = \left(\frac{15}{a_1}\right)^{-\frac{1}{2}} R_L^{-\frac{1}{2}} L. \quad 2.4$$

where turbulent Reynolds number  $R_L = \frac{u' L}{\nu}$  as described in section 2.2.3. As Taylor microscale  $\lambda$  is derived from the large eddy scale  $L$ , the Kolmogorov length can be obtained on the basis of a universal equilibrium theory. As a result,  $\eta$  is only a function of kinetic viscosity  $\nu$  and the rate of energy dissipation  $\varepsilon$ :

$$\eta = \left( \frac{\nu^3}{\varepsilon} \right)^{1/4} . \quad 2.5$$

Introducing Eq.2.2 produces

$$\eta = \left( \frac{\nu^3 L}{a_1 u'^3} \right)^{1/4} = a_1^{-1/4} R_L^{-3/4} L \quad 2.6$$

Eqs.2.4 and 2.6 represent the mathematical relations between macro and micro length scales,  $L$ ,  $\lambda$  and  $\eta$ . The coefficient  $a_1$  is of an order of unity and different in various studies as described in the following chapters.

### 2.2.1.1 The Case of Two Eddy Theory

Based on the experiments and the related reference values cited by Abdel-Gayed et al.

[1981],  $a_1 = 0.37 \left( \frac{15}{a_1} = 40.4 \right)$  was adopted under the turbulent condition of  $R_L > 60$ .

This leads to Lees calculation system. From Eq.2.4 and 2.6, Taylor and Kolmogorov length scales are expressed as ;

$$\lambda = 6.4 L R_L^{-0.5} \quad 2.7$$

$$\eta = 1.28 L R_L^{-3/4} . \quad 2.8$$

### 2.2.1.2 The Case of Kido's Model

Kido et al. [1983] developed a model for small-scale structure of isotropic turbulence under the compression stroke in a closed cylindrical chamber. This model took into account the effect of turbulence decay which contributed to the relations among length scales including integral length  $L$ , Kolmogorov length  $\eta$  and Taylor length  $\lambda$ . Similar to Corrsin's model [1962], this model suggested that the dissipative eddies consist of vortex sheets with a thickness of the order of Kolmogorov length  $\eta$  and a spacing of the order of integral length  $L$ . Then the energy dissipation rate was defined in terms of the volume fraction of the vortex sheets  $\frac{\eta L^2}{L^3}$ , thus Eq.2.2 can be defined as

$$\varepsilon = a_1 \frac{(u')^3 \eta L^2}{L L^3} = a_1 \frac{(u')^3 \eta}{L L}, \quad 2.9$$

Combining with Eqs.2.1 and 2.5, the following formulas are obtained,

$$\lambda = \frac{\sqrt{15}}{a_1^{0.4}} LR_L^{-0.2} \quad 2.10$$

$$\eta = a_1^{-0.2} LR_L^{-0.6} \quad 2.11$$

with  $a_1 = 28.9$  derived from the experiments, then

$$\lambda = LR_L^{-0.2} \quad 2.12$$

$$\eta = 0.51 LR_L^{-0.6}. \quad 2.13$$

Eq.2.12 is employed to obtain the turbulent strain rate in Chapter 5. Concerning the combined effect of the compression and decay of the turbulence, Kido's model was considered as closer to the present study [Ting et al. 2001].

## 2.2.2 Time Scales

Characteristic timescales are generally used to make comparisons between the turbulent flow and chemical reaction fields. The flame characteristic velocity scale and length scale are flame propagation speed and flame thickness.

A number of measurements have shown that most turbulent flames belong to a regime where the chemical reaction dominates the flow and the turbulence only wrinkles the flame surface rather than affecting the reaction zone. Consequently, the turbulent flame retains the inner structure of laminar flames and the chemical time is defined by

$$\tau_c = \frac{\delta}{S_L} \quad 2.14$$

for both the turbulent and laminar flames, representing a residence time in a laminar flame. The inverse of chemical time ( $1/\tau_c$ ) is also termed the chemical strain.

Corresponding to the structure of turbulent field, there are two kinds of designated turbulent turnover time in the small and large eddy structures, respectively,

$$\tau_{t-small} = \frac{\eta}{u'_\eta} \quad 2.15$$

$$\tau_{t-large} = \frac{L}{u'} \quad 2.16$$

where  $u'_\eta$  is the turbulent fluctuation velocity at Kolmogorov scales,

$$u'_\eta = (\nu\varepsilon)^{1/4} \text{ [Heywood 1988]}. \quad 2.17$$

Introducing Eq.2.2, Eq.2.15 can be defined as

$$\tau_{t-small} = \left( \frac{L\nu}{a_1 u'^3} \right)^{1/2}. \quad 2.18$$

### 2.2.3 Dimensionless Scales

Several important dimensionless scales are used to characterize the turbulent combustion flames as follows:

- 1) The turbulent Reynolds number  $R_L$  based on integral length scale  $L$  is represented by

$$R_L = \frac{u' L}{\nu} . \quad 2.19$$

This expression shows that the Reynolds number combines both the integral length scale and turbulent intensity. Andrews et al. [1975] interpreted  $R_L$  as the ratio of the rate of production to the rate of dissipation of turbulent energy. If the length scale for production and dissipation is the same, no balance can exist between the source and sink. This can explain that the dissipation takes place in smaller length scales than the production. From this viewpoint, as  $R_L$  increases, smaller dissipative eddies must be created to keep the balance.

- 2) Turbulent Karlovitz number  $K_a$  is the ratio of flame chemical time to small scale turbulence time, expressed as

$$K_a = \frac{\tau_c}{\tau_{t-small}} . \quad 2.20$$

If the flame thickness is characterized by

$$\delta = \frac{\nu}{S_L} , \quad 2.21$$

putting Eqs.2.14 and 2.18 into Eq.2.20 and with  $a_1=1$ ,

$$K_a = \left( \frac{u'}{S_L} \right)^{3/2} \left( \frac{L}{\delta} \right)^{-1/2} . \quad 2.22$$

The reason for  $a_l=1$  here is to be consistent with the discussion of the turbulent combustion regimes. However, the value of  $a_l$  will not change the qualitative trend. On the other hand, combining Eqs.2.5, 2.15 and 2.17, the Kalovitz number can also be expressed as the square of the ratio of the flame thickness and Kolmogorov length, that is

$$K_a = \left( \frac{\delta}{\eta} \right)^2. \quad 2.23$$

The expressions of flame thickness are discussed below. Peters [1986] argued that Eq.2.21 was accurate enough for the order of magnitude arguments regardless of non unity Prandtl number.

3) Turbulent Damköhler number  $Da$  is the ratio of the large turbulent time scale to the chemical time scale, given by

$$D_a = \frac{\tau_{t-large}}{\tau_c} = \frac{L S_L}{u' \delta}. \quad 2.24$$

Substituting Eqs.2.19, 2.21 and 2.22 into Eq.2.24, a relation among these three dimensionless scales is produced, that is

$$K_a D_a = R_L^{1/2}. \quad 2.25$$

### 2.3 Definitions of Laminar Flame Thickness

The flame thickness introduced in this study is to characterize the chemical reaction time. Several definitions of laminar flame thickness have been adopted in terms of thermal diffusivity, mass diffusivity and kinetic viscosity of the unburned gas. The

choices appear to be arbitrary, e.g. Bradley et al. [1996] used the flame thickness based on kinetic viscosity,

$$\delta_d = \frac{\nu}{S_L}; \quad 2.26$$

Kwon et al. [1992B], Tseng et al. [1993], Law [1988], Trouvé et al. [1994] chose mass diffusivity to obtain

$$\delta_m = \frac{D}{S_L}; \quad 2.27$$

Tanoue [2003] and Peters [1986] employed thermal diffusivity in their studies

$$\delta_{th} = \frac{\alpha}{S_L}. \quad 2.28$$

To discern the difference, it is necessary to introduce some useful dimensionless parameters:

- 1) Lewis number which is detailed in section 2.7.1.
- 2) Prandtl number,  $Pr = \frac{\nu}{\alpha}$ .
- 3) Schmidt number,  $Sc = \frac{\nu}{D}$ .

Under the condition of  $Le = Pr = Sc = 1$ , Eqs.2.26, 2.27 and 2.28 are identical, but this condition is too strict to be fulfilled. For typical hydrocarbon-air mixtures,  $Pr$  is approximately 0.7 [Abdel-Gayed et al. 1977A]. Therefore, the kinetic viscosity is smaller than the thermal and mass diffusivity, thus the  $\delta_d < \delta_{th}$  and  $\delta_m$ . Due to the difficulty of the measurement of the flame thickness, the sensitivity analysis of the definition has not yet been explored.

## 2.4 Premixed Turbulent Combustion Regimes

It is well known that premixed turbulent combustion is determined by the interaction of the flame with the turbulent flow field. To quantify the effects of turbulence on premixed turbulent burning velocity, it is necessary to define the turbulent combustion regimes because the turbulent effects vary substantially in different regimes. The interaction is dependent on the comparisons of characteristic velocity and length scales between the flame and the entire range of turbulent flow field, i.e.,  $u/S_L$ ,  $\delta/L$  and  $\delta/\eta$ . Through these comparisons, the combustion regimes could be roughly defined. Although several kinds of phase diagrams are used based on the various coordinate descriptions [Gülder et al. 2000A, Peters 1986, Wu et al. 1990], the physical descriptions are quite similar.

Here as illustrated in Figure 2.1, the Borghi-Peters diagram cited by Vervisch [VKI 1999] is adopted. Both the coordinates are logarithmic, representing the length ratio of  $L/\delta$  and velocity ratio of  $u/S_L$ , respectively. In this diagram, the regimes of premixed turbulent combustion are divided by several boundaries,  $R_L=1$ ,  $Da=1$ ,  $Ka=1$  and  $u/S_L=1$ . As a result, the following regimes are characterized:

- 1)  $R_L < 1$ , is defined as the laminar flame with negligible turbulence influence.
- 2)  $Da < 1$ ,  $Ka > 1$ , is termed the thickened flame or stirred reactor regime [Williams 1985], in which the chemical timescale is slow compared with that of turbulence. Fewer investigations are devoted in this regime due to its complexity and limited application. Thus, this regime is not of interest in the present study.



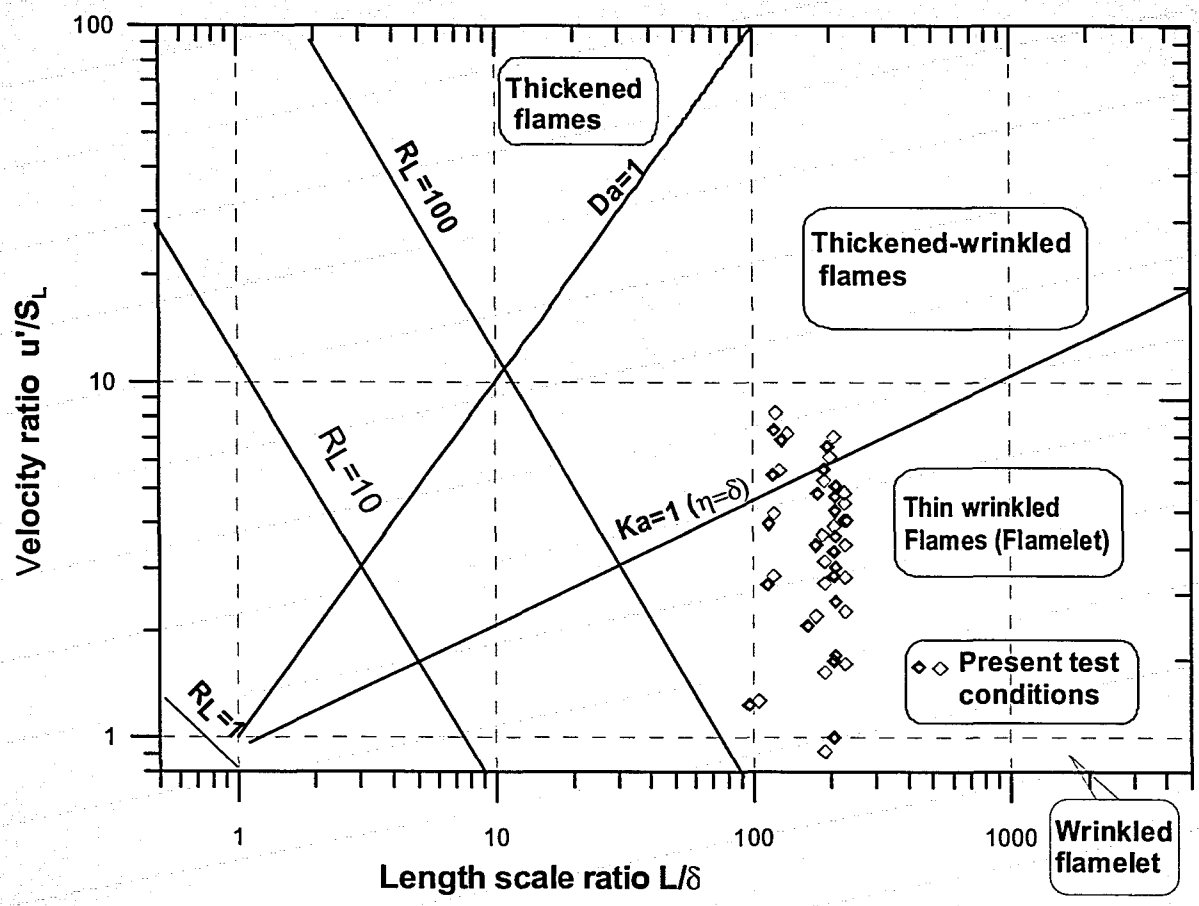


Figure 2.1 Turbulent Combustion Regimes

3)  $Ka > 1$ ,  $Da > 1$  and  $R_L > 1$ , is called the thickened-wrinkled flame regime, where the smallest eddies can enter into the flame structure because  $\delta > \eta$ , thus broadening the flame structure. However, similar to a laminar flame, the reaction zone in this regime remains thin. A few of the present test points fall in this regime which will be further discussed in section 2.5.

4)  $Ka < 1$ ,  $Da > 1$  and  $R_L > 1$ , is the thin wrinkled flamelet regime, in which the turbulent length scale is still larger than flame thickness and the turbulent flow motions are too slow to affect the flame structure. Therefore, the flame front remains thin and the turbulence motions wrinkle the flame surface, leading to large reacting area and hence fast burning velocity. This concept leads to the wrinkled laminar flamelet theory that is detailed in section 2.5.

The thin and thickened wrinkled flamelet regimes are two regimes of major interest, since many applications of premixed turbulent combustion can be characterized in these two zones.

The present test conditions, (discussed in Chapter 5), are also illustrated in this regime map, which mainly fall in the thin wrinkled flame regime with a few in the thickened-wrinkled flame regimes.

## 2.5 Laminar Flamelet Theory

Due to the complexity of turbulent combustion, a complete theoretical description has not been developed yet. This necessitates using assumptions to interpret the interactions between chemistry and turbulence. A widely accepted approximation is that the turbulent flame is composed of a set of laminar-like flamelets defined as asymptotically

thin layers where combustion takes place. These asymptotically thin layers are subjected to the turbulent flow and there is a well-defined inner structure called a flamelet [Peters 1986]. As shown in Figure 2.2, the turbulent flamelets propagate at the laminar flame speed with the surface wrinkled by the turbulent distortion [Checkel et al. 1994, Trouvé et al. 1994, Gülder et al. 2000B]. The effect of turbulence results in an increase of the flame surface area and thus the burning velocity. This flamelet theory readily simplifies the turbulent combustion into two basic parameters characterizing the flame and turbulent flow interactions as follows:

- 1) The speed of the flame inner structure.
- 2) The surface area of the flame front.

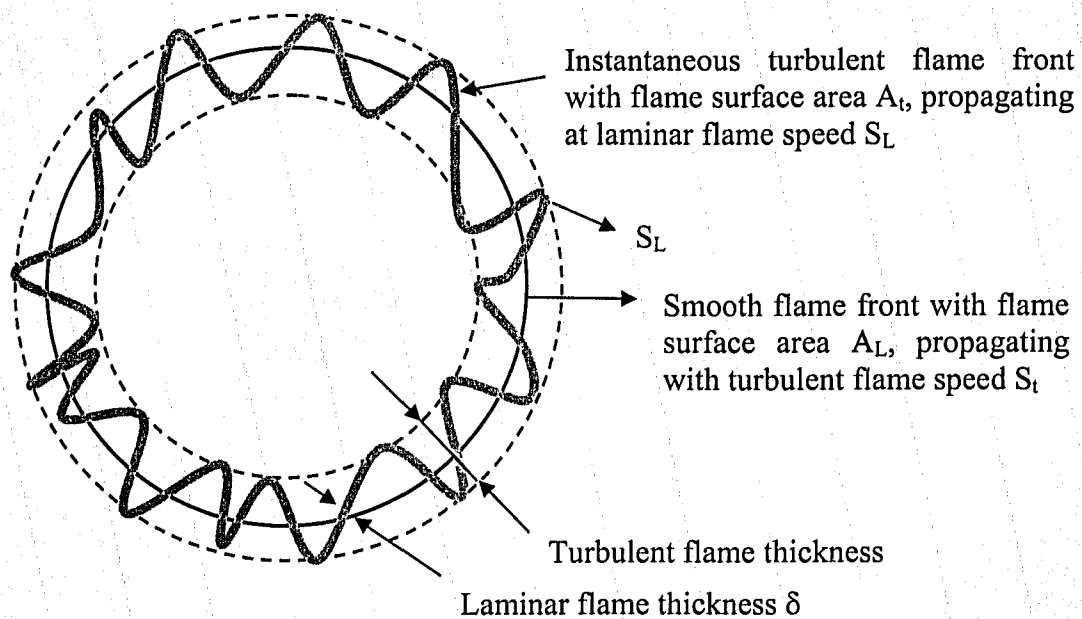


**Figure 2.2 Turbulent Flame Structure**

The wrinkling effect is associated with flame properties, i.e. Markstein number and Lewis number. It has been found that with positive  $Ma$  or  $Le < 1$ , the flame tends to be unstable and any wrinkles increase in magnitude. With negative  $Ma$  or  $Le > 1$ , the flame appears to be capable of smoothing out the protrusions, and hence is considered stable. Following this interpretation, the turbulence is more effective to increase flame surface area under negative  $Ma$  or  $Le < 1$  condition than flames with positive  $Ma$  or  $Le > 1$ . Therefore, the unstable flames take more benefits of turbulent flow than stable flames by more effectively accelerating burning velocity within the flame tolerance limit to the turbulence. This viewpoint will be detailed in section 2.7.1 and 2.7.2.

The flamelet concept was first proposed by Damköhler, who suggested for the large scale turbulence that the interaction between the wrinkled flame front and turbulent flow field was purely kinematic. This led to the unburned gas mass consumption rate ( $\dot{m}_u$ ) being equal to the laminar burning velocity multiplied by the turbulent flame surface area or to the turbulent burning velocity multiplied by the flow smooth surface area (Figure 2.2) and unburned gas density, namely,

$$\dot{m}_u = \rho_u S_L A_t = \rho_u S_t A_L. \quad 2.29$$

It follows that

$$\frac{S_t}{S_L} = \frac{A_t}{A_L}. \quad 2.30$$

Eq.2.30 represents that the increase of flame surface area is proportional to the increase of the burning velocity. This proposal provided a simple interpretation for the complicated turbulent combustion, but its validity and subtlety needs to be further

explored, particularly combining with the effect of preferential diffusion and flame stretch.

To define this flamelet in turbulent flame regime, two sets of dimensionless scales are employed. From the viewpoint of timescale, the characterized chemical time is  $\frac{\delta}{S_L}$ , while the turbulent timescale is defined in the smallest turbulence spectrum (Kolmogorov structure) as shown in Eq.2.15. If the chemical time is smaller than the turbulent time, the laminar flamelet exists in the turbulent flame structure. From the view of length scale, the alternative criterion is the ratio of the flame thickness to Kolmogorov length,  $\delta/\eta$ . If this ratio is less than unity, this means the laminar flamelet concept is applicable.

Furthermore, Peters [1999] extended the flamelet regime farther to  $\frac{\delta}{\eta}=10$  instead of unity by postulating a chemically inert preheat zone and a thin reaction zone. As  $\eta$  is smaller than  $\delta$ , the small eddies of the turbulence seem to penetrate into the preheat zone but not into the reaction zone. Thus the chemical time remains the same as for the laminar flame.

Corresponding to the latter boundary of the flamelet, another dimensionless parameter should be introduced. Damköhler number is the ratio of the turbulent time for large turbulence length scale,  $L$ , to the chemical time (Eq.2.24). For large values of  $Da$  ( $Da \gg 1$ ), the flame front is thin and its inner structure is not affected by turbulent motions which only wrinkle the flame surface.

Peters [1986] argued that if flame stretch combined with unbalanced heat and mass diffusivity (non unity Lewis number  $Le \neq 1$ ), the flame speed was assumed variable due to the temperature change in the thin reaction layer as follows:

1) For positive flame stretch (defined as the protrusion segment towards the unburned gas), the temperature in the thin layer increases or decreases as  $Le < 1$  or  $Le > 1$ , respectively, thereby the flamelet responds by an acceleration or deceleration in speed.

2) For negative flame stretch (defined as concave towards burned gas), the temperature decreases or increases as  $Le < 1$  or  $Le > 1$ , respectively, therefore the flamelet speed decelerates or accelerates.

Moreover, for  $Le < 1$ , a cellular pattern will emerge because the initial fluctuation of the flame front is intensified. In contrast, the flame surface with  $Le > 1$  becomes stable and tends to remain smooth.

Similarly, Clavin et al. [1979] concluded that the major influence of non unity Lewis number was that the flame surface wrinkling by turbulent motion resulted in temperature change which is determinant in flame speed. Many measurements [Haq et al. 2002, Renou et al. 2000, Kwon et al. 1992A, Wu et al. 1991, Trouvé et al. 1994] have provided evidence for this phenomenon.

It is worthwhile to mention that even if the turbulent flame consists of wrinkled laminar flamelets, the flame structure is still not entirely solved [Clavin et al. 1979]. In studying the turbulent burning velocity through wrinkled flame models, some arbitrary approximations need to be introduced such as the flame shape. Moreover, some of the dimensionless parameters characterizing the turbulent combustion may mask the nature

of interaction between the combustion and turbulent motion [Checkel et al. 1994]. Due to the limitation of experimental approaches, the wrinkled flamelet theory needs to be further confirmed.

## **2.6 Measurement of the Wrinkled Flame Surface**

To provide experimental support for the wrinkled flamelet theory that the turbulent burning velocity can be approximated by the product of the laminar burning velocity and flamelet surface area, two types of studies are considered. Firstly, the laminar burning velocity can be correlated with the effect of stretch and flame curvature, and these studies have been reported by Bradley et al. [1996], Tseng et al. [1993], Kwon et al. [1992B]. Secondly, the investigations of flamelet surface area as a function of turbulence parameters have been performed in several studies [Peters 1986, Gülder et al. 2000B, Smallwood et al. 1995, Lee 2000, Kwon et al. 1992A]. The former investigations will be described in section 2.7, while this section concentrates on the flame surface investigation.

The approaches for characterizing and estimating the flamelet surface area fall into two categories:

- 1) Fractal geometry using cutoff scales and fractal dimension.
- 2) Flame surface density ( $\Sigma$ ), defined as the ratio of mean flamelet surface area to the corresponding volume.

### **2.6.1 Fractal Geometry Application**

Since data reported in the literature have shown the fractal nature of turbulent premixed flame surfaces, the fractal geometry method should provide some reasonable estimates

for turbulent burning velocity using the Damköhler proposal shown in Eq.2.30. For an isotropic fractal surface, the fractal dimension  $D_3$  of the surface in three dimensions can be derived from the corresponding fractal dimension  $D_2$  of the boundary in two dimensions by;

$$D_3 = D_2 + 1. \quad 2.31$$

The two dimensional value,  $D_2$ , can be derived using variable measurement scale  $\omega$  to measure outline length  $\iota$  for two dimensional flame images. From plots of  $\iota$  as a function of  $\omega$ ,

$$D_2 = -\frac{\log \iota}{\log \omega}. \quad 2.32$$

Similarly, the inner and outer cutoff scales ( $\omega_i$  and  $\omega_o$ ) which represent the lower and upper limits of the scales are produced from the physical condition. The ratio of the instantaneous flame surface area to the cross-sectional area of the flame can be related to the ratio of inner to outer cutoff scales and fractal dimension using:

$$\frac{A_i}{A_L} = a_2 \left( \frac{\omega_o}{\omega_i} \right)^{D_3-2}, \quad 2.33$$

and applying Eq.2.30 yields

$$\frac{S_i}{S_L} = a_2 \left( \frac{\omega_o}{\omega_i} \right)^{D_3-2}. \quad 2.34$$

The correlation coefficient,  $a_2$ , has been defined in several ways by Smallwood et al. [1995] and Gülder et al. [2000B].

The experiments of Smallwood et al. [1995] and Gülder et al. [2000B] showed that fractal dimension  $D_3$  increased with the normalized turbulent intensity  $u/S_L$ . Kwon et al.



[1992A] found that the values of  $D_3$  exhibited a progressive increase with increasing flame radius. This indicates that wrinkling of the flame surface and thus the turbulent burning velocity progressively increased with the flame growth. Nevertheless, the calculated  $A_t/A_L$  appeared not strongly dependent on the major turbulence parameter, turbulent intensity.

It is notable that the turbulent burning velocity derived from the fractal dimension is much less than the directly measured values. These discrepancies cast doubts on either the fractal method or the wrinkled laminar flame theory. On one hand, if the fractal geometry concept can yield a true flame front, several possible reasons responsible for the phenomenon are listed as follows [Smallwood et al. 1995]:

- 1) The ratio of  $S_t/S_L$  may not be associated with the ratio of  $A_t/A_L$ , in the wrinkled flamelet regime.
- 2) The turbulent burning velocity may not be a meaningful parameter for the measured flames. The mean turbulent reaction rate tends to be a better representation for premixed turbulent combustion.
- 3) Apart from the surface area increases, the turbulent transfer of species and heat may play an important role in turbulent combustion in the wrinkled flame regime. In other words, the flames may propagate at more than the laminar flame speed.

On the other hand, the validity of the experimental results using fractal geometry is associated with the measurement scale. This may also be responsible for the contradiction between the measurement and the wrinkled flamelet theory.

### **2.6.2 Flame Surface Density**

The wrinkling effect of turbulence in wrinkled flamelet regimes of turbulent combustion can be described by the flame surface density ( $\Sigma$ ) [Bray 1990]. The mean rate of conversion of reactants into products in turbulent premixed combustion may be defined as

$$\dot{w} = \rho_u S_L I_o \Sigma = \rho_u S_u \Sigma. \quad 2.35$$

$I_o$  is the mean stretch factor accounting for both the flame stretch and curvature. Referring to the flame surface density, it is worthwhile to mention the well-known BML algebraic expression [Bray 1990]

$$\Sigma = \frac{g\bar{c}(1-\bar{c})}{\sigma_y L_y}. \quad 2.36$$

In this equation,  $\bar{c}$  is the mean progress variable, defined in the experiment.  $L_y$  is the characteristic length scale of flame wrinkling, which can be approximated as a function of turbulence integral length scale  $L$  and  $u/S_L$ . Parameters  $g$  and  $\sigma_y$  are experimentally dependent variables.

Based on Eq.2.36, Lee et al. [2000] measured the flame surface density of methane-air flames embedded in a turbulent flow by processing PLIF (Planar Laser-Induced Fluorescence) images and correlated  $\Sigma$  with the turbulent parameters, e.g.  $L$  and  $u/S_L$ . The conclusions that the maximum flame surface density increases as  $u/S_L$  increase or as the integral length scale decreases agree well with the commonly accepted experimental results.

The experimental evidence of the wrinkled flame surface of turbulent flame front has provided valuable guidelines for modeling. However, to solve the turbulent  $\Sigma$  equation, closure assumptions are still needed and the validity of some approximations are still

not accessible by experimental methods. Therefore, the wrinkled flamelet theory is still an open issue in turbulent combustion science.

## 2.7 Effects of Mixture Characteristics on Burning Velocity

When studying the turbulence effect on the burning rate, the intrinsic properties of the mixture always plays an important role and it has been found that laminar burning velocity is not a sufficient description of the mixture. Kido et al. [2001] found that mixtures with same value of laminar burning velocity exhibited different turbulent burning velocity under the equivalent turbulent condition. Karpov et al. [1980] observed that the peak turbulent burning velocity occurred in lean methane-air but in rich propane-air. This phenomenon drew attention to the molecular property in terms of Lewis number, or the preferential diffusion associated with Markstein number.

### 2.7.1 Lewis Number

In the thermal diffusive theory, Lewis number,  $Le$ , can be used as a criterion of the flame stability, e.g.  $Le < 1$  gives an unstable wrinkled flame and  $Le > 1$  gives a stable smooth flame. Investigations of the  $Le$  effect on the flame stability complement more elaborate descriptions.

By definition,  $Le$  is the ratio of thermal diffusivity to the mass diffusivity,

$$Le = \frac{\alpha}{D}, \quad 2.37$$

and  $\alpha$  can be estimated by

$$\alpha = \frac{k}{\rho C_p}, \quad 2.38$$

Eqs.2.37 and 2.38 clearly show that  $Le$  is dependent on the molecular transport coefficient, e.g. thermal conductivity and indirectly associated with viscosity. Table 2.1 shows that  $Le$  is variable with equivalence ratio. For methane-air mixtures,  $Le$  varies from less than unity for lean mixtures to larger than unity for rich mixture.

From the viewpoint of diffusion coefficient, Karpov et al. [1980] explained the mechanism responsible for the peak turbulent burning velocity. Taking the diffusion coefficient of nitrogen-oxygen as a baseline, if the relevant value of the fuel-air mixture is higher, the turbulent burning velocity peak will be shifted to the lean side. With lower diffusion coefficients than nitrogen-oxygen, the turbulent burning velocity peak is shifted to the rich side. Hydrogen-air mixtures have a very high diffusion coefficient. Of the common hydrocarbons, only methane-air mixtures have a higher diffusion coefficient than nitrogen-oxygen [Tseng et al. 1993]. With this interpretation, it becomes reasonable that lean methane-air and hydrogen-air have much higher turbulent burning velocity than lean propane mixtures relative to the corresponding laminar burning velocity.

In studying the small-scale eddy effect on the flame kernel development, Lipatnikov et al. [1998A] found that as  $Le < 1$ , the reactant supply by molecular diffusion into a highly curved small kernel prevailed over the energy loss by molecular heat transfer. As a result, the temperature in the kernel was increased and hence the combustion was intensified.

To accurately explain the effect of the Lewis number on the turbulent combustion, it is worth considering that the turbulence combustion is determined by processes localized to thin laminar zones characterized by large transient spatial gradients. The current

burning rate and temperature inside these zones can be altered significantly by the difference between heat loss by thermal and mass diffusivity which can be affected by fluctuating turbulent motion [Zel'dovich et al. cited in Lipatnikov et al. 1998B]. Based on this concept, Lipatnikov et al. [1998B] concluded that the strong effect of the Lewis number can not be explained by the weakly stretched laminar flamelet approach which treats turbulent flames to be a set of laminar flamelets stretched by turbulent eddies. This is because the linear relationship between the current burning rate and the flame stretch does not exist for moderately perturbed laminar flames. This point needs more experimental evidence to verify.

With respect to flame stretch and curvature, for non-unity Lewis number, the differential diffusion of heat and species results in a certain sensitivity of the local flame structure to strain rate and curvature. Using high-speed laser tomography, Renou et al. [2000] studied these effects for mixtures with Lewis numbers at 0.3, 1.0 and 1.4. A greater wrinkling effect was found for those mixtures with  $Le = 0.3$  and 1.4 than for those with  $Le = 1$ . The experimental phenomenon showed that

- 1) As  $Le < 1$ , the local flame temperature was increased by the positive stretch (the flame convex to the reactants), thus the burning rate increases. On the other hand, the flame temperature decreased with a negative stretch (the flame concave to the reactants), which led to a low burning rate.
- 2) As  $Le > 1$ , the flame temperature tended to be low in regions with positive flame stretch, thus reducing the current burning rate. Regions with negative flame stretch resulted in increased temperature then followed by an increase of burning rate.

On balance, the flame surface with  $Le > 1$  is less influenced by the turbulent flow than that with  $Le < 1$ . According to this analysis, the flame of  $Le = 1$  should be less stable than that of  $Le > 1$  because of the balanced heat and mass diffusivity. However, this is not in agreement with the observed result in Renou's [2000] investigation that more wrinkles appeared on the flame contour as  $Le > 1$ . This point needs to be investigated.

Similarly, Law [1998] found that as  $Le \geq 1$ , the laminar flame was stable in that the burning rate was more (less) intense in the receding (protruding) segment towards to reactants, which tended to advance (recede) to resume its undisturbed shape. In contrast,  $Le < 1$ , the flame was unstable with the opposite reactions to curvature.

The effect of Lewis number is also taken account in modeling work. Trouvé et al. [1994] employed DNS (direct numerical simulation ) to simulate flame surface density for various mixtures in terms of Lewis number. This study clearly showed that the relative increase of flame surface area rose with decreasing Lewis number. For  $Le = 1.0$  and  $1.2$ , the flame surface area initially increased with time until it reached a maximum, and then the rate decreased. It appeared that this kind of flame was capable of adapting itself to the turbulent environment. However, the flame with  $Le = 0.3$  and  $0.8$  exhibited a significant difference. The degree of the flame wrinkling kept increasing without saturation, so the  $Le = 0.8$  and  $0.3$  flames were defined as unstable in the turbulent case. This modeling also suggested that only for  $Le$  close to unity, e.g.  $0.8 \leq Le \leq 1.2$ , can the turbulence effect on the flame be attributed only to the surface wrinkling. For flames with a strong imbalance in thermal and mass diffusivity, e.g.  $Le = 0.3$ , the flame surface density was not the only factor responsible for the effect of turbulence; the change in flamelet burning velocity also contributes to the turbulent burning velocity.

In addition, contradictions still exist among the experimental investigations. Abdel-Gayed et al. [1984] observed that the quenching effect in turbulent conditions was greater for the lean propane and rich hydrogen mixtures. Lipatnikov et al. [1998B] argued that for lean hydrogen, the burning velocity is far more intensified by the effect of turbulence but with a small quenching turbulence value. In contrast, lean propane shows weaker turbulence enhancement but also has a small quenching turbulence value. This complicated result implies that the enhancement on burning velocity and flame quenching by a strong turbulence cannot be explained solely by the effect of Lewis number.

### 2.7.2 Markstein Number

When the flame propagates outwardly, the continual changes of flame surface area cause flame stretch (defined by Eq.2.45). Markstein number is introduced to represent a measure of laminar flame response to the flame stretch. This is generally measured at early stages of flame propagation under nearly constant pressure conditions where burning velocity varies linearly with flame stretch rate [Kwon et al. 1992B, Tseng et al. 1993]. As described before, the effect of flame stretch on the burning velocity is largely dependent on the thermal-mass diffusion in terms of  $Le$ . Haq et al. [2002] argued that the Markstein number is more applicable to reflect the influence of flame stretch on the flame propagation due to the ambiguous definition of Lewis number.

Based on the early proposal of Markstein, Clavin [1985] generalized and extended the limit of small stretch as follows,

$$S_L = S_{L0} - \xi K . \quad 2.39$$

where  $\mathcal{L}$  is referred to Markstein length, representing the sensitivity of  $S_L$  to the stretch rate  $K$  for a given mixture. The Markstein length is proportional to the characteristic flame thickness, so this readily yields a Markstein number:

$$Ma = \frac{\mathcal{L}}{\delta}. \quad 2.40$$

Ignoring the reactant flow motion (constant pressure combustion) and the effect of flame curvature by setting  $\delta/r \ll 1$ , it is convenient to obtain  $K$  from Eq.2.45 ( $K = \frac{2}{r} \frac{dr}{dt}$ ) for an outwardly propagating spherical laminar flame [Tseng et al. and Kwon et al. 1992B].  $K$  can be also transformed into a dimensionless parameter, Karlovitz number ( $K_{as}$ ) by dividing the chemical strain rate,  $S_L / \delta$ , as

$$K_{as} = \frac{K}{(S_L / \delta)}. \quad 2.41$$

From Eqs.2.39-2.41, the following expression is obtained:

$$\frac{S_{L0}}{S_L} = 1 + (\mathcal{L}/\delta)(K\delta/S_L) = 1 + MaK_{as}. \quad 2.42$$

From Eq.2.42, it can be clearly shown that with positive  $K_{as}$

- 1) If  $Ma$  is negative, the burning velocity  $S_L$  increases with increasing stretch rate,
- 2) If  $Ma$  is positive,  $S_L$  decreases with growing stretch.

In other words, if  $Ma$  is negative, the bulges in the flame surface towards the fresh gas (positive flame stretch) will grow due to the increasing burning velocity, thus leading to an unstable flame. Conversely, with the same flame stretch and a positive  $Ma$ , the burning velocity will decrease in similar flame bulges, thereby smoothing the flame surface and the flame tends to be stable.



Bradley et al. [1996] accounted for two kinds of Markstein number corresponding to the effects of strain rate and flame curvature, respectively. However, the effect of flame curvature was negligible [Tseng et al. 1993 and Kwon et al. 1992B] because the ratio of flame thickness to flame radius  $\delta/r \ll 1$ . The values from measurements seem more applicable because the simplified Markstein number might combine several effects, some of which may still not be explored.

For comparison use, some mixture Markstein numbers are given in Tables 2.1-2.3 for two typical hydrocarbon mixtures (methane-air and propane-air), as well as hydrogen-air. Where data from two sources are listed in the case of methane-air, the difference between them is strikingly large, especially the point of transition from negative to positive. However, the qualitative trend that Markstein number increases with equivalence ratios agrees well in these two sets of data. Tables 2.1 and 2.3 show that for both methane-air and hydrogen-air,  $Ma$  increases with increasing equivalence ratio. As expected, the opposite trend exists in the case of propane-air (Table 2.2) and most other hydrocarbons. This seems to be in accordance with the observation of Karpov et al. [1980]. In regard to the laminar burning velocity, it seems to be independent of Markstein number.

**Table 2.1 Properties of Methane-Air (300 K, 1 atm)**

$\phi$	$S_{LO}$ (cm/s) [Aung et al. 1995]	Ma [Tanoue 2003]	Ma [Aung et al. 1995]	Le [Tanoue 2003]
0.6	5	1.34	-1.1	0.965
0.7	14	2.45	0.01	0.961
0.9	28	5.5	1.4	0.955
1	34	6.3	1.3	
1.1	35	7.4	1.6	1.1
1.2	33	8.4	1.8	1.1
1.35	26	5.5	3.2	1.1

**Table 2.2 Properties of Propane-Air (300 K, 1 atm)**

$\phi$	$S_{LO}$ (cm/s) [Kwon et al. 1992B]	Ma [Kwon et al. 1992B]
0.775	22	5.5
0.85	26	4.3
0.985	35	4.3
1.16	41	4.3
1.362	38	3.1
1.548	26	0.6
1.708	13	-1.8
1.878	7.7	-2.2

**Table 2.3 Properties of Hydrogen-Air (300 K, 1 atm)**

$\phi$	$S_{LO}$ (cm/s) [Aung et al. 1997]	Ma [Aung et al. 1997]
0.6	88	-0.8
0.75	134	0.25
0.9	180	1.09
1.05	210	1.72
1.2	240	2.8
1.5	260	2.35
1.65	260	3.5
1.8	261	3.72
2.1	250	4.26
2.35	239	3.46
2.6	212	3.9
3	193	4.27

### 2.7.3 Preferential Diffusion

Corresponding to the effect of Lewis number, it seems that the mechanism responsible for flame instability can be expressed by Markstein number. As mentioned by Kwon et al. [1992B], the effect of the flame stretch on the burning velocity involved two aspects of preferential diffusion: diffusive-thermal and diffusive-diffusive preferential diffusion, respectively. The first one has already been outlined in terms of Lewis number; the latter is associated with preferential diffusion of one reactant with respect to another.

Nevertheless, as it is impossible to separate these two specific mechanisms, it is common to attribute the preferential diffusion to the combination of these two. Particularly, the transition from a stable to an unstable condition was found to depend on neither the peak value of flame temperature nor the laminar burning velocity. Instead, it is a function of equivalence ratio that depends on either the Lewis number or the Markstein number. From the typical mixtures listed in Tables 2.1-2.3, this point has been sufficiently confirmed.

It is worth noting that Markstein number is a function of Lewis number, and becomes negative at some critical value of  $Le$ . The value of the critical Lewis number for many practical flames is less than unity [Clavin 1985]. Tromans, cited in [Abdel-Gayed et al. 1984], argued that for Lewis number greater than 0.85, the straining of the flame reduced the laminar burning velocity. Although from the view of the thermo-diffusive instability, the bounding value of Lewis number is unity, from the view of Markstein number, the critical value of  $Ma$  is zero corresponding to a Lewis number which is lower than unity.

#### **2.7.4 Flame Instability**

For flame instability caused by preferential diffusion, the hydrodynamic instability must be mentioned [Law 1998]. The hydrodynamic instability originates from the heat release of the burned gas, assuming a flame sheet exists between reactant and product, both of which have a constant gas density, and the flame is extending at a constant laminar flame speed. The difference of the gas density between the reactants and products results in the acceleration of denser reactants towards the less dense product zone. Law [1998] argued that without the effect of flame stretch the flame would be unstable by the hydrodynamic

stretch based on the fact that both the protruding and receding segment of the flame will be intensified further due to the unchanged laminar burning velocity. It is also concluded that the hydrodynamic stretch can not affect the flame intensity but only alters the flame surface area. However, Kwon et al. [1992A] argued that comparing with the effect of preferential diffusion, the hydrodynamic instability was relatively weak and generally obscured in laboratory scale experiments.

With respect to the preferential diffusion effect, the turbulent distortion of the flame surface is intensified in unstable conditions and retarded for stable conditions, thereby giving the same influence on the turbulent burning velocity. Fortunately, the stable condition is more commonly employed in the practical combustor, e.g. heavier-than-air hydrocarbons at lean conditions are widely used as the main fuel in industry [Wu et al. 1991].

### **2.7.5 Flame Stretch Rate**

Experimental studies [Aung et al. 1997, Tseng et al. 1993 and Kwon et al. 1992B] and a computational study [Bradley et al. 1996] have sufficiently shown the influence of flame stretch rate on the laminar burning velocity in terms of the Markstein number. As mentioned by Bradley et al. [1996], the contributions of flame curvature and strain rate are strikingly different in affecting the burning velocity. This makes the study more complicated. The investigation of the flame stretch in the laminar case forms a basis for interpreting the interactions between flame surfaces and turbulence within the wrinkled thin laminar flamelet regime of premixed turbulent flames.

In the laminar case, due to the relative simplicity of measurement of flame stretch rate and burning velocity, the outwardly propagating spherical flame is widely adopted

[Dixon-Lewis 1990]. For example, a general definition of stretch rate,  $K$ , at any point on a flame surface is the time rate of change of the infinitesimal surface area surrounding this point, specially,

$$K = \frac{1}{A} \frac{dA}{dt} \quad [\text{Law 1998}]. \quad 2.45$$

By the definition of stretch rate, the stretch acts on the surface tangential to the element. For general flame geometries and velocity field, the strain rate consists of two physical processes. One is the tangential strain rate on the flame surface which is associated with current velocity gradients in the reactant just upstream of the flame and the other one is the propagation of a curved flame, which can be characterized by the local curvature and local propagation velocity relative to the reactant fluid.

One simplification for the case of spherical outwardly propagating flame with infinite small flame thickness (with negligible flame curvature) at constant pressure (with negligible local flow motion) is that the flame stretch rate and instantaneous quiescent burning velocity can be readily given by

$$K_L = \frac{2}{r} \frac{dr}{dt}, \quad 2.46$$

$$S_L = \frac{\rho_b}{\rho_u} \frac{dr}{dt} \quad [\text{Law 1998}]. \quad 2.47$$

Therefore the stretch rate in the laminar case can be expressed as a function of laminar burning velocity by

$$K_L = \frac{2}{r} \frac{\rho_u}{\rho_b} S_L. \quad 2.48$$

The contribution of turbulence to the flame stretch can be associated with the life time of turbulent eddies [Abdel-Gayed et al.1987], e.g. the turbulence strain rate

$$K_t = \frac{u'}{\lambda}. \quad 2.49$$

With both  $K_L$  and  $K_t$ , the combined effect of flame stretch rate can be expressed as

$$K = \frac{2}{r} \frac{\rho_u}{\rho_b} S_L + \frac{u'}{\lambda}. \quad 2.50$$

This refers to the effective flame strain rate in turbulent conditions. It is worth noting here that the expression of  $K_L$  is based on the unconfined outwardly propagating spherical flame, namely no flow motion. Therefore, for the constrained flame of which the flame radius is larger than a certain size, Eq.2.46 is not applicable due to the pressure rise of the chamber. This was the case in the current investigation with flame radii of  $r = 46$  mm and 55 mm in a chamber of effective radius 62 mm.

Frequently, the stretch rate is expressed as a dimensionless parameter to characterize the flow field in Eq.2.41. The Karlovitz number  $K_{as}$  refers to the ratio of chemical characteristic time to the hydrodynamic time scale ( $1/K$ ). If the flame thickness is defined by mass diffusivity, Eq.2.27 will be substituted into Eq.2.41, which then becomes

$$K_{as} = \left(\frac{D}{S_L^2}\right)K. \quad 2.51$$

Thus the effect of stretch as represented by  $K_{as}$  can be increased by increasing the stretch rate or mixture diffusivity or by decreasing the flame burning velocity. In the turbulence case, in order to increase the turbulent burning velocity, it is necessary to decrease the flame stretch rate. This means that higher turbulent intensity does not

always increase the burning velocity. This point has been identified by the investigation of Abdel-Gayed et al. [1987] where the turbulent burning velocity initially increased with  $u'$ , but as  $u'$  increased further, the rate of increasing turbulent burning velocity with  $u'$  decreased until a maximum value of  $St$  was reached. Then a decrease of burning velocity followed until the flame was finally quenched with increasing  $u'$ .

## 2.8 Effect of EGR and RG

When EGR and RG are added in basic fuel-air mixtures, it is expected that properties concerning burning velocity of the mixture will vary in several ways. Because the major component of EGR is  $CO_2$ , many studies are devoted to study effect of  $CO_2$  on flames, e.g. non-gray radiation enhances the burning velocity with higher  $CO_2$  dilution [Ruan et al. 2001], soot emission and  $NO_x$  are reduced [Liu et al. 2003], the ignition timing is slowed down and temperature is reduced [Chen et al. 2002]. The well-known effect of EGR is to reduce the flame temperature, a major factor in the  $NO_x$  formation, but accompanied by an undesirable consequence of reduced burning velocity.

With respect to the RG, the main composition of  $H_2$  has a high flame speed and wide flammability limits. These properties are employed to extend the tolerance of engines to high levels of EGR. A good example was given by Allenby et al. [2001] that the addition of  $H_2$  extended EGR tolerance by 44 percent compared with operation on methane-air alone, giving a 77 percent reduction in raw  $NO_x$  emissions in the extreme operating condition without enrichment.

This study will not go into detail for all these aforementioned factors about EGR and RG but focuses on analyzing the following mechanisms:



1) Direct chemical effect.

2) The variation of the transport and thermal properties of the mixtures.

### 2.8.1 On Flame Chemistry

An understanding of the nature of flame chemistry is essential to interpret the burning velocity behavior. From the viewpoint of reaction mechanism, (using complete or reduced reaction mechanisms), sensitivity analysis has identified the most important controlling elementary reactions for hydrocarbons as follows [Dixon-Lewis 1990],



These two reactions show that the overall reaction is determinant on the radicals, H, O and OH.

Unlike an inert gas, the CO<sub>2</sub> in EGR can participate in the chemical reaction directly through the reverse reaction of R2.1. The competition of CO<sub>2</sub> for H radicals significantly decreases the reaction rate of R2.2, which is the most important chain branching reaction. As a result, the burning rate decreases with increasing CO<sub>2</sub> concentration by decreasing H radical concentration. The effect of RG (with major component H<sub>2</sub>), is to increase the burning rate through the same reaction mechanism by increasing the H radical concentration.

Liu et al. [2003] also concluded that the chemical effect of CO<sub>2</sub> in methane-air is much higher than that in hydrogen-air through the same reaction mechanism. The reason is that H radical concentration in hydrogen flames is relative high, so the reduction of radical H by CO<sub>2</sub> competition is less important. The current experimental laminar

burning velocity of methane-air mixed with EGR and RG (presented in Chapter 5) agrees well with the reaction analysis.

### **2.8.2 On Molecular Properties**

Adding EGR and RG makes the gas properties more complicated because with more than one reactant each contributes to the properties such as heat and mass diffusivity which affect Lewis number or Markstein number. In addition, the difference of the transport properties among the components of carbon dioxide, hydrogen and methane results in the complexity dealing with the combustion chemistry. The interaction between the turbulent flow and flame front varies with the strength of EGR and RG due to the aforementioned variation. Most combustion studies focus on one-reactant system [Clavin et al. 1979] without working with different conservation equations for energy and species. Even if the system is applicable to two-reactant systems, the validity is still restricted due to the assumption that both the reactants have either equal molecular coefficients or are highly diluted. However, the reactants in the current mixtures are highly diluted and the concentration of CO is weak comparing with methane and hydrogen in the mixtures, so the effect of CO is negligible. On the other hand, the hydrogen in RG increases both the heat and mass diffusivity of the fresh mixtures, but the heat diffusivity rises faster than the mass diffusivity. On the basis of analysis, it is reasonable to assume that the combined effect of RG can help stabilize the flame by increasing Lewis number of the reactants.

The computational method and results will be presented in section 4.3.

## **2.9 Effect of Turbulence Parameters**

The effect of turbulence on burning velocity falls into two categories: the turbulence intensity and turbulence length scale.

### 2.9.1 Turbulent Intensity

A huge volume of investigations has been devoted to the effect of turbulence intensity on the burning velocity. From both theoretical and experimental viewpoints, many expressions of turbulent burning velocity in terms of turbulent intensity have been given. Damköhler first proposed the simple formula

$$\frac{S_t}{S_L} = 1 + \frac{u'}{S_L} \quad 2.52$$

based on the assumption of continuous wrinkled laminar flame.

Moreover, Lipatnikov et al. [2002] reviewed a number of expressions derived from experiments. They argued that regardless of various models, a very close dependence of  $S_t$  on  $u'$  is yielded within moderate turbulence, giving

$$S_t \sim u'^{a_4} \quad 2.53$$

with  $0.5 \leq a_4 \leq 1$ .

Later, Williams [1985] used statistical turbulence to conclude that

- 1) For an intermediate range of intensities, (e.g.  $u'/S_L$  is of order of unity), the formula can be

$$\frac{S_t}{S_L} = 1 + a_3 \left( \frac{u'}{S_L} \right). \quad 2.54$$

- 2) For high turbulence levels, (e.g.  $u'/S_L > 1$ ), the formula becomes

$$\frac{S_t}{S_L} = \left( \frac{u'}{S_L} \right)^{0.7}. \quad 2.55.$$

The linear relation (Eq.2.53) between  $St/S_L$  and  $u'/S_L$  has been verified by the work of Ting et al. [1994] conducted in this laboratory. However, the question rises whether under the same value of  $u'/S_L$ , the coefficient  $a_3$  is variable or constant. Ting et al. [1994] found that  $a_3$  was fixed for various levels of mixture strength. The current investigation exhibited that  $a_3$  was varied with the mixture compositions. This point will be discussed in section 5.2.1.

Eqs.2.52-2.55 imply an increase in turbulence intensity would increase turbulent flame velocity, irrespective of fuel concentration of the mixture, which is in fact inconsistent with experimental observations in three aspects:

- 1) At high level turbulence, a “bending” effect has been found [Abdel-Gayed et al.1987]. As the turbulent intensity increases further, there is a slight decrease of turbulent burning rate. Shy et al. [2000] also found that a transition from increasing to decreasing effect of turbulent intensity on burning rate.
- 2) The coefficient of  $a_3$  is variable with the fuel mixture [Shy et al. 2000].
- 3) Most of the investigated flames are defined as fully-developed. However, the flame propagation velocity is varying within the range of development, especially for the currently investigated flames. In such engine-scale flames, the flame cannot reach to the developed stage, therefore the expression should take account into the flame size.

With respect to the transition of the effect of turbulent intensity, Shy et al. [2000] proposed another expression formula

$$\frac{S_t}{S_L} = 1 + a_5 \left( \frac{u'}{S_L} \right)^{a_6} . \quad 2.56$$

By plotting the experimental points, it showed that a turning point across which the slope  $a_6$  changes from positive to negative. The critical value of  $u'/S_L$  is around 12, and for this bound, Lipatnikov et al. [2002] argued that it is significantly dependent upon the Lewis number.

### 2.9.2 Turbulent Length Scale

Unlike the turbulent intensity, the effect of the turbulence scale  $L$  on the burning rate is inconsistent among the studies. Direct experimental investigation of the effect of  $L$  on flame burning rate is scant. Ting et al. [1994] have investigated the effect of  $L$  from 2 to 8 mm (at ignition time) on burning rate by varying various turbulence-generation grids. A decrease in burning rate with increasing  $L$  was observed.

The indirect effect of  $L$  can be found from the direct proportional relation between turbulent burning velocity and turbulent Reynolds number ( $R_L = \frac{u' L}{\nu}$ ), e.g.  $S_t \propto (R_L)^{0.238}$  [Abdel-Gayed et al. 1977A] which clearly demonstrates that the burning rate increases with increasing  $R_L$  and hence with  $L$ .

From the given empirical approximations for turbulent burning rate in [Lipatnikov et al. 2002],  $S_t \propto u'(D_a)^{0.27}$  and  $S_t \propto u'(K_a)^{-0.3}$ , together with the expressions of dimensionless scales,  $D_a = \frac{L S_u}{u' \delta}$  (Eq.2.24) and  $K_a = \left(\frac{u'}{S_L}\right)^{3/2} \left(\frac{L}{\delta}\right)^{-1/2}$  (Eq.2.22), it readily implies an increase in  $S_t$  by  $L$ .

The contradiction may lie in the varied stage of flame propagation. Ting et al. [1994] drew this conclusion from developing flames. As flames grow to the fully developed state, the influence of  $L$  may distinct. Chen et al. [1991] observed the varied influence

of  $L$  throughout all stages of flame development from ignition to the fully-developed flame in SI engines. This study showed that an increase of integral scale slowed the flame development from laminar to partially developing turbulent flame. Once the flame attained the developed phase, the turbulent burning velocity was enhanced by increasing  $L$ . This observation appears to explain the observation of Ting et al. [1994]. Since the effect of length scale is not the emphasis of current study, a fixed value of  $L = 7.6 \text{ mm}$  at ignition time is employed throughout the study. However bear in mind that the results indirectly contain the influence of  $L$ .

## **2.10 Measuring Turbulent Burning Velocity**

Two major methods involving pressure history and visualization imaging are widely used in measuring turbulent burning velocity. Here the respective main features are described as well as the application.

### **2.10.1 Pressure Trace**

The turbulent burning velocity calculated from the pressure trace recorded during flame propagation corresponds to the burned gas production rate. Four assumptions were made by Karpov et al. [1978] as follows,

- 1) The product behind the transient turbulent flame front is identical to that of the laminar flame.
- 2) The instantaneous value of the pressure in the chamber is a function of the amount of products, independent of their distribution in the volume.
- 3) The product and reactant are separated by a spherical surface with a radius from the spark center.

4) The burning velocity is taken as the increasing rate of the radius of the spherical surface relative to the unburned mixtures.

Based on the aforementioned assumptions, the turbulent burning velocity can be derived by comparing the pressure rise between turbulent and laminar cases for identical initial condition, that is

$$\frac{S_t}{S_L} = \frac{(dP/dt)_t}{(dP/dt)_L} \quad 2.57$$

This method has been adopted by many researchers [Checkel et al. 1994] and [Kido et al. 2001].

The drawback of pressure trace methods is the noise disturbance, especially at the initial stage of the flame growth, where the pressure rise is relatively weak compared with the noise. Usually the curve is not applicable until the ratio of pressure to noise is high enough that the noise is negligible completely.

### **2.10.2 Visualization Method**

Although pressure trace is widely used in measuring burning velocity, the flame visualization is still an indispensable measure, especially for studying the flame at the early stage where the pressure rise is too small to be measured, and analyzing the flame tomograms.

Checkel et al. [1992] employed a high speed video camera to capture schlieren images of the early stages of flame growth. The flame was assumed to be a uniform sphere with the same cross-sectional area as the schlieren image, and the flame front was designated the extreme outer edge of the schlieren images. This led to slightly over-estimating the flame size and burning velocity compared with the pressure-based observation.

Further, Bradley et al. [2003A] presented typical flame contours by using the planar Mie images, as well as the schlieren images trace. They postulated an important definition of flame radius for turbulent flames such that the volume of unburned gas inside a sphere of this radius is equal to the volume of burned gas outside it. By means of this definition, the turbulent burning velocity measured from schlieren images was proved to correspond to the mass turbulent burning velocity. It is worthwhile to mention here that the expansion factor due to the expansion of the burning element is used to derive the burning velocity, specially

$$S = \frac{\rho_b}{\rho_u} V_F. \quad 2.58$$

Here  $V_F$  is the propagation speed of the local part of the flame front, which is determined by using the sequential flame images. A similar method was also introduced [Kido et al. 2001, Tseng et al. 1993 and Renou et al. 2000].

By observing the flame surface images, the wrinkling effect of turbulence has been previously studied [Renou et al. 2000, Kaminski et al., Smallwood et al. 1995 and Haq et al. 2002], and all of these studies substantially support the wrinkled flame theory.

## 2.11 Concluding Remarks

This chapter gives a review of research in premixed turbulent flame propagation. It is concluded that the wrinkled flamelet theory is qualitatively effective for turbulent combustion and the gas properties significantly affect the interactions between turbulent field (flame stretch) and flame chemistry in terms of turbulent burning velocity.

Due to the need to build a combustion model for spark engines under EGR and RG operational condition, this research is designed under engine like combustion



conditions: wrinkled laminar flamelet turbulent combustion regime and not-fully-developed flames. The burning velocities are obtained from measured pressure trace. The effects of gas properties (Lewis number and Markstein number) on wrinkling flame surface are also studied because the turbulence enhancement is evidently altered with varying the concentrations of EGR and RG. Based on these viewpoints, the influence of turbulence intensity on burning velocity is dependent on the fuel type and flame growth state. With negligible laminar flame stretch effect, turbulent stretch effects on the flame propagation are also investigated in the present study. The turbulent burning velocities are correlated with some dimensionless timescales to examine the effectiveness of the established empirical expressions in developing flames. The details of these investigations and conclusions are clarified in Chapter 3, 4 and 5.

## CHAPTER 3: EXPERIMENTAL METHOD

This chapter describes the experimental system involving apparatus, control, procedure and data processing.

The basic experimental set up consists of a cubical combustion chamber, gas filling station, turbulence generation mechanism and data acquisition (DAQ) system as shown in Figure 3.1. This set up was employed in many previous investigations [McDonell 1988, Modien 1991, and Ting 1992]. However, some major modifications were made for these studies. A Virtual Instrumentation (VI) equipment combining hardware and software was developed to replace the previously used FM tape recorder and A/D converter. Also, new circuits were developed for the sensor box to allow the DAQ board to send and receive control and data signals to and from the relevant apparatus.

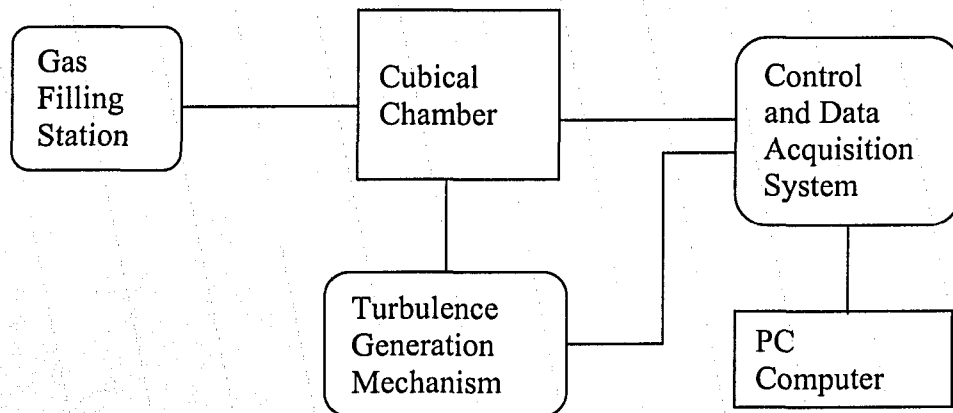
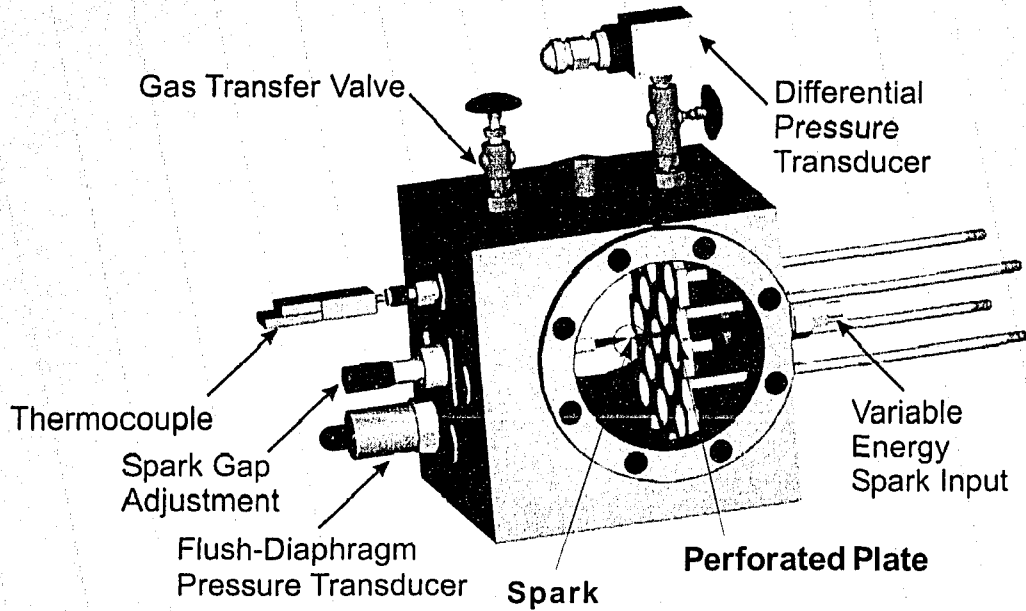


Figure 3.1 Schematic Diagram of the Experimental Setup

### 3.1 Combustion Chamber



**Figure 3.2 Combustion Chamber Configurations**

This chamber as shown in Figure 3.2 was described in detail by McDonell [1988], Modien [1991], and more recently by Ponnusamy [2005]. The major instrumentation of this study is the same used by Ponnusamy. This includes a chromyl-alumel (Type K) thermocouple measuring the initial temperature of each run, a Validyne digital pressure transducer recording the initial pressure of the mixture prior to ignition, and a flush diaphragm pressure transducer (Precise Sensor model 7820) to record the pressure rise during flame growth. The initial temperature was fixed as the same ambient room temperature ( $23 \pm 1$  °C). The initial pressure was set as 101.3 kPa with error of  $\pm 0.15$  kPa (error of 0.133 kPa was produced from barometer reading and error of 0.014 kPa is generated from Validyne reading).

A Swagelok port connected to the gas filling system (section 3.2) for vacuuming and charging gas. The two spark electrodes passed through the centre of the cell with one

adjustable to allow changeable spark gap, a high-voltage capacitor circuit supplied the spark energy. This study adopted a spark gap of 4 mm and constant thermal ignition energy of 112.5 mJ (300 V and 2.5  $\mu$ F) for all runs. A modification was also made in the preciously used capacitor discharge ignition circuit as shown in Figure 3.8.

### **3.2 Gas Filling Station**

The gas filling apparatus consists of CH<sub>4</sub>, N<sub>2</sub>, CO<sub>2</sub>, CO and H<sub>2</sub> commercial cylinders, an air pipeline connected to the laboratory compressed air system, a mixing chamber and a vacuum pump as shown in Figure 3.3. The fuel-air/diluents mixtures were determined using the partial pressure method. To reduce the error caused by the charging process, the mixtures were first mixed in the mixing chamber at a final pressure that was higher than the initial pressure of the test run and sufficient for several tests using the same mixture.

To ensure the gas flowing to the right direction, the manifold upstream pressure was always kept higher than the mixing chamber pressure. After one gas finished filling, the manifold was evacuated and then flushed with air three times to make sure that the old gas was removed completely prior to introducing new gas. When the mixing chamber was filled with proper mixture, the gases in the vessel were allowed to reach homogeneous status by waiting several minutes [Ting 1992], and then the mixtures were ready to be charged into the combustion chamber. Prior to introducing the prepared mixtures, the combustion chamber was evacuated and flushed with compressed air three times. The final pressure of the cubical chamber was one

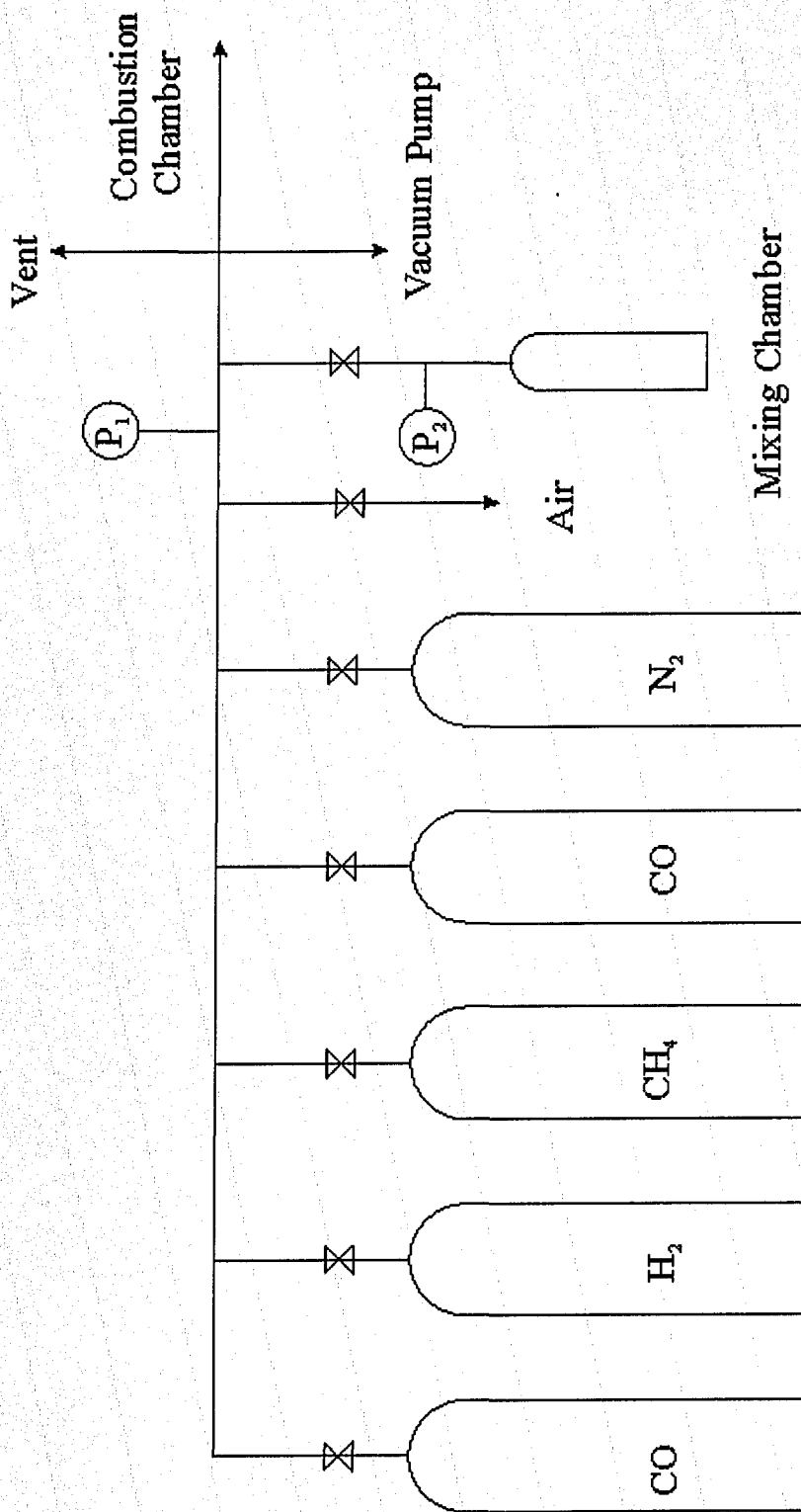


Figure 3.3. Schematic Diagram of Gas Filling System

atmosphere (101.3 kPa) for all the current tests. After a test, the chamber was immediately evacuated and purged with air to remove the burned products and moisture.

### **3.3 Turbulence Generation Mechanism**

#### **3.3.1 Plate Motion Mechanism**

The current turbulence generation mechanism as shown in Figure 3.4 is the same as that used in the previous investigations [Modien 1991, McDonell 1988 and Ting 1992]. This mechanism contains a 60 % solid perforated plate, a steadily rotating flywheel with protruding tooth, a stirrup attached by four rods to the perforated plate, a hydraulic shock absorber and two electromagnets. To initiate plate motion, a solenoid fired a pin across a slot in the stirrup, engaging the tooth and pulling the perforated plate across the chamber. As the tooth clears the pin, the stirrup mechanism moves on by means of its own momentum until it is caught by the hydraulic shock absorber and two electromagnets that hold the plate at the end of the chamber for two seconds. The shock absorber position is also adjustable to allow a longer damping stroke for higher plate speed.

#### **3.3.2 Plate Speed Measurement**

The actual plate position and speed are deduced from the recorded output of an optical sensor focused on white and black strips at 10 mm intervals on the stirrup. Figure 3.10 shows a typical plate position trace. The high voltage of 5 V corresponds to the white stripe, while the low voltage is associated with the black stripe. The time duration is

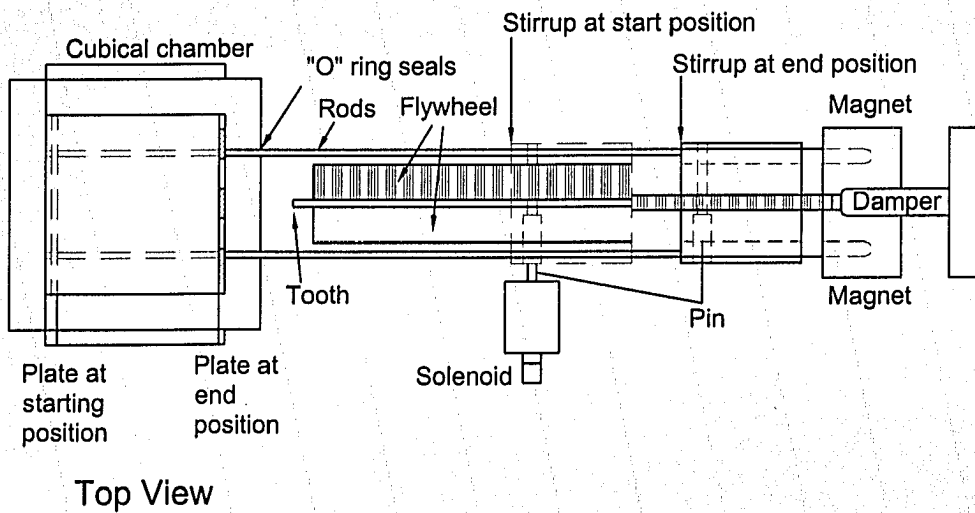
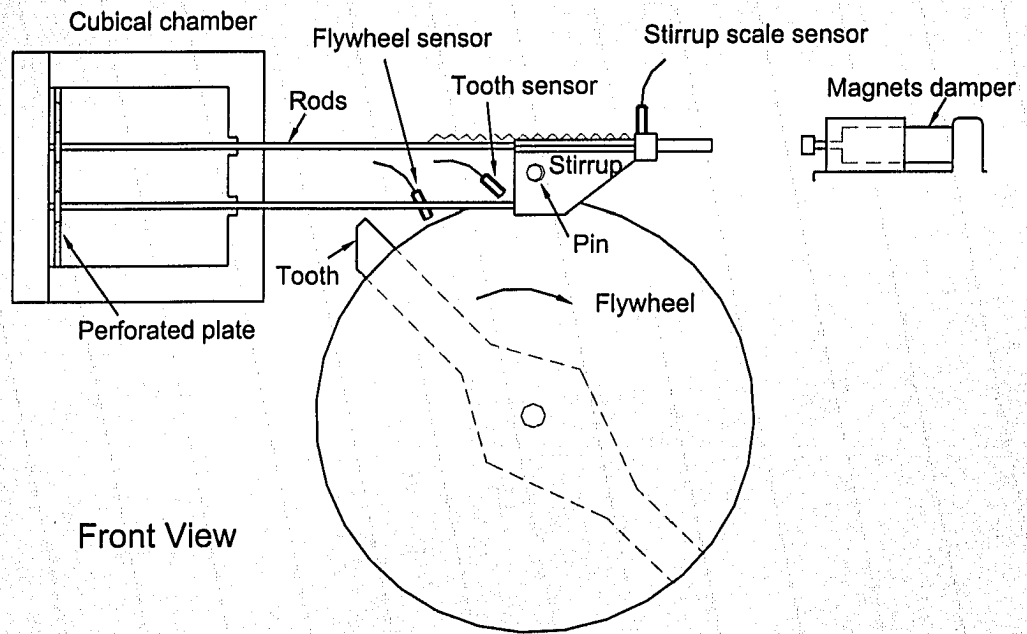


**Figure 3.4 Turbulence Generation Mechanism [Modien 1991]**

conveniently read from the LabVIEW show panel. Note that the plate position is the distance of the leading edge of the plate from the chamber wall where the plate initially rested. The calculated plate speed is an average over the range of positions from 5 to 110 mm. Specially, the plate speed can be calculated from the expression

$$V = \frac{105 \text{ mm}}{\text{Time Duration}} \quad 3.1$$

### 3.4 Data Acquisition and Control System

As shown in Figure 3.5, the data acquisition system consists of a sensor box, a National Instruments personal computer interface card and custom LabVIEW software program. The control aspect uses the same software program and computer interface card to fire a solenoid which triggers each experiment.

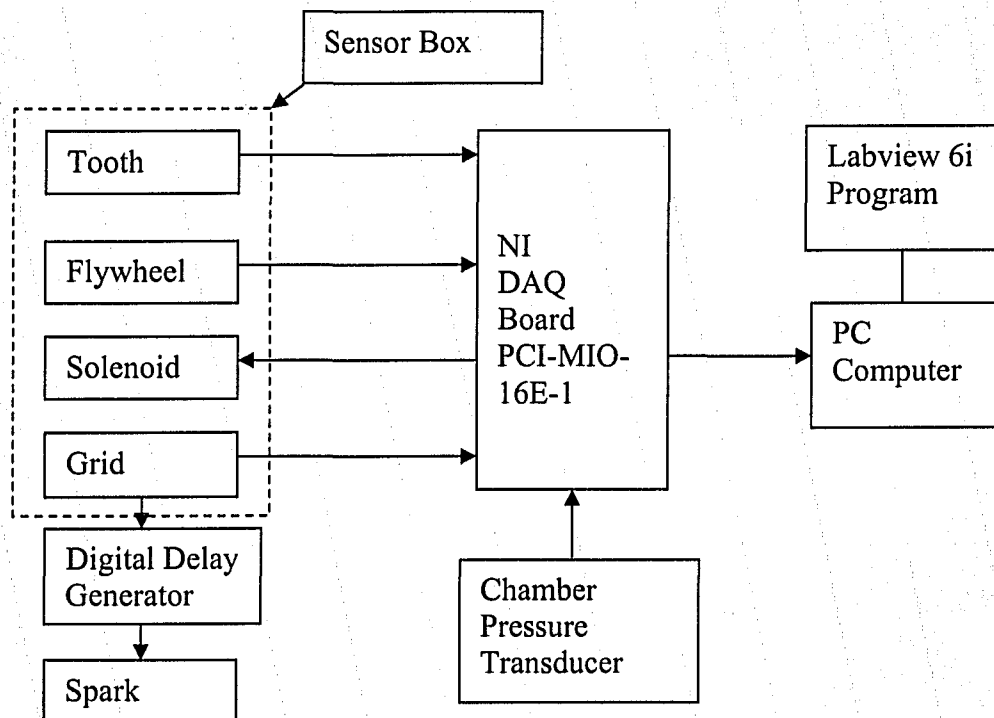


**Figure 3.5 Schematic Diagram of Data Acquisition and Control System**



### **3.4.1 Sensor Box**

The sensor box uses optical sensors to sense tooth, flywheel and grid positions. Measuring the white and black mark on the relevant apparatus, the reflective object sensors generate voltage signals. More details can be consulted in McDonell [1988] and Modien [1991]. High sensitivity OPB704 phototransistors were used in this study replacing the old models. With a load resistance of  $10 \Omega$ , the corresponding rise and fall time is  $200 \mu\text{s}$  which gives an estimate of the time measurement accuracy.

As shown in Figure 3.6, the signals from flywheel, grid and spark were optically isolated from ground and went to the National Instruments PCI-MIO-16E-1 board. There are two grid sensors put in use, one for recording grid speed and one for trigger the spark for turbulent-run combustion (called turbulent spark). Note that the isolated signals of tooth and spark were not directly used in this study.

Shown in Figure 3.7 is a circuit designed to allow the solenoid and magnets power supply to hold for two seconds after the pin in the stirrup was fired by the pulse from PCI-MIO-16E-1 board. This is to make sure the perforated plate remains at the end of the chamber during the combustion. Otherwise the flame shape will be distorted by the plate prior to contacting the chamber wall.

### **3.4.2 Virtual Instrument Channels**

Table 3.2 lists the functions of the seven Virtual Instrument (VI) channels. The first five are inputs. The sixth is a trigger output which triggers the pin to engage the flywheel tooth. The seventh (spark out) is a digital trigger for laminar flame runs. Shown in Figure.3.9 is the diagram of the channels designated in the National Instruments PCI-

MIO-16E-1 board. The corresponding custom LabVIEW program can be consulted in APPENDIX A.

### 3.5 Experiment Control Procedure

The plate speed, flywheel frequency and pressure trace were monitored on PC with a Virtual Instruments PCI-MIO-16E-1. A dedicated LabVIEW program controlled the experimental procedure and presented the raw data for calculation use.

**Table 3.1 VI Channel Inputs and Outputs**

VI Channels	Range (V)	Function
Pressure 0-10V	0 to 10	Maximum pressure
Pressure 0-5V	0-5	High resolution pressure
Grid	0-10	Plate motion
Tooth	0-10	For future use
Flywheel ( also connected to Counter 1)	0-10	Flywheel frequency
Solenoid trigger	output	Trigger the pin
Spark out	output	Trigger the spark (Laminar runs)

For each experiment, the first step was to adjust the flywheel to a desirable frequency shown in the LabVIEW's show panel. Secondly, LabVIEW sent a digital signal to the solenoid to fire the pin. Then the plate was drawn by a stirrup to the end of the chamber and held for two seconds until the combustion finished. The progress of the plate and

stirrup assembly was sensed and recorded by the program. At the same time the grid travel the “spark” sensor which triggered the digital delay generator (California Avionics Laboratories, Inc., model 201AR). After a preset delay time, the digital delay generator generated a 12 V pulse to trigger the ignition circuit and the program recorded the pressure transducer output. The delay preset time was planned in corresponding to the plate speed to give desired turbulence values.

The DAQ board recorded all the corresponding data in four analog channels during the procedure. The plate speed was used to calculate the r.m.s turbulence velocity and the pressure rise was employed to calculate the burning velocity. The sample rate used for pressure here was 10,000 points per second. Figure 3.10 shows the data output of a typical turbulent experiment. The LabVIEW 6i programming code is given in Appendix A.

### **3.6 Mixtures Investigated**

All mixtures used in this study consist of stoichiometric methane-air along with simulated stoichiometric EGR and stoichiometric RG-air. Methane-air stoichiometric mixture is composed of 9.5 % CH<sub>4</sub> and 90.5 % in volume. Simulating the real exhaust gas recirculation (EGR) by means of the similar molar mass and specific heat capacity, the EGR in this study consists of 18.5 % CO<sub>2</sub> and 81.5 % N<sub>2</sub> by volume. Hence, a mixture which is designated EGR5 will include  $0.05 * 18.5 \% = 0.0925 \% \text{ CO}_2$ . The reformer gas (RG) is composed of 25 % CO and 75 % H<sub>2</sub> by volume to simulate the ideal steam reforming products of methane. Note that the value of percentage for RG refers to the stoichiometric mixtures of CO, H<sub>2</sub> and air. Consequently in the RG total

mixture consists of 22.1 % H<sub>2</sub>, 7.4 % CO, 70.5 % of air and a mixture designated as RG11 contains 0.11 \* 22.1 % = 2.4 % H<sub>2</sub>.

Four kinds of mixtures are investigated as shown by detailed volumetric compositions in Table 3.2.

**Table 3.2 Compositions of Tested Mixtures (volumetric fraction)**

	Methane-air	Methane-air/ EGR5	Methane-air/ EGR15	Methane-air/ EGR5/RG11
CH <sub>4</sub>	0.0948	0.0901	0.0806	0.0780
O <sub>2</sub>	0.120	0.181	0.162	0.178
N <sub>2</sub>	0.716	0.720	0.730	0.703
CO <sub>2</sub>		0.00925	0.0278	0.00925
CO				0.00812
H <sub>2</sub>				0.0244

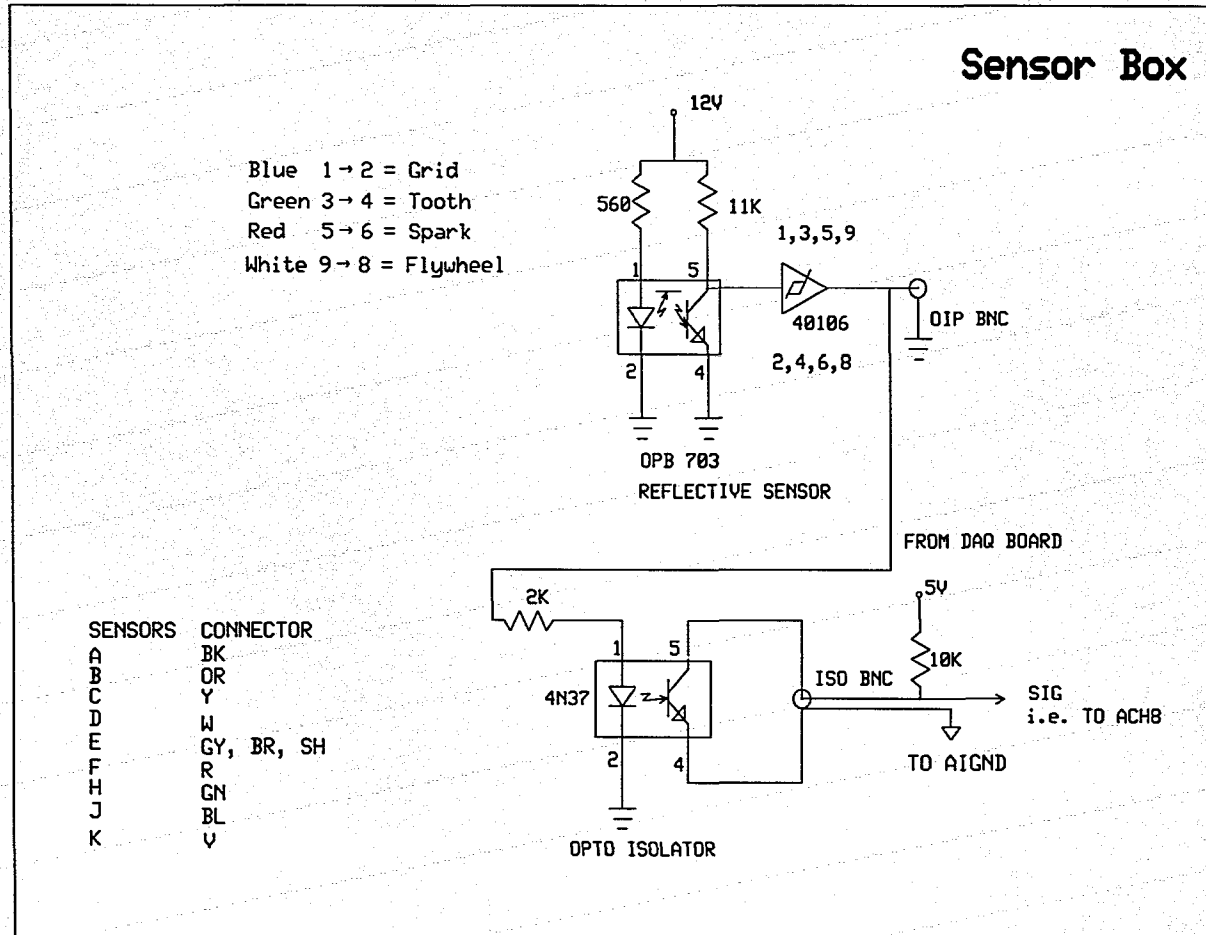


Figure 3.6 Circuits for Tooth, Flywheel, Spark and Grid in Sensor Box

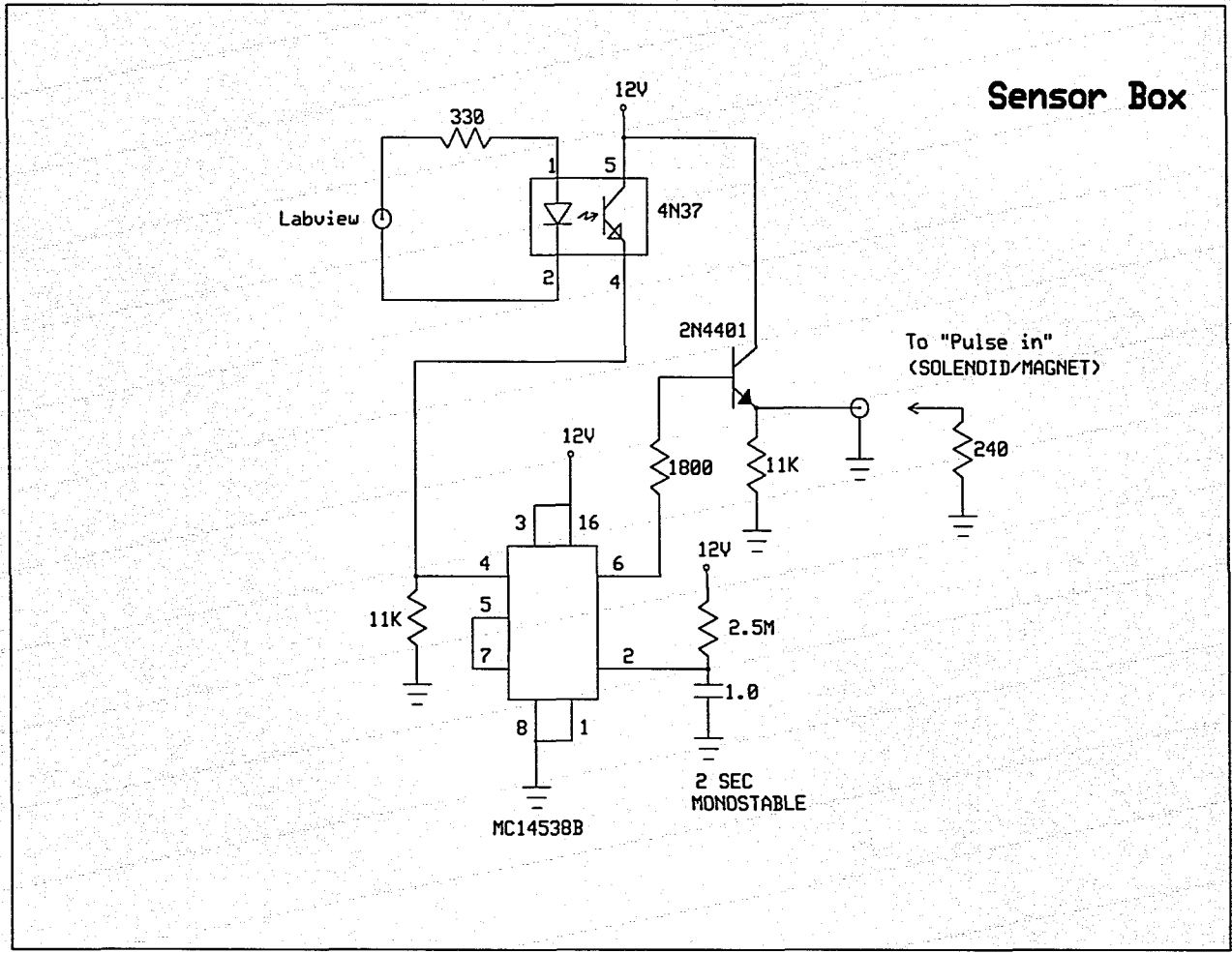
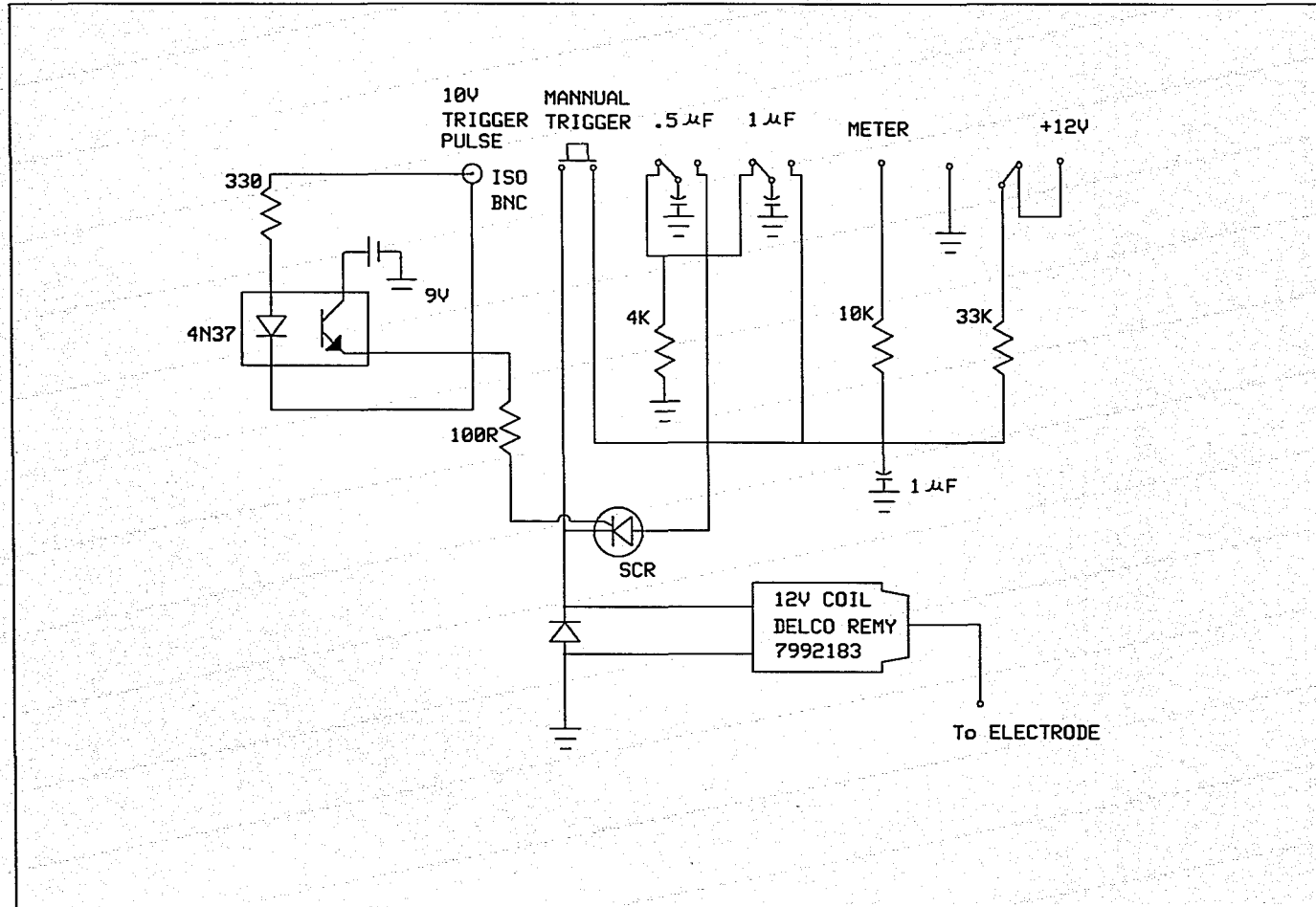
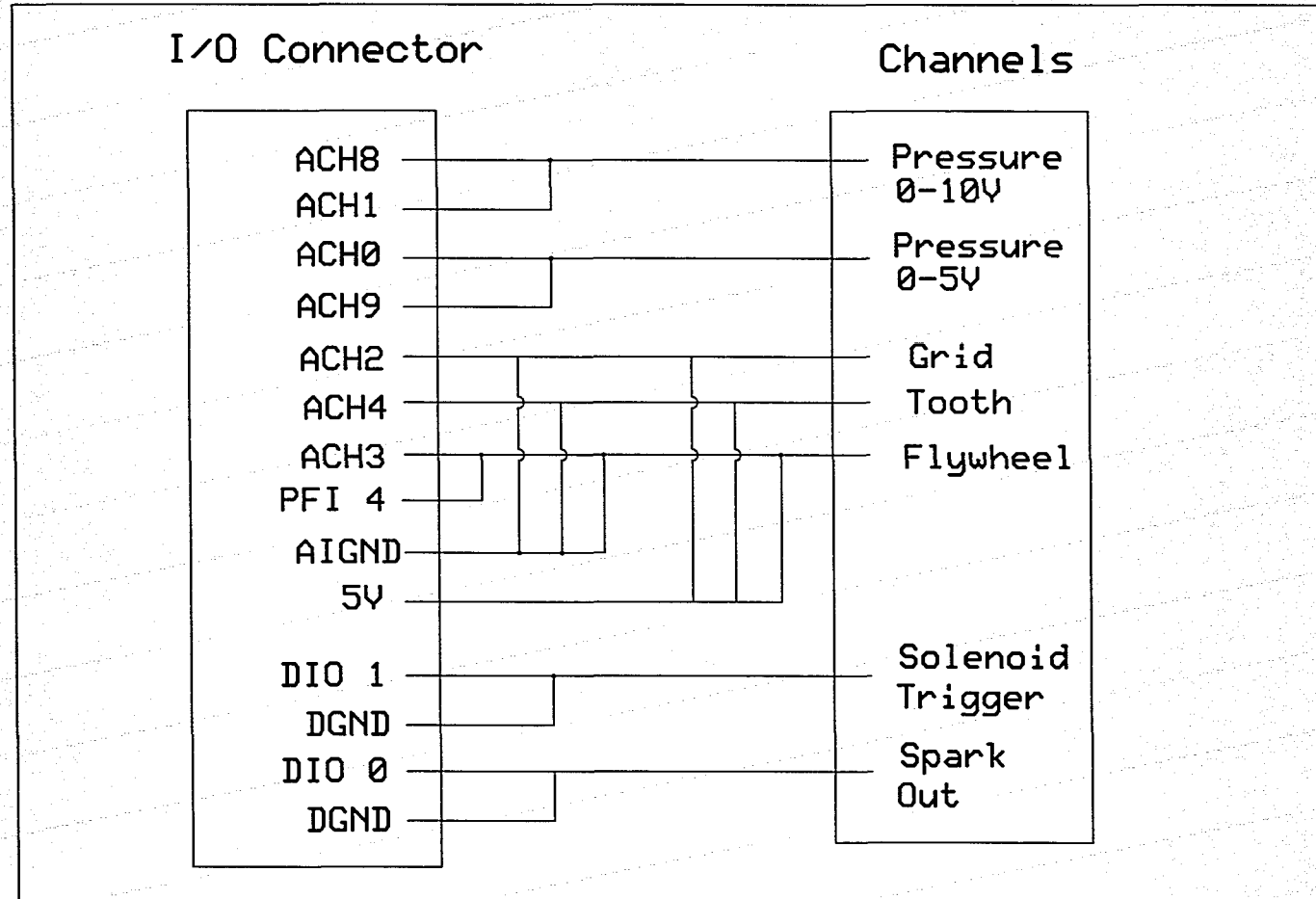


Figure 3.7 Circuits for Solenoid Trigger and Magnet



**Figure 3.8 Modified Circuits for Capacitance Discharge Ignition**



**Figure 3.9 Schematic Diagram of the Data Channel Connections**



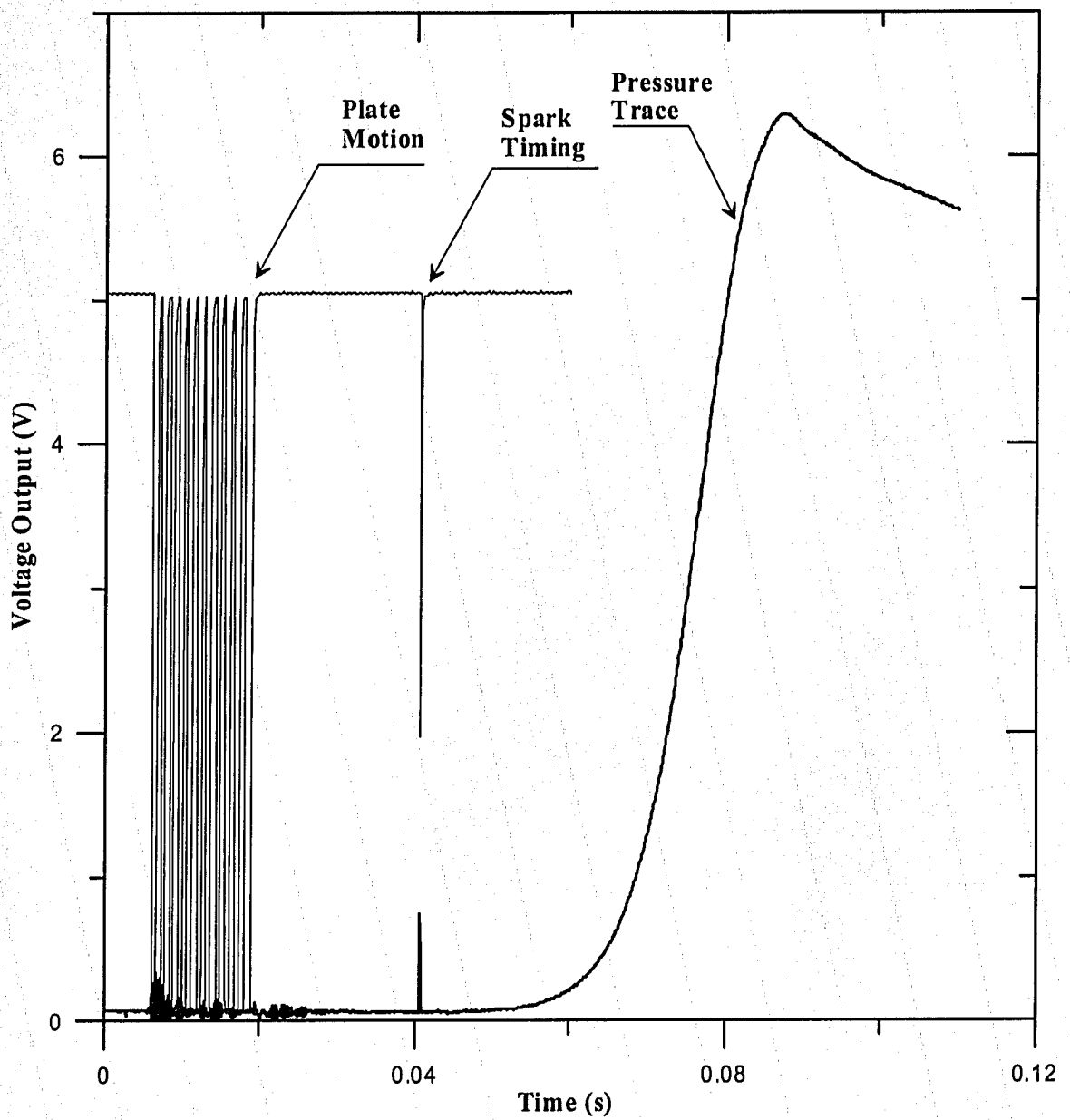


**Figure 3.10 Typical Data Recorded**

**(Pressure Rise and Plate Motion as a Function of Time)**

methane-air/EGR15,  $V = 8.2 \text{ m/s}$ ,  $X/D=10.7$ ,  $u'_{ig} = 1.2859 \text{ m/s}$

Chamber peak pressure: 745 kPa,

Combustion time duration: 46.9 ms.

## CHAPTER 4: CALCULATION METHODS

This chapter describes the calculations used throughout this study, involving turbulent burning velocity, turbulence parameters and mixture property parameters such as Markstein number and Lewis number.

### 4.1 Calculation of Turbulent Burning Velocity

The turbulent burning velocity is a function of the corresponding laminar burning velocity, turbulence parameters such as turbulence intensity and integral scale, and the flame stability in terms of Markstein number or Lewis number. The laminar burning velocity, an important intrinsic property of the fuel gas, is determined by the mixture composition, equivalence ratio and combustion conditions such as temperature and pressure. With respect to the developing phase of turbulent flame investigated, the instantaneous quiescent burning velocity replacing laminar burning velocity is employed as a basis value with benefit of negligible effect of temperature and pressure. Also, the application of instantaneous burning velocity leads to the effect of turbulence is associated with flame size.

For flames growing in a closed vessel, the turbulent burning velocity can be determined from the pressure trace as outlined in section 2.10.1 in conjunction with a thermodynamic model. Both the quiescent and turbulent burning velocities were derived from the pressure history monitored during the spherical flame propagation in the cubical chamber. Specially, the turbulent flame size was approximated from the pressure trace at the same increased pressure predicted by the thermodynamic model for a given amount of burned mixtures.

#### 4.1.1 Multi-zone Thermodynamic Equilibrium Model

To calculate the burning velocity, this study adopted an established multi-zone thermodynamic equilibrium model [Ting 1992] (MTEM). This program code is given in Appendix B. Here a brief description is given focusing on the major characteristics.

This model is applicable to spherical flame propagation in a constant volume combustion vessel. By using a shell method, the gases in the vessel are divided into three regions: previously burned gas, unburned gas and currently burning gas as shown in Figure 4.1. The first two are assumed frozen in chemical composition and are compressed isentropically by the burning gas. The burning gas is assumed to reach an

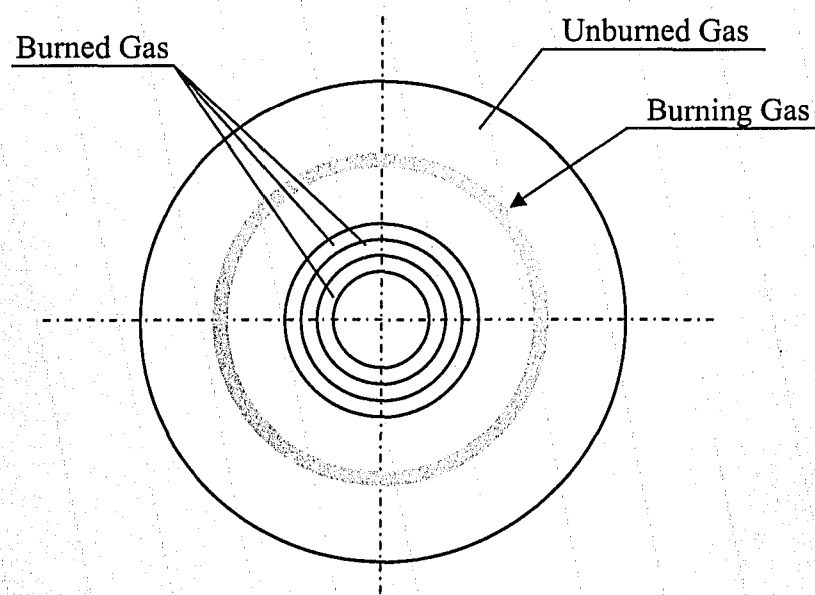


Figure 4.1 Schematic of the MTEM

equilibrium state, where carbon dioxide and water-gas dissociation are the only reactions taken into account.



Therefore, the thermodynamic properties of the burned gas are calculated using six species such as CO<sub>2</sub>, CO, O<sub>2</sub>, N<sub>2</sub>, H<sub>2</sub>, and H<sub>2</sub>O. From the view of energy and species effects, it has been confirmed that these two dissociations could meet the calculation requirements [Modien 1991].

Conservation of mass and energy equations are applied to solve the unknown pressure of the vessel after burning each shell of unburned gas. Considering adiabatic, constant volume combustion with negligible heat loss, the internal energy difference between reactant and product of the burning shell is equal to the compression work done on all the volume of previously burned and unburned gas:

$$EI_{reactant} - EI_{product} = \sum (W_{burned}) + W_{unburned} \quad 4.1$$

In the burned gas zone, different pressure and temperature are considered in each of the previously burned shells. The total compression work is the sum of the work in these shells plus the unburned gas which can be treated as a uniform volume.

With the pressure solved, mass conservation is used as a closure equation for the model. The chamber volume after each combustion step is equal to the sum of volumes of unburned gas, previously burned gas after compression by the burning shell and the burning shell after combustion.

In this process, the burned mass fraction and mean flame radius are solved as a function of the pressure. Therefore, the measured pressure from the experiment can be used to derive the actual flame front radius and mass burning fraction by interpolation. In order

to account for the change of flame area with flame growth during each time step, a defined geometric average flame radius is used in calculating burning velocity rather than the instantaneous flame radius. More details can be consulted in [Ting et al.1994]. The burning velocity now can be calculated as the engulfment rate of the unburned gas between measurement points of the pressure trace, namely

$$S = \frac{\Delta r}{\Delta t} \quad 4.2$$

Here  $\Delta r$  is a designated flame radius difference between two adjacent measured points.

This thermodynamic program code (Matlab Edition) is given in Appendix B.

#### **4.1.2 Multi-Zone Thermodynamic Equilibrium Model for Turbulent Flames**

Since the flame in quiescent condition is nearly spherical and its thickness is thin, using Eq.4.2 to calculate burning velocity gives more reliable results without much argument. In the case of turbulent combustion, the situation varies in two aspects. One is that the flame front is not smoothly spherical due to the turbulence distortion of the flame surface. The other is that the flame front becomes thicker due to the distortion of small scale turbulent eddies. During measuring the turbulent burning velocity, the definition of flame surface is an issue. For example, the surface area of a statistically spherical turbulent flame substantially depends on the choice of the reference surface [Lipatnikov et al.2002]. According to Checkel et al. [1992], the “smoothed” flame radius can be defined for turbulent combustion such that the area of a smooth sphere of that radius has a volume equal to the gas already burned. This is essentially the same definition as the quiescent burning velocity and thus provides a result on the basis of an “average smooth” radius in the turbulent flame thickness. The validity of an analogous

calculation has been verified [Kauffman 1980] by calibrating the flame radius measured by ionization gauges.

In the current study two points were selected to study the effect of turbulence on burning velocity, namely flame radius  $r = 46$  mm and  $r = 55$  mm. There are three reasons responsible for this selection.

1) At early stage of combustion, the burning velocity derived from pressure history is significantly affected by noise. Thus, only after the pressure rise reaches a certain value to exceed the noise disturbance can the pressure trace produce consistent results. When the flame radius is larger than 42 mm, the signal is about two orders of magnitude larger than noise [Ting 1992], so it is reasonable to use flames over 42 mm radius to measure.

2) The physical dimension of the cubical chamber constrains the measurement to a flame radius smaller than 61 mm [Ting 1992]. When the flame ball hits the chamber wall, the limiting pressure is approx.  $2.2 \cdot P_{ini}$  under the current experimental condition. After this point, the flame front may contact the chamber wall, so the assumption that flame shape is ideally spherical is not applicable. Also, when the flame contacts the chamber wall, there is a large heat loss, contradicting the computational model of negligible heat transfer to outside the chamber.

3) The flame curvature and relative flame thickness are small at these two points. This makes it reasonable to assume that the flame is one dimensional and thin. Clark et al. [1995] argued that the flame stretch caused by curvature and thickness can be ignored as well as laminar flame stretch when the flame ball was relatively large.

#### **4.1.3 Application of Instantaneous Burning Velocity**

Several models were proposed [Andrews et al. 1975] where the turbulent burning velocity was based on laminar burning velocity. Due to the physical size of the current combustion chamber, the flames investigated are relatively small and the whole range of the flame is still in the developing stage similar to the operational condition in spark engines [Checkel 1986]. Therefore, both the instantaneous turbulent and quiescent burning velocities are considered in this study replacing developed turbulent flame velocity and laminar burning velocity. Consequently, the burning velocity for both quiescent and turbulent combustion is a function of flame radius.

The instantaneous burning velocity maybe more appropriate because the pressure and temperature of the unburned mixture are varied from the initial state as the flame grows.

According to the empirical power law equation,

$$S_L = S_{L0} \left( \frac{P}{P_{int}} \right)^{a_9} \left( \frac{T}{T_{ini}} \right)^{a_{10}}, \quad 4.3$$

the burning velocity deviates from the laminar burning velocity at the standard state. The difference between the standard and instantaneous burning velocities for different mixtures investigated can be consulted Table 5.1 in section 5.1.

It has been commonly accepted that the temperature rise increases the flame burning rate, while the pressure rise has opposite effect on the burning rate. With respect to the exponents of  $a_9$  and  $a_{10}$ , many studies investigated the effects of temperature and pressure on the burning velocity. For example, Heywood [1988] gave the coefficients of  $a_9 = -0.16$  and  $a_{10} = 2.18$  for stoichiometric methane-air mixture.

In the case of constant volume combustion, the unburned gas temperature is a function of pressure due to the isentropic compression of expanding flame. As the flame grows,

the chamber pressure increases as well as the temperature. The instantaneous burning velocity is determined by the combined effect of pressure and temperature.

Despite of the discrepancies of  $a_9$  and  $a_{10}$  among the studies, the instantaneous quiescent burning velocity is used to normalize the turbulent burning velocity under the same pressure and temperature, so the uncertainty caused by pressure and temperature can be avoided.

Using the instantaneous burning velocity, Kido et al. [2001] found that under weak turbulence intensity, the turbulent burning velocity maybe considered as independent of the equivalence ratio of the mixture. Checkel et al. [1992] also concluded that using instantaneous quiescent burning velocity as a standard, the effects of moderate changes in lean equivalence ratio on the linear relationship between  $S_t/S_L$  and  $u'/S_L$  was negligible.

## **4.2 Estimation of Turbulent Intensity and Integral Length Scale**

To correlate the turbulent burning velocity with turbulence flow field, the estimation of turbulent intensity and scales is of critical importance. Various turbulence generation mechanisms are responsible for the transient behavior of the expanding turbulent flame. This makes it essential to address the current approach of estimating turbulence parameters.

The current turbulence is generated by drawing a perforated plate across the test cell. The turbulence decays rapidly without combustion, while the turbulence parameters during combustion are intensified significantly by the compression effect of the



expanding flame. Using the rapid distortion model to correct decaying turbulence, the current turbulent intensity and scales are assessed.

## 4.2.1 A Decay model

### 4.2.1.1 Theoretical background

Without combustion, the turbulence intensity ( $u'$ ) can be deduced from a well established decay model as a function of plate speed ( $V$ ), preset delay time ( $t_d$ ) and hole diameter ( $d$ ). The model was originally constructed in the wind tunnel using a hot wire anemometer and applied to the turbulent combustion bomb on the basis of geometric similarity [Checkel 1986, McDonell 1991]. The basic concept is that the spatial decay of r.m.s turbulence intensity measured downstream of a fixed perforated plate in the wind tunnel with a steady flow of bulk velocity  $V$  is a power law with the same exponents as that for the temporal decay of turbulence at a fixed point behind a similar plate drawn across the cell at a constant velocity  $V$ . That is:

$$\frac{\text{anemometer output } (u')}{V} = c_1 \left(\frac{X}{d}\right)^{c_2}, \quad 4.4$$

where  $X/d$  is the dimensionless distance, representing distance downstream of the plate:

$$X = V * t_d, \quad 4.5$$

$t_d$  is delay time starting from the plate passing by the ignition gap at the chamber center to the ignition time. Previous investigations [Checkel 1981 and McDonell 1991] using the combustion chamber showed that for  $X/d$  greater than 5, the mean flow broke down completely and did not affect the flow field. Therefore, the turbulence at this moment was approximated as isotropic, meaning the two component velocities in the plane parallel to the direction of the plate motion were probability distributed. Moreover,

statistical arguments were used to show that the mean of the anemometer output was approximately 1.2 times the root square turbulence intensity parallel to the perforate plate. That is:

$$\text{mean signal} = 1.2\sqrt{u'^2} . \quad 4.6$$

Based on Eq.4.6, the decaying r.m.s velocity in the direction of plate motion can be derived from an ensemble mean anemometer signal in the region of negligible mean flow.

By definition, the integral length scale is the integral of the autocorrelation coefficient of the fluctuating velocity at two adjacent points in the flow with respect to the variable distance between points [Heywood 1988]. Due to the difficulty of measuring two points simultaneously, it is more convenient to derive the integral length scale from the Eulerian time correlation for a single probe:

$$\mathfrak{R}(t) = \frac{1}{N-1} \sum_{i=1}^N \frac{u(t_0)u(t_0+t)}{u'(t_0)u'(t_0+t)} . \quad 4.7$$

In addition, a simple empirical formulation cited [McDonell 1991] was employed to derive the integral time scale  $\tau_I$ ,

$$\mathfrak{R}_E(t=\tau_I) = \exp(-1) . \quad 4.8$$

the integral length scale is readily obtained from

$$L = V\tau_I \quad 4.9$$

Similar to the turbulent intensity, a power law function was found in deriving the relation between the length scale and grid-generated turbulence,

$$\frac{L}{d} = c_3 \left(\frac{X}{d}\right)^{c_4} \quad 4.10$$

#### 4.2.1.2 Coefficients of Empirical Equations

Based on aforementioned concept, the coefficients  $c_{1-4}$  were derived from considerable experiments, Checkel (unpublished) produced a decay model which separated the decay of turbulence into three regions in term of the range of  $X/d$ . The coefficients  $c_{1-4}$  tabulated in Table 4.1 are used in this study for calculating turbulence intensity and integral scale.

So far, Eq.4.4 and 4.10 are applied to calculate the turbulent intensity and turbulent length scale under the cold run condition.

**Table 4.1 Turbulent Coefficients [Ting 1992]**

Regime	$c_1$	$c_2$	$c_3$	$c_4$
$5 < X/d < 10$	10.96	-1.812		
$X/d < 14.3$			0.38	0
$10 < X/d < 20$	2.627	-1.191		
$14.3 < X/d$			0.1	0.5
$20 < X/d < 40$	0.773		-0.783	

#### 4.2.2 A Rapid Distortion Model

As discussed before, the combustion is affected by turbulence intensity and scale. In a closed vessel with turbulence, the compression of a growing flame can contribute to a further increase in turbulent burning velocity due to the enhancement of turbulence. It

can be explained that the vorticities just in front of the flame front are stretched by the curved advancing flame. Note that the Rapid Distortion Theory (RDT) is effective provided that:

- 1) The fluid element distortion must take place faster than there is time for viscous and non-linear transfer effects to become significant;
- 2) Displacement between particles resulting from the distortion must be much larger than those caused by the turbulence fluctuations.

Chew et al. [1992] used RDT to estimate the degree of turbulence enhancement by the mechanism of vortex stretching. They also verified that for typical turbulent combustion experiments with moderate turbulent intensity, the RDT requirements are reasonably satisfied.

As the rapid distortion of an element of fluid acts on the turbulence in that element, it was found that the energy for the longitudinal direction (as shown in Figure 4.3) velocity component is reduced. On the other hand, the energy for the lateral direction (Figure 4.3) velocity component is increased. Putting the two effects together, the total energy is increased by rapid distortion. Chew et al. [1992] also presented a mathematical formulation of the energy ratio. As shown in Figure 4.2, assuming an element in a confined vessel propagates spherically from the original point (before ignition),  $r_{ini}$ , to the flame front,  $r_b$ , the volumetric compression ratio is :

$$\zeta = \left( \frac{\rho_u}{\rho_{ini}} \right)^{-1} \quad 4.11$$

and the normal geometric strain of the element is:

$$s = \left( \frac{r_{ini}}{r_b} \right)^2. \quad 4.12$$

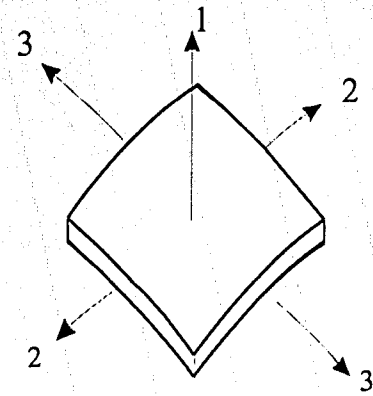
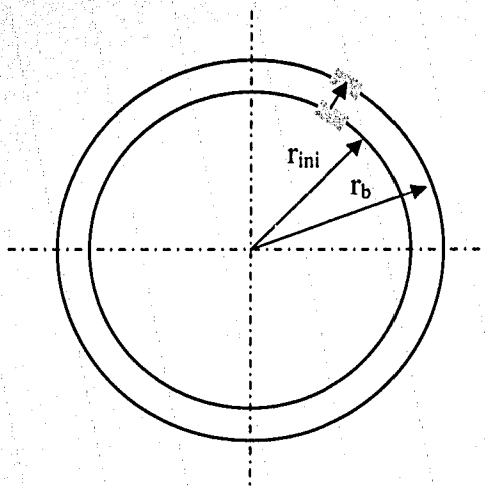


**Figure 4.2 Spherical Propagation Flame**      **Figure 4.3 Schematic Coordinates of an Element** [Chew et al. 1992]

In the radial (1) direction, the ratio of the kinetic energy due to the distortion effect is

$$\psi_1 = \zeta^{-3} s^{-2} \frac{3}{4} \left( \frac{e^2 - 1}{e^3} \tan^{-1} e + e^{-2} \right) . \quad 4.13$$

In the transverse (2 and 3) directions, the ratio of the kinetic energy is:

$$\psi_2 = \psi_3 = \frac{3}{4} \frac{s}{\zeta} + \frac{3}{8} \frac{1}{\zeta^5 s^5} \left( \frac{1}{e^3} \tan^{-1} e - \frac{1}{e^2(e^2 + 1)} \right) \quad 4.14$$

$$e = \sqrt{\frac{1}{\zeta^2 s^3} - 1} . \quad 4.15$$

Therefore, the total rapid distortion enhancement on turbulence intensity is

$$\frac{u'_{rd}}{u'_d} = \sqrt{\frac{\psi_1 + \psi_2 + \psi_3}{3}} \quad 4.16$$

where  $u'_{rd}$  is the turbulence intensity including the effects due to rapid distortion.  $u'_d$  represents the decaying turbulence intensity derived from decay model Eq.4.4. The value of time  $t$  during combustion is the time duration from the ignition to current flame

radius plus preset time. Unless otherwise described,  $u'$  during combustion in this study is the value of  $u'_{rd}$ , which is derived from Eq.4.16.

Applying ideal gas law,

$$\zeta = \left( \frac{P_u T_{ini}}{P_{ini} T_u} \right)^{-1}, \quad 4.17$$

where  $P_u$  and  $T_u$  are the current properties of the unburned mixtures corresponding to the current flame radius. The value of  $r_{ini}$  can be obtained from the thermodynamic model for each burned mass fraction. It is approximately 26 mm and 33 mm for  $r = 46$  mm and 55 mm, respectively. As the flame expands, the amplification factor of turbulence energy increases. For example, the amplification factor is 1.47 at  $r = 46$  mm and 1.67 at  $r = 55$  mm.

In contrast to the effect of rapid distortion on the turbulent intensity, the turbulent scales are relatively unaffected. The eddy volumes are not affected by distortion stretching, only by the change of bulk density with compression. It can be assumed that the decaying scales obtained from the decay model are only associated with the current density of unburned mixture as affected by pressure and temperature:

$$L = \zeta * L_d. \quad 4.18$$

$L_d$  is calculated from Eq.4.10. Unless otherwise stated, the length scale used in this study during combustion is determined from Eq.4.18. The detailed program code for calculation of turbulence intensity and scales with consideration of RDT based on the experimental condition at ignition time is given in Appendix C.

### 4.3 Calculation of Lewis Number and Markstein Number

To explore the turbulence influence on burning velocity of methane-air with EGR diluents, it is important to understand the Markstein number or Lewis number for these fuels. As was shown in Table 2.1, researchers have measured Markstein number for a number of mixtures, including hydrogen-air, methane-air and propane-air within a range of equivalence ratio. Bradley et al. [1996] also investigated Markstein number by a computational method. However, since it is not easy to obtain Markstein number, either theoretically or experimentally, discrepancies exist among the values. Markstein number for Methane-air with EGR and RG has not yet been reported in the literature. On the basis of the correlation between Markstein and Lewis numbers, an attempt was made to use a theoretical method to calculate the Markstein number for methane-air with EGR and RG. Clavin [1985] estimated the Markstein number using a single step reaction rate:

$$Ma = \frac{1}{\gamma} \ln\left(\frac{1}{1-\gamma}\right) + \frac{1}{2} \beta (Le - 1) \frac{1-\gamma}{\gamma} \int_0^{\gamma^{(1-\gamma)}} \frac{\ln(1+x)}{x} dx, \quad 4.19$$

$$\text{Where } \beta = \frac{T_a(T_{ad} - T_u)}{T_{ad}^2}, \quad 4.20$$

$$\gamma = \frac{T_{ad} - T_a}{T_{ad}}, \quad 4.21$$

$$T_a = \frac{E}{R}, \quad 4.22$$

The equation shows that for unity Lewis number mixtures,  $Ma = \frac{1}{\gamma} \ln\left(\frac{1}{1-\gamma}\right)$ . Over a wide range of mixtures,  $Ma$  is approximately linear with  $Le$ .

Table 4.2 summarized the calculated results for the tested mixtures. The activation energy of methane adopted from the Chemkin database [Westbrook 1984] was

employed for all the mixtures. The kinetic viscosity ( $\nu$ ) was derived by dynamic viscosity which was calculated using the Wilke's formula [Bird et al. 1964]. The mass diffusivity ( $D$ ) was taken to be the binary diffusion coefficient of fuel (methane) in nitrogen using the Chapman-Enskog kinetic theory [Bird et al. 1964]. The thermal conductivity ( $k$ ) was estimated by applying Eucken's semi-empirical equation [Bird et al. 1964]. The specific heat ( $C_p$ ) was approximated by the equation and NASA coefficients cited by Heywood [1988].

From Table 4.2, it seems that EGR decreases the thermal conductivity slightly and increases the specific heat capacity. These two points together result in decreasing the thermal diffusivity, so the Lewis number for methane-air/EGR mixtures is lower than methane-air. With increasing EGR concentration, the values of both Lewis number and Markstein number decreases. Tanoue [2003] studied the property of 15 % EGR diluents (15 %  $\text{CO}_2$  + 85 %  $\text{N}_2$ ), similar to current composition) in methane-air, the same trend was found as the present investigation.

From the last column of Table 4.2, a notable difference occurs when adding 11 % RG, which increases the thermal conductivity by 21.6 %. This gives rise to a more stable mixture with Lewis number larger than unity and a sharply higher Markstein number.

The calculated  $Le$  and  $Ma$  numbers can be compared with other researchers for the limited case of stoichiometric methane-air. Save for the slight difference, Lewis number agreed well with the values in Table 4.3. It should note that Renou et al. [2000] and Haq et al. [2002] gave different definition of Lewis number as "*the ratio of molecular diffusivity to thermal diffusivity*" and "*the ratio of the diffusivity of the deficient reactant into nitrogen to the thermal conductivity of the unburned mixture*",



respectively. This may be responsible for their Lewis number larger than unity. From Table 4.3, it showed that a significant difference for Markstein number existed in the studies. As discussed in Section 2.7.2, Bradley et al. [1996] derived  $Ma$  from a computation model with more complicated definition of Markstein number, while Aung et al. [1995] obtained  $Ma$  from experiments which are more applicable to explain the transition from stable to unstable flame. The fact that calculated value of  $Ma$  for stoichiometric methane-air is reasonably close to the experimental results implies that this calculation method is effective for current investigation.

In summary, for methane-air/EGR5 and EGR15, the Lewis and Markstein number stay close to that of methane-air. This similarity implies that the dilution level used here did not greatly alter the thermo-diffusive property of methane-air. However, adding RG can significantly increase Lewis and Markstein number.

**Table 4.2 Properties of Tested Mixtures**

	Methane-air	Methane-air/EGR5	Methane-air/ EGR15	Methane-air/EGR5/RG11
$\mu$ ( $\text{g}\cdot\text{cm}^{-1}\cdot\text{s}^{-1}$ ) $\times 10^{-6}$	171.9	171.8	171.7	170.6
$\nu$ ( $\text{mm}^2\cdot\text{s}^{-1}$ )	15.05	14.95	14.77	15.14
$\kappa$ ( $\text{cal}\cdot\text{s}^{-1}\cdot\text{cm}^{-1}\cdot\text{K}^{-1}$ ) $\times 10^{-5}$	6.0938	6.064	6.0052	7.411
$C_p$ ( $\text{cal}\cdot\text{mol}^{-1}\cdot\text{K}^{-1}$ )	7.1119	7.1215	7.141	7.1042
$\alpha$ ( $\text{mm}^2\cdot\text{s}^{-1}$ )	20.73	20.61	20.36	25.25
$D_{\text{CH}_4\text{-N}_2}$ ( $\text{mm}^2\cdot\text{s}^{-1}$ )	21.4	21.4	21.4	21.4
Le	0.97	0.96	0.95	1.18
Ma	1.97	1.85	1.5	4.47
$\delta_{\text{th}}$	0.061	0.736	0.135	0.0721
$\delta_{\text{d}}$	0.0443	0.0533	0.0985	0.0433
$\delta_{\text{m}}$	0.0629	0.0764	0.143	0.0611

All cases are in the temperature and pressure 296K and 1atm, respectively.

**Table 4.3 Comparison of *Ma* and *Le* for Stoichiometric Methane-air**

Le	[Renou et al. 2000]	[Haq et al. 2002]	[Smallwood et al. 1995]	This Study
	1.02	1.05	0.975	0.97
Ma	[Bradley et al. 1996]	[Gu et al. 2000]	Aung et al. [1995]	This Study
	3.85	4.2	1.3	1.97

## CHAPTER 5 RESULTS AND DISCUSSION

Experimental results of premixed turbulent burning velocity for methane-air diluted by 5 % and 15 % EGR, methane-air with 5 % EGR and 11 % RG as well as methane-air with equivalence ratio of unity are reported in this chapter. The detailed compositions of each type are listed in Table 3.1. All the mixtures were ignited at 1 atm and 23 °C. The turbulence test conditions were within the wrinkled flame regimes with turbulent Reynolds number in a range of 100 ~ 1300. The plate hole size of 20 mm leading to a 8 mm integral length scale at ignition time was only considered here.

The current turbulence was adjusted by the compression and distortion of the burned gas on the basis of the normal decay. Both the turbulent and quiescent burning velocity considered here were the instantaneous values at flame radii equal to 46 mm and 55 mm.

In order to establish a useful database of turbulent combustion for methane-air diluted by EGR and enriched by RG, the ever measured turbulent burning velocity was employed to correlate with turbulent intensity ( $u'$ ), turbulent strain rate ( $u'/\lambda$ ), product of Karlovitz strain factor and Lewis number ( $K_{as}Le$ ), Damköhler number ( $Da$ ), and Karlovitz number ( $Ka$ ). Some empirical correlations were obtained from the existing data. Comparing with relevant correlations based on some well-established database by other teams, the current results were examined. Also, Perters's [1999] model was used to assess the accuracy.

### 5.1 Experimental Results

Four different stoichiometric mixtures were studied: methane-air, methane-air/EGR5, methane-air/EGR15 and methane-air/EGR5/RG11. The stoichiometric methane-air mixtures was used here as a baseline for other mixtures. The methane-air/EGR5/RG11 was chosen for its nearly identical laminar burning velocity to methane-air, whereas it coupled the effect of EGR and RG.

The r.m.s turbulence intensity at ignition time was varied as follows: 0.26 m/s ~ 1.57 m/s for methane-air, 0.51 m/s ~ 2.46 m/s for methane-air/EGR5, 0.17 m/s ~ 2.55 m/s for methane-air/EGR15 and 0.59 m/s ~ 2.31 m/s for methane-air/EGR5/RG11.

The instantaneous quiescent burning velocity was used to normalize the turbulence burning velocity. The current test conditions of flame radius  $r = 46$  mm and  $r = 55$  mm for quiescent combustion are listed in Table 5.1.

**Table 5.1 Current Conditions and Burning Velocity of Quiescent Flames at  $r = 46$  mm and 55 mm**

		Methane-air	Methane-air/ EGR5	Methane-air/EGR15	Methane-air/EGR5/RG11
$S_{L0}$ (cm/s)		$34 \pm 0.8$	$26 \pm 0.6$	$15 \pm 0.3$	$35 \pm 0.6$
$r = 46$ mm	$T_u$ (K)	$320 \pm 1$	$319 \pm 1$	$317 \pm 1$	$319 \pm 1$
	$P_u$ (kPa)	$135 \pm 0.15$	$134 \pm 0.15$	$133 \pm 0.15$	$134 \pm 0.15$
	$S_L$ (cm/s)	$36 \pm 0.2$	$25 \pm 1.2$	$15 \pm 1.0$	$37 \pm 1.4$
$r = 55$ mm	$T_u$ (k)	$341 \pm 1$	$340 \pm 1$	$336 \pm 1$	$340 \pm 1$
	$P_u$ (kPa)	$171 \pm 0.15$	$170 \pm 0.15$	$167 \pm 0.15$	$170 \pm 0.15$
	$S_L$ (cm/s)	$37 \pm 0.6$	$29 \pm 0.6$	$17 \pm 0.7$	$38 \pm 0.4$

At ignition,  $P_{ini} = 101.30 \pm 0.15$  kPa,  $T_{ini} = 296 \pm 1$  K

### 5.1.1 Combustion Duration

Generally, combustion duration is an important controlling parameter in SI engine cycle. This makes it practically useful to investigate combustion duration. The combustion time,  $t_{max}$ , is defined as the time duration between ignition ( $t = 0$ ) and the time when the chamber pressure reached the maximum, representing how fast the fuel gases are burned out.

Table 5.2 lists the detailed experimental results as well as the relevant standard deviations for eight explosions of the four mixtures. Measurement uncertainties for combustion duration and the maximum pressure were within 5 %. Shown in Figure 5.1 were time-pressure traces obtained directly from the measurements of these eight explosions.

In quiescent flame cases, it was clearly shown that  $t_{max}$  increased with increasing concentration of EGR. Particularly  $t_{max}$  of methane-air/EGR15 was nearly 3 times longer than that of methane-air (marked as referenced value in Figure 5.1). On the other hand, adding 11 percent RG,  $t_{max}$  of methane-air/EGR5 was brought back to the reference value even without turbulence enhancement.

In turbulent flame cases, a moderate turbulence level of approx. 1 m/s was employed to illustrate the effect of turbulence. The combustion was intensified substantially by the turbulent flow motion which resulted in that the turbulent  $t_{max}$  of methane-air/EGR15 was even shorter than the reference value. In this case, there appeared to be an initial fairly slow rise in pressure with time, then followed by a sharp increase in the rate of

increasing pressure in later combustion stage. This meant the turbulence was less effective on the early stage flame growth for slower burning mixture and more effective as the flame expanded to a certain size. In other words, the turbulent combustion could effectively extend the tolerance limit of EGR in combustion engine by decreasing the combustion duration.

The double effect of turbulence and RG was demonstrated in the case of methane-air/EGR5/RG11. The corresponding combustion duration was comparable to that of methane-air in similar turbulent condition and only half of the reference value.

The difference of the highest chamber pressure between the methane-air and methane-air with diluents implied that the flame temperature decreased due to adding EGR. The CO<sub>2</sub> in EGR with high specific heat played an important role to decrease the flame temperature and thus the NO<sub>x</sub> emission. A concave point was observed just prior to the pressure reaching to the peak, especially in quiescent cases. This may be caused by the sharp drop of flame temperature while the flame hit the chamber wall completely.

**Table 5.2 Summary of Experimental Results for Quiescent and Turbulent Combustion**

	Methane-air	Methane-air/ EGR5	Methane- air/EGR15	Methane-air/ EGR5/RG11
Quiescent Combustion ( $u' = 0$ )				
$t_{\max}$ (ms)	56.4	78.7	144	58.3
Std Deviation	2.5	4.3	1.4	0.9

**Table 5.2 (Cont'd)**

	Methane-air	Methane-air/ EGR5	Methane- air/EGR15	Methane-air/ EGR5/RG11
$P_{\max}$ (kPa)	766.8	735.0	642.0	731.5
Std Deviation	5.7	4.4	1.8	1.7
$df_b/dt$ at $r = 46$ mm	5.87	4.87	2.6	6.45
Std Deviation (1/s)	0.26	0.53	0.21	0.26
$df_b/dt$ at $r = 55$ mm	10.78	8.45	4.94	10.99
Std Deviation (1/s)	0.16	0.18	0.08	0.17
<b>Turbulent Combustion</b>				
$u'_{ig}$ (m/s)	0.93	1	1.28	1.1
$t_{\max}$ (ms)	26.0	32.2	47.7	26.0
Std Deviation	0.1	0.3	1.5	0.8
$P_{\max}$ (kPa)	829.5	799.3	738.0	799.0
Std Deviation	3.5	2.1	7.5	6.8
$df_b/dt$ at $r = 46$ mm	13.89	11.95	9.20	15.34
Std Deviation (1/s)	0.35	0.39	0.80	0.38
$df_b/dt$ at $r = 55$ mm	26.15	22.7	17.74	28.31
Std Deviation (1/s)	1.01	0.27	0.65	0.47



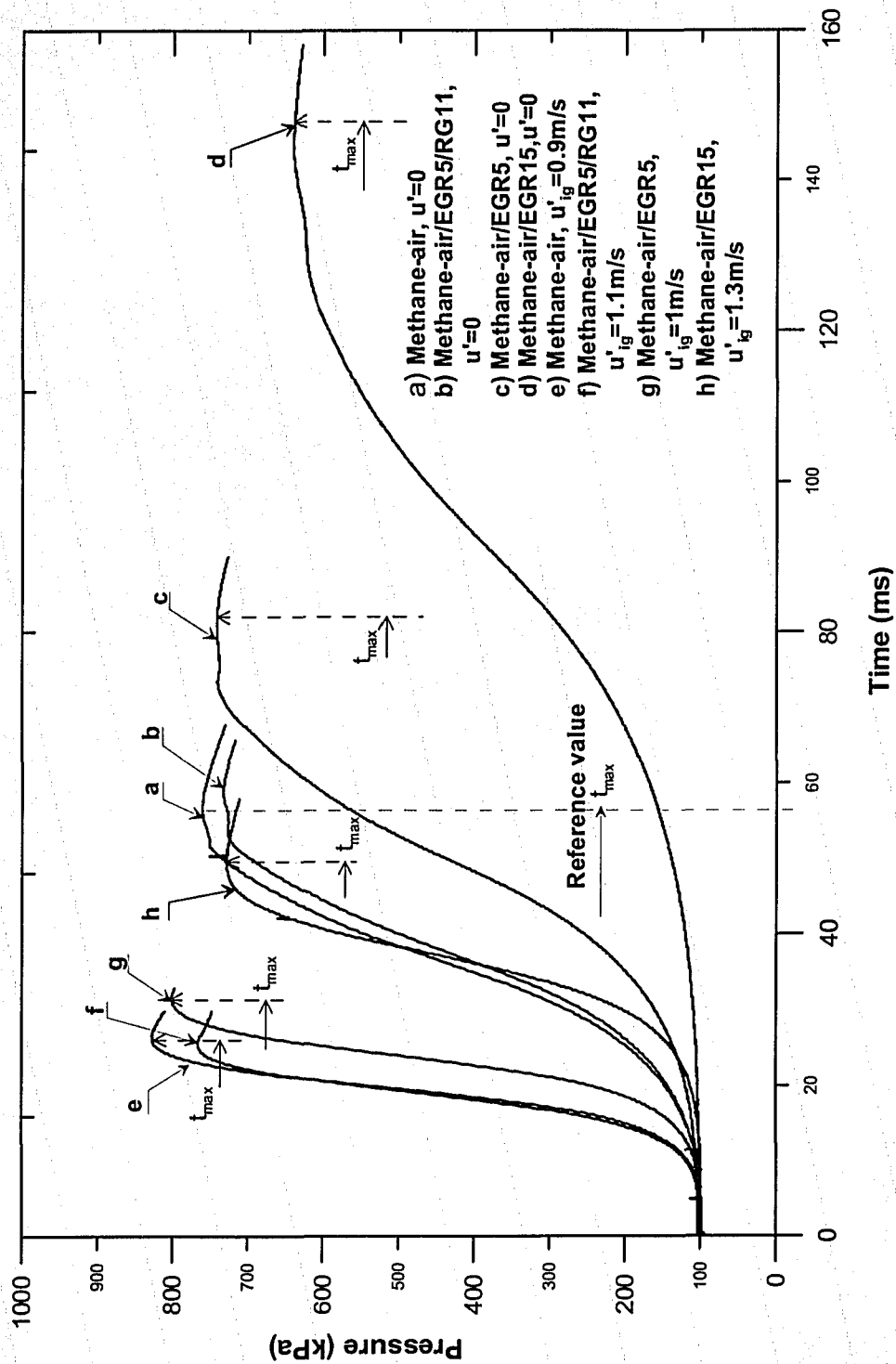


Figure 5.1 Comparisons of Pressure Trace

### 5.1.2 Rate of Burned Mass Fraction

Shown in Figure 5.2 for the same explosions as in Figure 5.1 were the variations of burned mass fraction rate with the flame radii. The detailed experiment data was given in Table 5.2. The measurement uncertainty of burned gas fraction rate was within 9 % for flame radius  $r = 46$  mm and 4 % for  $r = 55$  mm. These curves demonstrated the fundamental measurements of this study in terms of unburned gas consumption rate corresponding to pressure trace.

By definition [Andrews, et al. 1972], the unburned mass consumption rate can be expressed as

$$\dot{m}_u = \frac{dm_u}{dt} = -\rho_u A S_L, \quad 5.1$$

where  $\rho_u$  is the density of unburned gas,  $A$  the flame surface area,  $m_u$  the mass of unburned gas,  $m_u = m_{tot} - m_b$ ,  $m_{tot}$  the mass of total mixture,  $m_b$  the mass of burned gas.

Combining with mass conservation during combustion in the constant volume,  $S_L$  can be represented by

$$S_L = \dot{m}_b \frac{1}{\rho_u A}. \quad 5.2$$

Also,  $m_b = f_b m_{tot}$  and  $v_{tot} = \frac{m_{tot}}{\rho_{ini}}$ , where  $f_b$  is the burned mass fraction and  $v_{tot}$  is the

chamber volume,  $\rho_{ini}$  the density at initial state, so

$$S_L = \frac{v_{tot}}{A} \frac{\rho_{ini}}{\rho_u} \frac{df_b}{dt}. \quad 5.3$$

Due to the similarity of thermodynamic properties among the tested mixtures, at the same flame radii, the value of term  $\frac{v_{tot} \rho_{ini}}{A \rho_u}$  was close. Therefore the burning rate was primarily determined by  $\frac{df_b}{dt}$ .

In the turbulence conditions, the laminar flamelet structure of the turbulent flame supported the assumption that the flame propagated with the same mean spherical shape as the relevant quiescent flame at the same pressure. The turbulence enhancement contributed to the flame surface wrinkling, so the burning rate increased with increasing flame surface area. Consequently, the turbulent flame radius was a mean value equivalent to that of the quiescent flame under the same chamber pressure.

These plots clearly showed that the progressively increasing rate of the mass fraction rate as the turbulent flames developed. In contrast, the slopes of quiescent flames were much flatter. For the same flame radii, the notable difference of burned mass fraction rate between the turbulent and quiescent conditions illustrated the intensified effect of turbulence on combustion. It could be seen in the example of methane-air/EGR15 that even without adding reformer gas, not only could the typical turbulent motion restore the reduced burning rate, but also the turbulent burning rate was much higher than that of the referenced methane-air.

Again, taking account of the effect of RG, the burned gas fraction rate of methane-air/EGR5/RG11 increased nearly 3 times faster than that of the referenced quiescent flame of methane-air at both flame radiuses of 46 mm and 55 mm as marked in the plot.

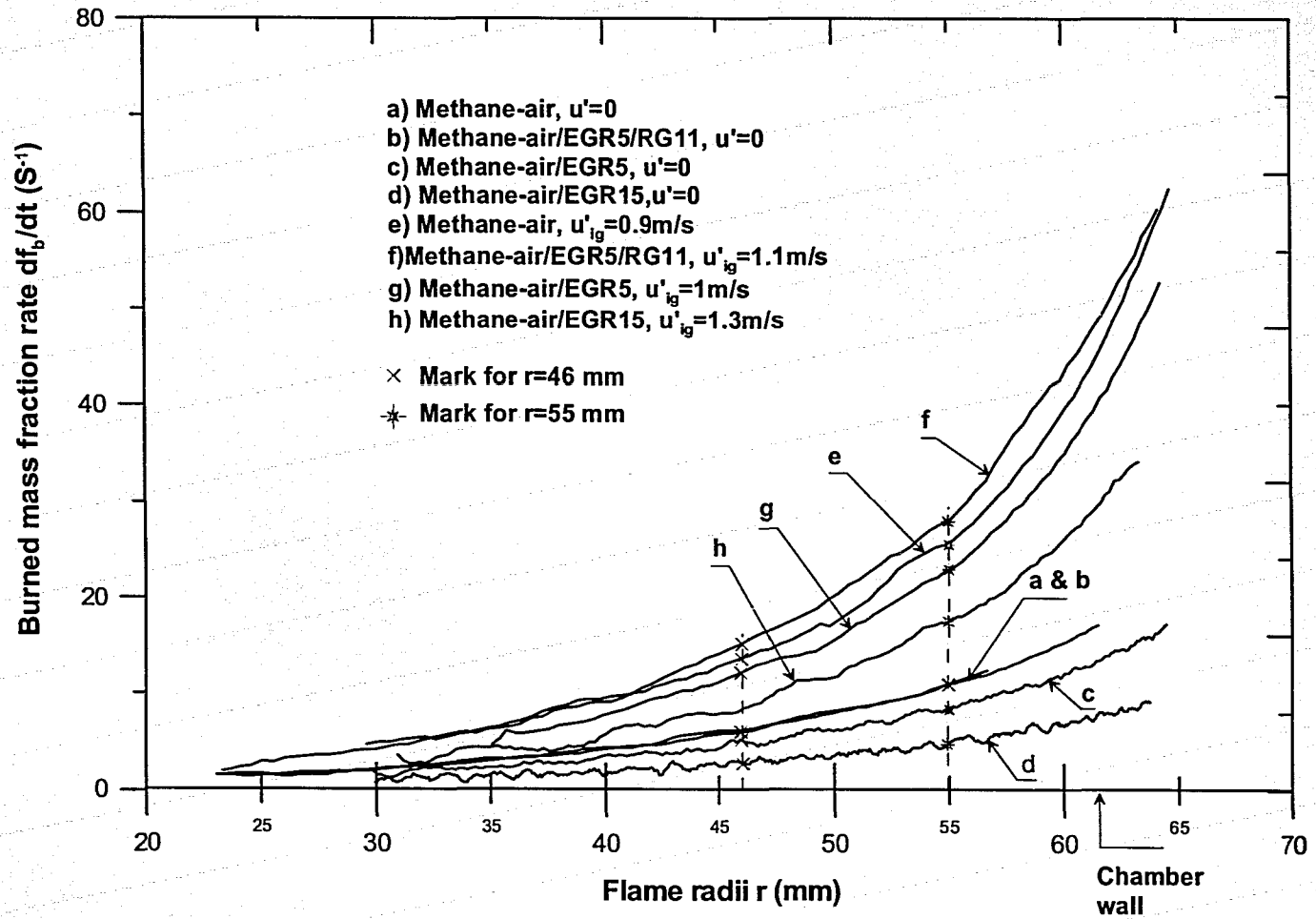


Figure 5.2 Comparisons of Burned Mass Fraction

The large uncertainty of the mass burning rate was observed at early stage of flame expansion. The explanation lay in the fact that the noise was high compared with pressure signal at this stage. Only at the flame ball greater than 45 mm in radius could the noise disturbance be negligible. Especially the burning rate was more stable at flame radii  $r = 55$  mm. The chamber wall position ( $r = 62.5$  mm) was also marked in the plot.

## 5.2 Correlations of Turbulent Burning Velocity

Tables 5.3-5.10 are summaries of detailed turbulent test conditions and experimental results for the mixtures currently investigated. All the data in this table were average transient values of three to five runs at certain flame radius, e.g.  $r = 46$  mm and 55mm. The relevant standard deviation of turbulent burning velocity was also listed in the tables. The measurement uncertainty of  $St$  is within 7 % at  $r = 46$  mm and 4 % at  $r = 55$  mm.

In these tables,  $u'$  and  $L$  are derived from Eq.4.16 and 4.18 respectively with taking account of the compression effect of burned gas. Kolmogorov length scale ( $\eta$ ) was calculated from Eq.2.6 with  $a_1 = 1$  and used to define the turbulent combustion regimes for this investigation.  $St$  was instantaneous turbulent burning velocity derived from monitored pressure trace. Taylor microscale,  $\lambda$ , was determined by Kido's model (see Eq.2.12) which was employed to obtain turbulence strain rate. Flame thickness

$\delta$  here was identical to  $\delta_d$  (see Eq.2.26), specially  $\delta = \frac{v_u}{S_L}$ .

For  $u'$  and  $L$ , the measurement error was dependent on the preset delay time and measurement variability of plate speed. After calibrating the digital delay generator by

Digital Phosphor Oscilloscope TD3014B with 100MHz, the error magnitude of the delay time is proved as  $10^{-8}$ , so the uncertainty from delay time can be negligible. The measurement variability of plate speed was controlled within  $\pm 3\%$  by repeating experiments. Therefore, the error in  $u'$  and  $L$  measurement was  $\pm 3\%$  as well as  $\eta$  and  $\lambda$  through analyzing the systematic error.

**Table 5.3 Turbulent Experimental Conditions and Results for Methane-Air at** **$r = 46 \text{ mm}$** 

<b><math>T_u = 320 \text{ K}, P_u = 135 \text{ kPa}, S_L = 37 \text{ cm/s}, \nu_u = 12.9 \text{ mm}^2/\text{s}, \delta = 0.036 \text{ mm}</math></b>									
$u'_{ig} \text{ (m/s)}$	$u' \text{ (m/s)}$	$L \text{ (mm)}$	$\eta \text{ (mm)}$	$\lambda \text{ (mm)}$	$R_L$	$Da$	$Ka$	St and Std Deviation (cm/s)	
0.26	0.33	6.85	0.142	2.5	175	208	0.064	47	1.7
0.48	0.55	6.85	0.097	2.2	292	125	0.137	59	1.5
0.94	0.98	6.85	0.063	2.0	520	70	0.326	81	0.5
1.20	1.13	6.85	0.057	1.9	600	61	0.403	84	1.0
1.57	1.42	7.49	0.049	2	824	53	0.543	98	3.1

**Table 5.4 Turbulent Experimental Conditions and Results for Methane-Air/EGR5****at  $r = 46 \text{ mm}$** 

<b><math>T_u = 319 \text{ K}, P_u = 134 \text{ kPa}, S_L = 25 \text{ cm/s}, \nu_u = 12.8 \text{ mm}^2/\text{s}, \delta = 0.051 \text{ mm}</math></b>									
$u'_{ig} \text{ (m/s)}$	$u' \text{ (m/s)}$	$L \text{ (mm)}$	$\eta \text{ (mm)}$	$\lambda \text{ (mm)}$	$R_L$	$Da$	$Ka$	St and Std Deviation (cm/s)	
0.51	0.55	6.87	0.096	2.2	295	61	0.281	50	2.5
1.00	0.93	7.30	0.066	2.1	530	38	0.600	69	1.7
1.60	1.32	7.42	0.051	2.0	765	28	1.006	89	6.0
1.95	1.54	7.84	0.046	2.0	943	25	1.233	93	2.0
2.46	1.76	8.09	0.042	2.0	1112	22	1.483	111	8.0

**Table 5.5 Turbulent Experimental Conditions and Results for Methane-Air/EGR15 at  $r = 46$  mm**

$T_u = 317$ K, $P_u = 133$ kPa, $S_L = 15$ cm/s, $v_u = 12.6$ mm <sup>2</sup> /s, $\delta = 0.084$ mm									
$u'_{ig}$ (m/s)	$u'$ (m/s)	L (mm)	$\eta$ (mm)	$\lambda$ (mm)	$R_L$	Da	Ka	St and Std Deviation (cm/s)	
0.17	0.19	6.86	0.211	2.7	103	64	0.158	19	2.0
0.48	0.43	7.84	0.119	2.6	268	33	0.502	31	2.1
0.88	0.64	7.9	0.088	2.4	401	22	0.909	41	1.5
1.28	0.85	8.3	0.072	2.4	560	17	1.357	54	3.5
1.74	1.08	8.9	0.061	2.4	763	15	1.877	61	3.8
2.55	1.23	8.00	0.054	2.1	781	12	2.406	69	3.5

**Table 5.6 Turbulent Experimental Conditions and Results for Methane-Air/EGR5/RG11 at  $r = 46$  mm**

$T_u = 319$ K, $P_u = 134$ kPa, $S_L = 37$ cm/s, $v_u = 13.7$ mm <sup>2</sup> /s, $\delta = 0.037$ mm									
$u'_{ig}$ (m/s)	$u'$ (m/s)	L(mm)	$\eta$ (mm)	$\lambda$ (mm)	$R_L$	Da	Ka	St and Std Deviation (cm/s)	
0.59	0.60	6.87	0.095	2.2	301	114	0.152	61	1
0.87	0.84	6.87	0.074	2.1	421	82	0.251	76	2.1
1.13	1.05	6.87	0.063	2.0	527	65	0.351	89	1.5
1.53	1.29	6.87	0.054	1.9	647	53	0.478	95	1.7
1.83	1.51	6.87	0.048	1.8	757	45	0.605	111	2.0



**Table 5.6 (Cont'd)**

<b><math>T_u = 319 \text{ K}, P_u = 134 \text{ kPa}, S_L = 37 \text{ cm/s}, \nu_u = 13.7 \text{ mm}^2/\text{s}, \delta = 0.037 \text{ mm}</math></b>									
$u'_{ig}$ (m/s)	$u'$ (m/s)	L(mm)	$\eta$ (mm)	$\lambda$ (mm)	$R_L$	Da	Ka	St and Std Deviation (cm/s)	
2.15	1.69	6.87	0.044	1.8	847	41	0.716	112	0.6
2.31	1.81	6.87	0.042	1.8	908	38	0.794	120	3.0

**Table 5.7 Turbulent Experimental Conditions and Results for Methane-Air at  $r = 55 \text{ mm}$**

<b><math>T_u = 341\text{K}, P_u = 171 \text{ kPa}, S_L = 38 \text{ cm/s}, \nu_u = 11.3 \text{ mm}^2/\text{s}, \delta = 0.037 \text{ mm}</math></b>									
$u'_{ig}$ (m/s)	$u'$ (m/s)	L (mm)	$\eta$ (mm)	$\lambda$ (mm)	$R_L$	Da	Ka	St and Std Deviation (cm/s)	
0.26	0.37	6.28	0.116	1.7	206	206	0.070	52	0.6
0.48	0.61	6.28	0.079	1.3	339	125	0.148	66	0.0
0.94	1.06	6.28	0.053	1.0	589	72	0.338	89	1.0
1.20	1.24	6.28	0.047	0.9	689	61	0.428	98	0.0
1.57	1.51	7.10	0.042	0.9	949	57	0.541	112	1.5

**Table 5.8 Turbulent Experimental Conditions and Results for Methane-Air/EGR5**at  $r = 55$  mm

$T_u = 340$ K, $P_u = 170$ kPa, $S_L = 29$ cm/s, $\nu_u = 11.3$ mm <sup>2</sup> /s, $\delta = 0.037$ mm									
$u'_{ig}$ (m/s)	$u'$ (m/s)	L (mm)	$\eta$ (mm)	$\lambda$ (mm)	$R_L$	Da	Ka	St and Std Deviation (cm/s)	
0.51	0.60	6.37	0.081	2.2	338	79	0.233	57	0.6
1.00	1.01	6.86	0.056	1.8	613	51	0.490	79	1.0
1.60	1.41	6.99	0.044	1.5	872	37	0.800	98	2.0
1.95	1.65	7.40	0.039	1.4	1081	33	0.985	114	1.5
2.46	1.92	7.65	0.035	1.4	1300	30	1.216	124	1.7

**Table 5.9 Turbulent Experimental Conditions and Results for Methane-air /EGR15 at  $r = 55$  mm**

$T_u = 336$ K, $P_u = 167$ kPa, $S_L = 17$ cm/s, $\nu_u = 11.1$ mm <sup>2</sup> /s, $\delta = 0.065$ mm									
$u'_{ig}$ (m/s)	$u'$ (m/s)	L (mm)	$\eta$ (mm)	$\lambda$ (mm)	$R_L$	Da	Ka	St and Std Deviation (cm/s)	
0.17	0.21	6.3	0.175	2.2	119	78	0.140	23	0.5
0.48	0.46	7.41	0.101	1.6	307	42	0.418	38	1.5
0.88	0.68	7.54	0.076	1.4	462	29	0.744	52	2
1.28	0.93	7.83	0.060	1.2	656	22	1.168	61	0.5
1.74	1.17	8.45	0.052	1.1	891	19	1.587	71	1.5
2.55	1.25	7.90	0.048	1.0	890	16	1.813	78	2.1

**Table 5.10 Turbulent Experimental Conditions and Results for Methane-Air/EGR5/RG11 at  $r = 55$  mm**

$T_u = 340$ K, $P_u = 170$ kPa, $S_L = 38$ cm/s, $v_u = 11.4$ mm <sup>2</sup> /s, $\delta = 0.03$ mm									
$u'_{ig}$ (m/s)	$u'$ (m/s)	$L$ (mm)	$\eta$ (mm)	$\lambda$ (mm)	$R_L$	$Da$	$Ka$	St and Std Deviation (cm/s)	
0.59	0.65	6.29	0.076	1.3	359	123	0.155	67	2.3
0.87	0.92	6.29	0.059	1.1	508	87	0.260	85	1.5
1.13	1.15	6.29	0.050	1.0	635	69	0.364	98	2.3
1.53	1.40	6.29	0.043	0.9	772	57	0.488	108	2.5
1.83	1.65	6.29	0.038	0.8	910	48	0.625	125	1.7
2.15	1.81	6.29	0.035	0.8	999	44	0.718	128	3.1
2.31	1.94	6.33	0.034	0.7	1077	41	0.794	138	2.1

Note: The data are the average values of three to five runs at the same test conditions.

### 5.2.1 With Turbulent Intensity

As shown in Figures 5.3 - 5.7 were a group of plots of turbulent burning velocity as a function of turbulent intensity for the four mixtures as outlined earlier. The turbulence enhancement on burning velocity at different flame radius, namely 46 mm and 55 mm, were illustrated by the linear fit approach  $\frac{S_t}{S_L} = a_{11}(\frac{u'}{S_L}) + a_{12}$  and the coefficient of determination  $C^2$ . The slope " $a_{11}$ " of the straight line characterized the intensified effect

by the turbulence.  $a_{12}$  represented the extent of deviation from the corresponding quiescent burning velocity ( $u'=0$ ).

The measurement uncertainty for each point is shown in Figure 5.3 as error bars at  $\pm 1$  standard deviations for repeated experiments. It clearly showed the level of confidence in the accuracy of flame radius  $r = 55$  mm is much higher than that of flame radius  $r = 46$  mm. This is attributed to the pressure noise disturbance in the early stage of flame growth. In addition, by calculating the student t - test for the slopes of these two sets of data at  $r = 46$  mm and 55 mm for methane-air, the statistic difference between the two sample slopes is 1.481 which led to a 18 % probability that they were from the same population. In other words, the effect of turbulence on flame is significantly increasing as the flame develops.

Introducing the wrinkled flamelet theory, the wrinkled flame surface can be treated as a smooth sphere with a surface area,  $A_L$ , distorted by the turbulent flow. The turbulent flame surface area,  $A_t$ , can be expressed as the sum of  $A_L$  and an excess flame area  $A_{ex}$ . [Ashurst et al. 1994]. A sequent expression:

$$\frac{S_t}{S_L} - 1 = \frac{A_{ex}}{A_L} \quad 5.4$$

derived from Eq.2.30 combined with the present linear relation  $\frac{S_t}{S_L} - 1 = a_{11} \frac{u'}{S_L}$ ,

producing the following equation:

$$\frac{A_{ex}}{A_L} = a_{11} \frac{u'}{S_L} \quad 5.5$$

The ratio of  $A_{ex}/A_L$  represented the degree of the flame wrinkling such that the higher value of the ratio, the more intensive wrinkling effect of turbulence.

From the plots, an apparent trend was observed that the linear coefficients of  $r = 55$  mm were about 1.2 times larger than those of  $r = 46$  mm for all the mixtures investigated. In other words, the flame wrinkling was progressively intensified as the flame expanded. This observation was thoroughly confirmed by the flame visualization [Haq et al. 2001, Kwon et al. 1992A], that the flame surface distortion increased with mean flame radius, accordingly the increasing rate of  $S_f/S_L$  increased as  $u'/S_L$  increased. The results demonstrated a developing period of flame growth within the reach of present measurements. Extending to the application in SI engines where the combustion was confined in a chamber with limited volume, it was impossible for the flame to reach steady state. This made the present study of developing flame more reasonable than developed flame for SI engines.

It should be pointed out that the intercept values of " $a_{12}$ " were negative for all the full line curves regardless of zero expected. Particularly for methane-air/EGR15, the curve deviated from the origin at a large value, e.g.,  $a_{12} = -0.3$  at  $r = 46$  mm and  $a_{12} = -0.16$  at  $r = 55$ mm. This was probably associated with over estimating the turbulence intensity for the developing flame by rapid distortion theory. In slower burning case, the turbulence did have time to decay comparing with the fast burning condition. Thus the error of turbulence intensity estimated by RDT was obvious for weak mixtures. Ting et al. [1994] suggested that the actual  $u'$  should fall between the values estimated by normal decay and RDT. Regardless of this discrepancy, the striking consistency of the measurement for all various mixtures demonstrated that a strong linear relation lay in between  $S_f/S_L - 1$  and  $u'/S_L$  as well as  $A_{ex}/A_L$  and  $u'/S_L$ . Here it was worth mentioning that this linear relationship was only applicable for developing flames. The "bending effect"

of  $u'$  on burning velocity was found for fully developed flames [Abdel-Gayed et al. 1981].

The comparisons of the linear coefficients at  $r = 55$  mm for the four tested mixtures showed that the turbulence effect on burning velocity increased with increasing the quiescent burning velocity  $S_L$ . For instance, the smallest  $S_L$  for methane-air/EGR15 at  $r = 55$  mm was 17 cm/s, so the smallest slope of 0.51 was obtained. On the other hand, the largest  $S_L$  for methane-air/EGR5/RG11 was 38 cm/s, so the largest slope of 0.57 was given. No evident similar trend was found at  $r = 46$  mm.

However, according to the aforementioned influence of Markstein number upon the flame, it was anticipated that the wrinkling effect should be more effective for the mixture with the lower Markstein number. This meant the " $a_{11}$ " of methane-air/EGR15 should be the biggest due to its smallest Ma in spite of the actual smallest one obtained. Similarly, the highest Markstein number occurred in methane-air/EGR5/RG11, so the flattest slope was expected. However, the opposite trend was observed.

The primary source of error in the measurements was likely associated with overestimating  $u'$  for slower burning flames. This gave rise to lower linear coefficient than actual value for methane-air/EGR15. But this explanation was not applicable to methane-air/EGR5/RG11 which had comparable quiescent burning velocity and much higher Ma than that of methane-air. The lower value of " $a_{11}$ " than that of methane-air was expected, but both values were close. Therefore this assumption can not sufficiently explain the observed discrepancy.

On the other hand, all the Markstein numbers of the mixtures were positive and close except for methane-air/EGR5/RG11 with much higher values. The similarity might

obscure the flame sensitivity to the influence of the turbulence stretch due to the systemic discrepancy of the experiments. Haq et al. [2002] investigated the curvature PDFs for lean and stoichiometric methane-air. Little difference was found in the same moderate turbulence condition, despite much lower Markstein number appeared in lean methane-air. Also, Ting et al. [1994] did not find the difference between methane-air at equivalence ratio of 0.7 and 0.9 using the same method as the present experiments. Bradley et al. [2003B] suggested that the influence of Ma was partially dependent on the range of turbulent Reynolds number  $R_L$ . At low values of  $R_L$ , namely  $R_L < 100$ , turbulence was more effective to wrinkle the flamelet and hence the turbulent burning velocity. The current  $R_L$  over a range of 100 ~1300 was beyond this bound. This appeared to explain the observed phenomenon. In general, in the regimes investigated, it seemed that the quiescent flame property was relatively important for the flame growth, while the influence of Ma was weak to affect the burning rate.

Regardless of the little difference among the slopes of the straight lines, the consistency of the data for the four mixtures made it possible assemble all the data shown in Figure

5.7, the best linear relationship was found to be :  $\frac{S_t}{S_L} - 1 \approx 0.55 \frac{u'}{S_L}$  for  $r = 55\text{mm}$  and

$\frac{S_t}{S_L} - 1 \approx 0.46 \frac{u'}{S_L}$  for  $r = 46\text{mm}$ . Corresponding to the Eq.2.56,  $a_6$  is unity,  $a_5$  equals to

0.55 and 0.46 for  $r = 46$  and  $55$  mm, respectively.

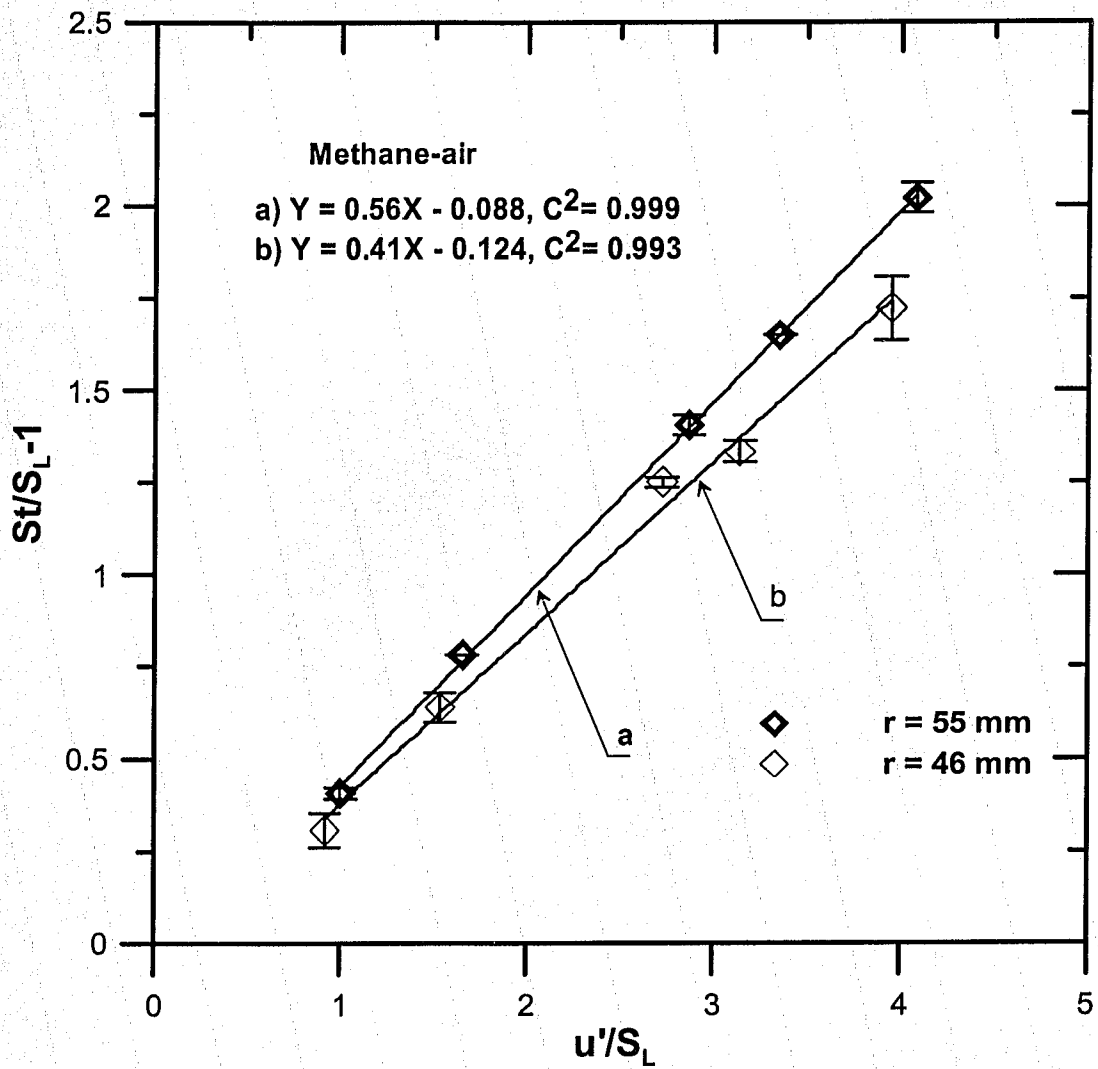


**Figure 5.3 Turbulent Burning Velocity as a Function of Turbulent Intensity and Flame Radius  $r$  for Methane-air.** (The error bar represents  $\pm 1$  standard deviation for repeated measurements at each point.)



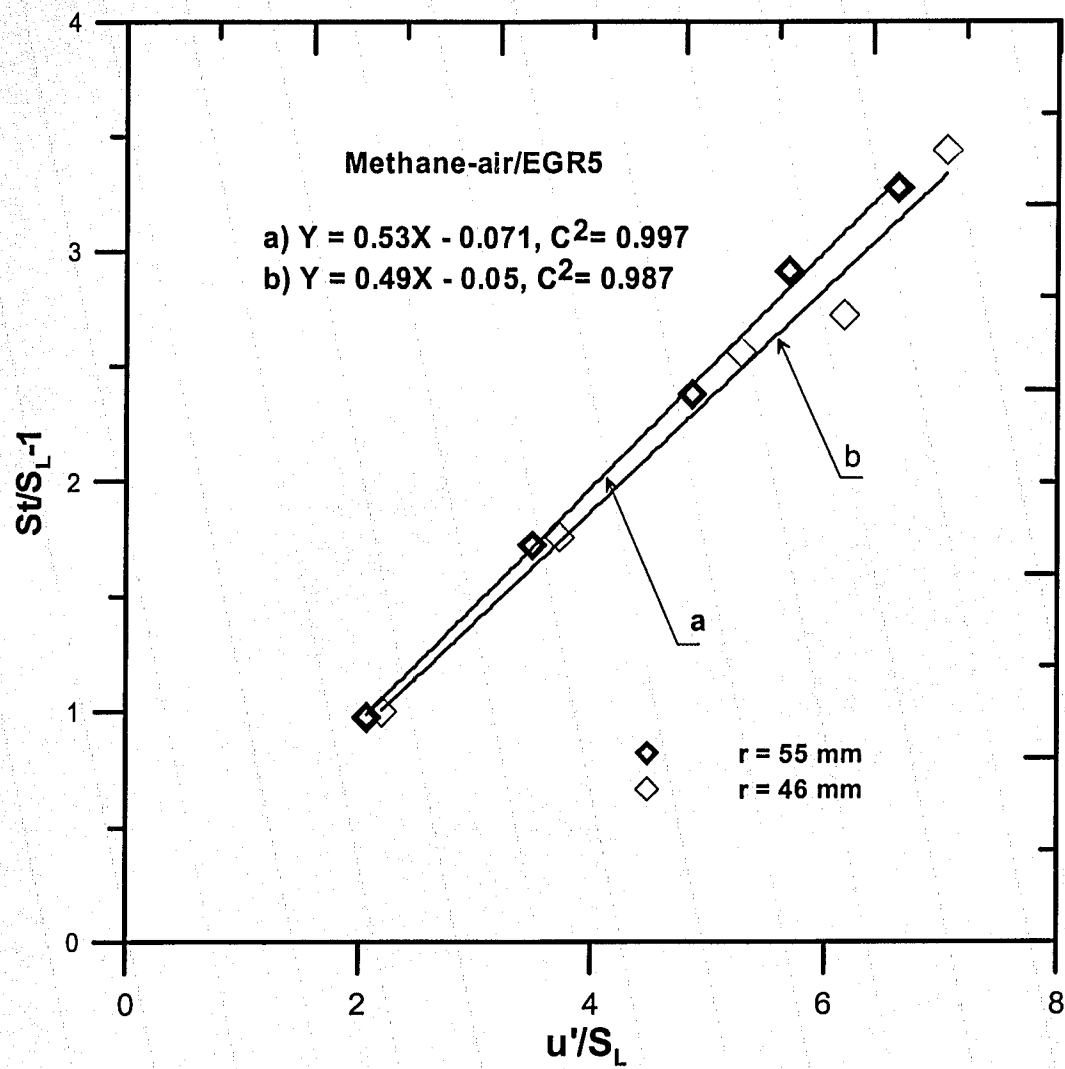


**Figure 5.4 Turbulent Burning Velocity as a Function of Turbulent Intensity and Flame Radius  $r$  for Methane-air/EGR5**

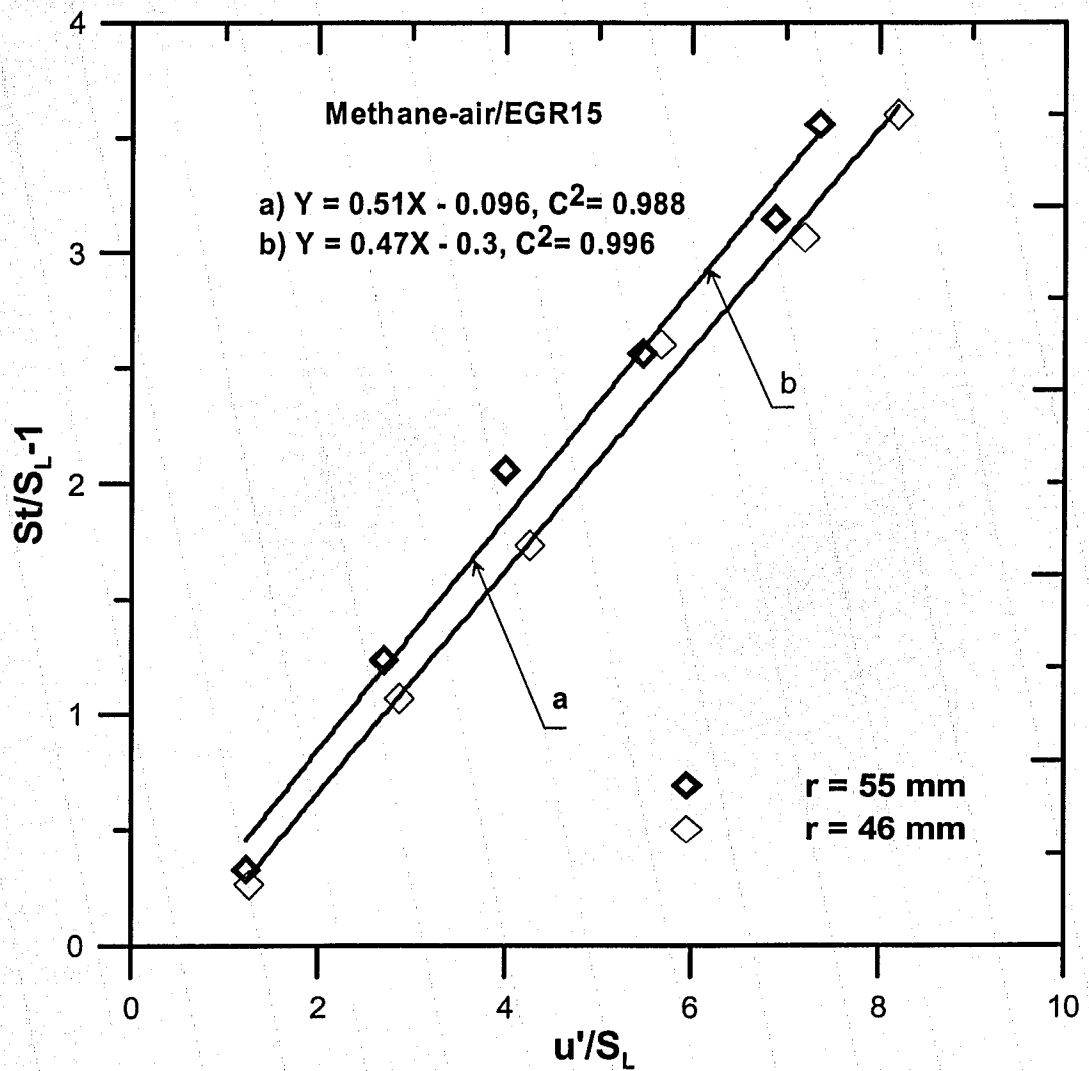


**Figure 5.5 Turbulent Burning Velocity as a Function of Turbulent Intensity and Flame Radius  $r$  for Methane-air/EGR15**

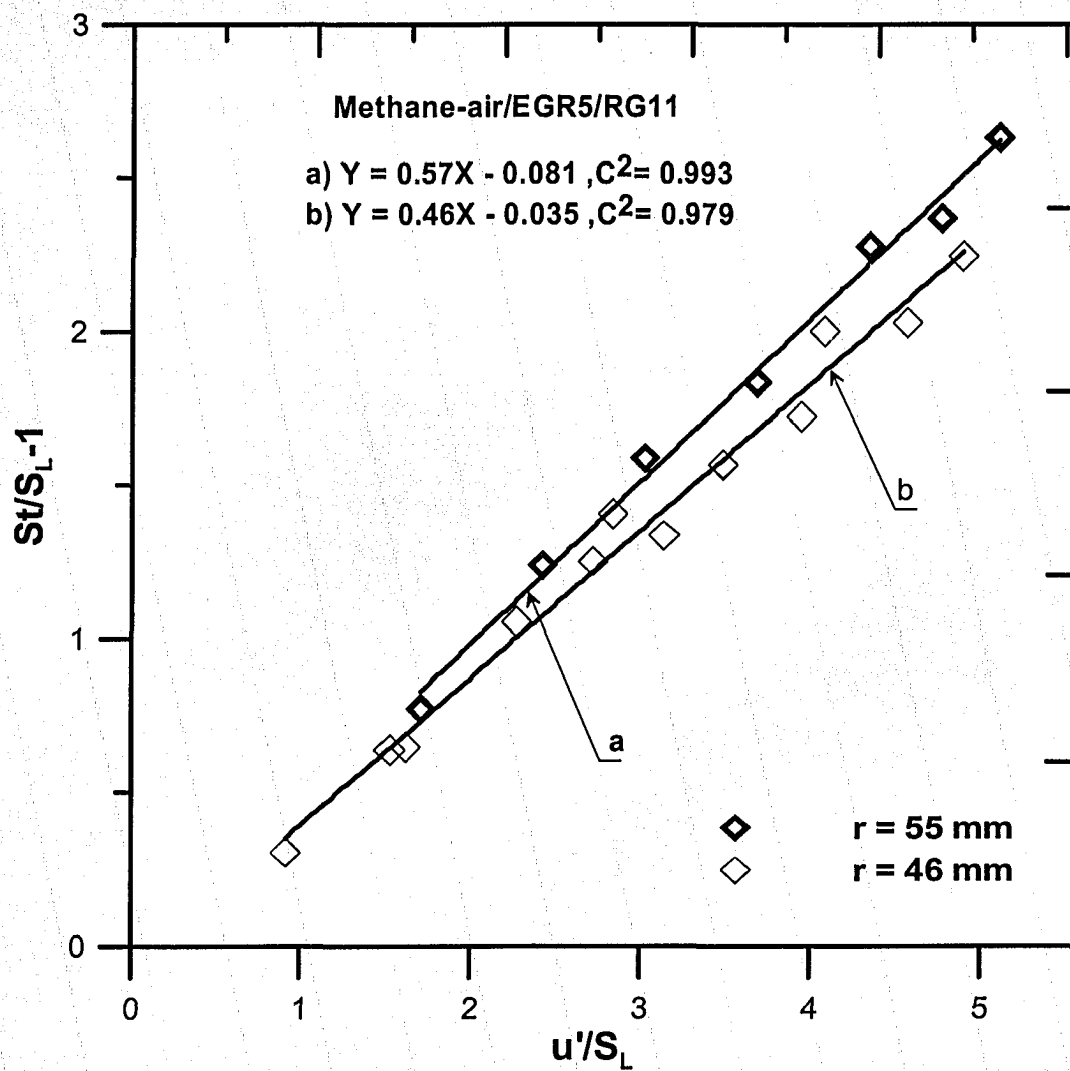


**Figure 5.6 Turbulent Burning Velocity as a Function of Turbulent Intensity and Flame Radius  $r$  for Methane-air/EGR5/RG11**

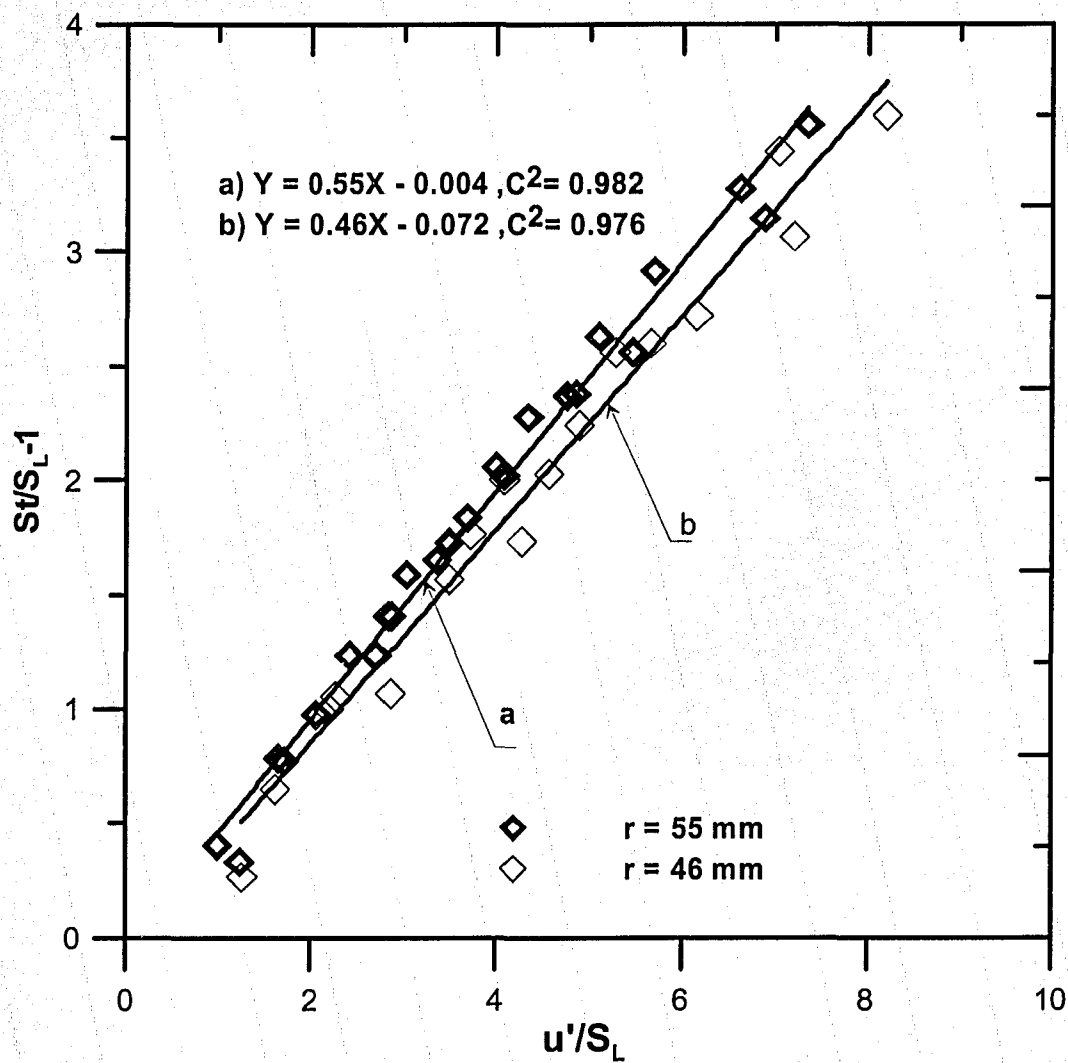


**Figure 5.7 Summary of Turbulent Burning Velocity as a Function of Turbulent Intensity and Flame Radius  $r$  for All Mixtures**

## 5.2.2 With Turbulent Strain Rate

In the laminar flame case, the strain rate can affect the burning rate substantially at early stage of the flame propagation. Furthermore, it was found that the strain effect was dependent on the Markstein number of the mixtures that were detailed in section 2.7.2. In turbulent flame case, the stretch rate was the sum of laminar stretch rate and turbulence strain rate as expressed in Eq.2.50. On the basis of this expression, the stretch rate of laminar flame was a function of flame radius and flame speed. However, this study was focusing on the developing flame at radius of  $r = 46$  mm and  $55$  mm, where the laminar flame stretch rate was relative small compared to the turbulent strain rate [Clark et al. 1995]. As a result, the turbulence strain rate was the only determinant strain effect on the flame propagation.

Since Taylor microscale,  $\lambda$ , can not be measured directly from the experiment, the question rose to assign a proper value of  $\lambda$ . Corresponding to present experimental condition where the turbulence was decaying by the nature of viscous dissipation, and on the other hand was being intensified by the compression of burned gas during the flame propagation, Ting et al. [2001] argued that Kido's [1980] model was more appropriate for the present test conditions. In Kido's [1980] model, the turbulence was studied in a constant volume chamber during compression stroke. Therefore, Eq.2.13 was adopted in this study, and the calculated results were listed in Tables 5.3 ~ 5.10.

Shown in Figures 5.8 and 5.9 were the turbulent burning velocity  $S_t$  plotted against the mean turbulent strain rate  $u''/\lambda$  at flame radii of  $r = 46$  mm and  $r = 55$  mm, respectively. The linear fits were used to show the enhancement extent of turbulent strain rate on

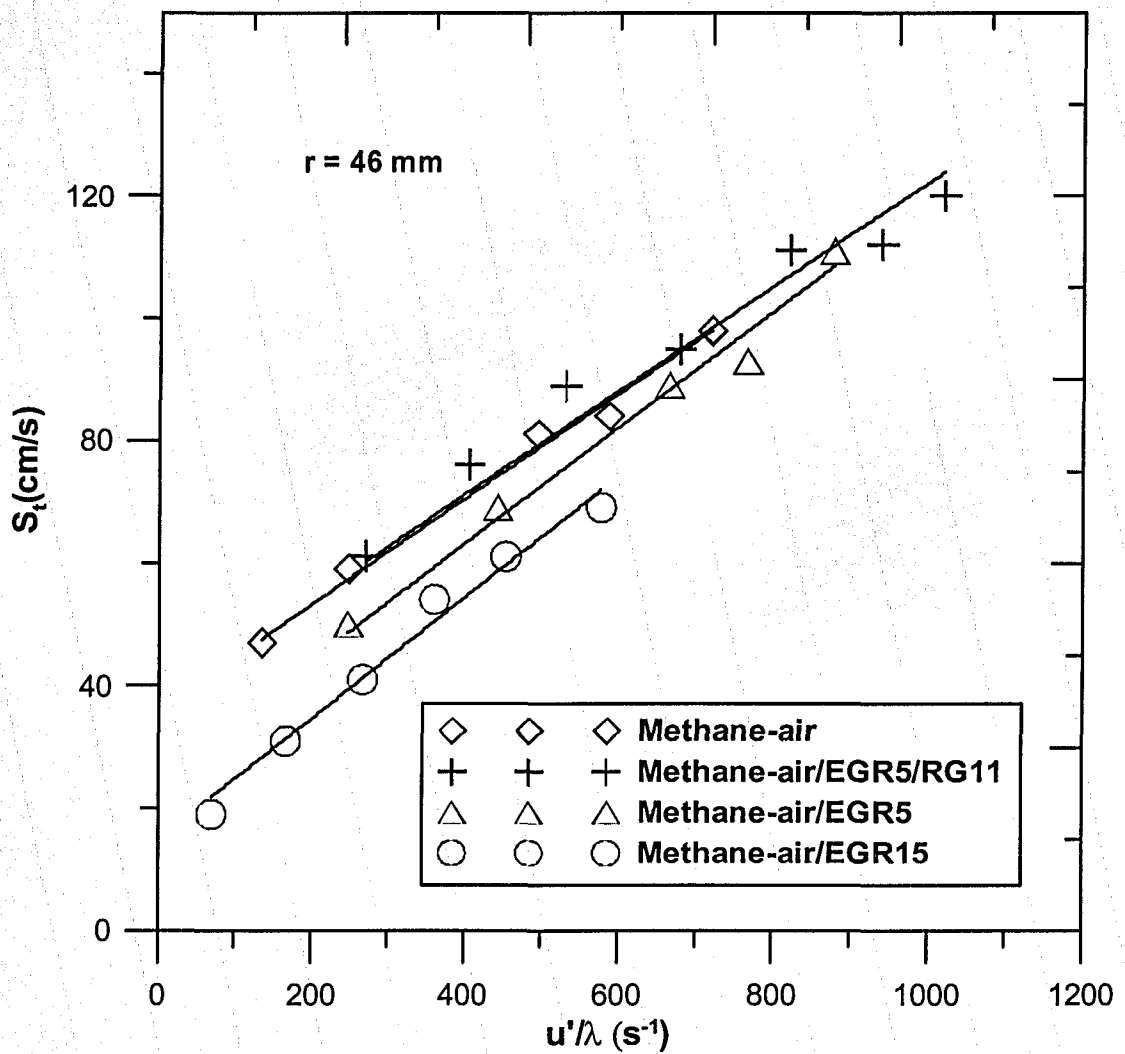
burning velocity, and the straight lines fitted the relevant quiescent burning velocity in terms of Y-intercept.

The comparison between Figures 5.8 and 5.9 clearly shows that the slope of turbulent burning velocity increased as the flame developed from  $r = 46$  to  $55$ mm. This exhibition was attributed to the reduction of eddy size as the flame grew. The large eddies broke up into small eddies which were more effective to enhance the burning rate by wrinkling the flame surface area. For this point, the measurement of the flame surface geometry in terms of flame surface density had confirmed that the wrinkling effect of turbulence was intensified with the flame expanding [Lee et al. 2000 and Knaus et al. 1999]. However, the current investigation showed a slight increase of 3 % from flame radius  $r = 46$  mm to  $r = 55$  mm.

Taking the value of methane-air as a baseline, both plots exhibited that the degree of increasing burning rate increased with more EGR adding, whereas adding RG enabled the slope of the fit line to be less gradual. For example, for both flame  $r = 46$  mm and  $r = 55$  mm, the slope of methane-air/EGR15 was around 1.2 times steeper than that of methane-air. The possible reason lay in the Markstein number which represented the flame response to the stretch effect. Although the property of Markstein number was obtained from the laminar flame, when the strain acted on the flame, both in laminar or turbulent case, the nature of the flame was still the same such that the flame with larger Markstein number tended to be more stable by smoothing out the protrusive segments [Haq et al. 2001]. The trends observed in the plots agreed well with the fact outlined above. The Markstein number of methane-air diluted by EGR decreased with increasing the EGR concentration. On the other hand, adding RG made the ever diluted mixtures

more stable by increasing Markstein number. Similar finding was reported by Ting et al. [2001] that the flame of methane-air at equivalence ratio of 0.9 was more stable than that of 0.7 due to the higher corresponding Markstein number.

For methane-air/EGR5/RG11, a careful observation showed that the influence of strain rate became relative weak at higher strain rate for this mixture. In other words, the effect of strain rate on the flame varied in different spectrum such that it was more effective at low strain rate. The enhanced effect on burning rate decreased until the flame was quenched as already observed by Abdel-Gayed et al. [1987].



Methane-air:  $S_t = 0.086 \frac{u'}{\lambda} + 36, C^2 = 0.99$

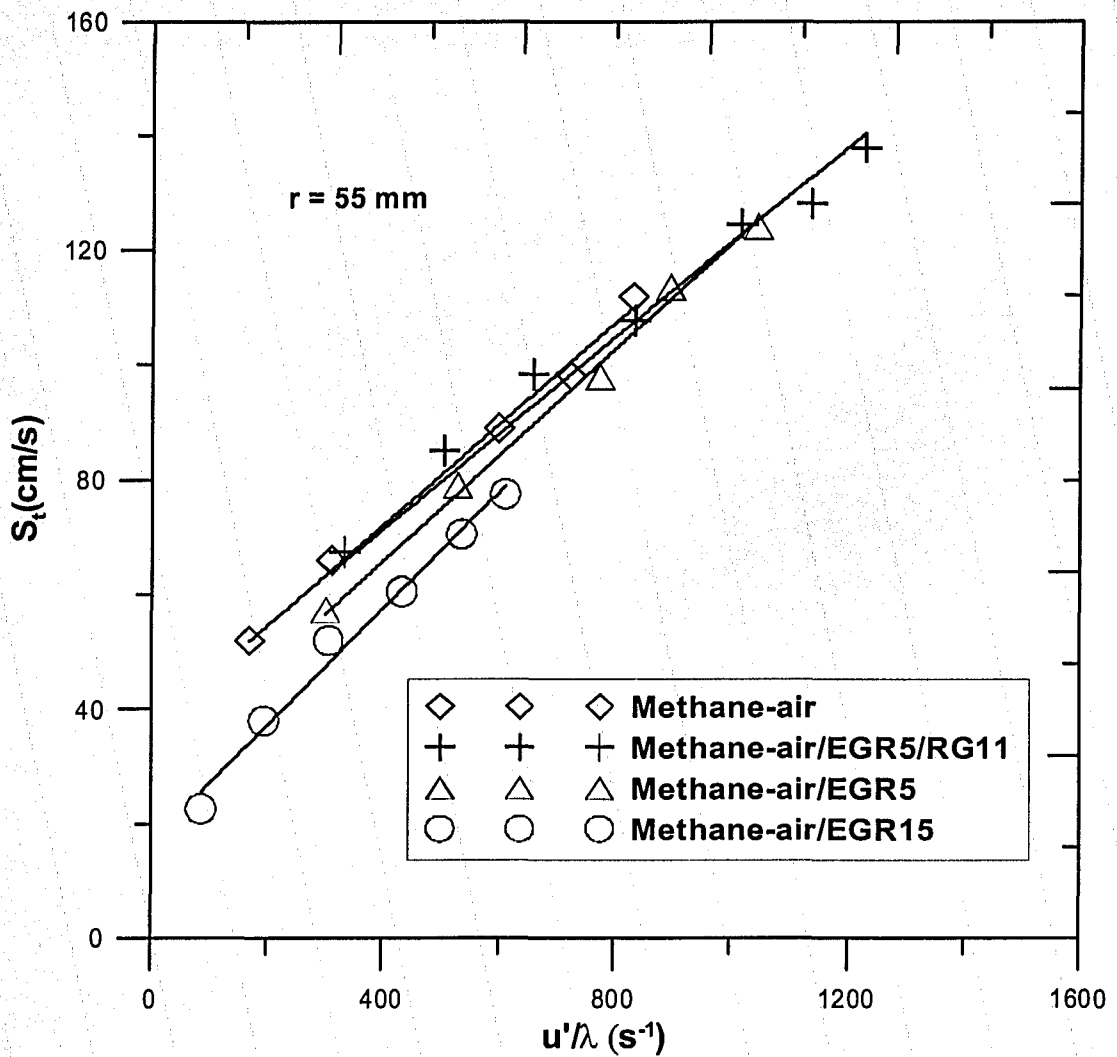
Methane-air/EGR5/RG11:  $S_t = 0.083 \frac{u'}{\lambda} + 37, C^2 = 0.96$

Methane-air/EGR5:  $S_t = 0.092 \frac{u'}{\lambda} + 25, C^2 = 0.98$

Methane-air/EGR15:  $S_t = 0.098 \frac{u'}{\lambda} + 15, C^2 = 0.98$

**Figure 5.8 Turbulent Burning Velocity as a Function of Turbulent Strain Rate  
(flame radius  $r = 46 \text{ mm}$ )**





Methan Methane-air:  $S_t = 0.088 \frac{u'}{\lambda} + 37, C^2 = 0.99$

Metahane-air/EGR5/RG11:  $S_t = 0.085 \frac{u'}{\lambda} + 38, C^2 = 0.98$

Methane-air/EGR5:  $S_t = 0.095 \frac{u'}{\lambda} + 29, C^2 = 0.99$

Methane-air/EGR15:  $S_t = 0.101 \frac{u'}{\lambda} + 17, C^2 = 0.96$

**Figure 5.9 Turbulent Burning Velocity as a Function of Turbulent Strain Rate  
(flame radius  $r = 55 \text{ mm}$ )**

### 5.2.3 With Combined Product of Strain Factor and Lewis number

The influence of the turbulent intensity  $u'$  on the burning rate  $S_t$  had been studied by a number of teams and a variety of empirical approximations were given on the basis of test conditions. The major trends were summarized in section 2.9.1. Despite the difference of experimental methods and test conditions, the basic trend exhibited a good agreement. However, it was not complete to express the turbulent burning velocity only in terms of  $u'$ . Based on 1650 experiments [Bradley et al. 1992] including a substantial number of fully developed turbulent flame in intense turbulence, an opposite effect of turbulence on burning rate was observed. As  $u'$  increased further the increasing rate of  $S_t$  with  $u'$  decreased until a maximum value of  $S_t$  was obtained.

In addition, as reviewed in section 2.7.1, Lewis number also played an important role in the interaction between turbulence and flame chemistry. From this viewpoint, in order to present the observed phenomenon, Bradley et al. [1992] correlated the turbulent burning velocity relative to effective turbulent intensity with the product of Karlovitz strain factor,  $K_{as}$ , (ratio of turbulent strain rate to the chemical strain rate), and Lewis number  $Le$ . The chemical strain factor was defined as the reciprocal of the chemical time  $\frac{\delta}{S_L}$ , where  $\delta$  is characterized by  $\frac{\nu}{S_L}$ , so

$$K_{as} = \frac{u' \delta}{\lambda S_L}. \quad 5.6$$

Thus, a well-known expression for the turbulent burning velocity was obtained as

$$\frac{S_t}{u_k'} = 0.88(K_{as} Le)^{-0.3} \quad 5.7$$

over a range of  $K_{as}Le$  from 0.01 to 0.63, where  $u_k'$  is a time-dependent effective turbulent intensity. The completeness of this expression lay in that not only did it correlate  $S_t$  with  $u'$ , but also the product of laminar chemical strain rate, turbulent strain rate and thermo-diffusive property of the mixture which was one of the determinants of the flame stretch effect on the flame.

Following this proposal, the present experimental results were shown in Figures 5.10 and 5.11 for flame  $r = 46$  mm and 55 mm, respectively. It was worth noting that Bradley et al. [1987] used the Taylor scale  $\lambda$  derived from two eddy theory [Abdel-Gayed et al. 1981], while here  $\lambda$  was estimated from Kido's model as mentioned earlier to keep the consistency. A power law expression,  $S_t = a_{13}*(K_{as}Le)^{a14}$  was used to fit the data points. The plots demonstrated that the data points fitted well with the power law curves with an accepted discrepancy, particularly for the flame radii of 55 mm. Unlike the developed flame analyzed by Abdel-Gayed et al. [1987], the present flames were still in developing stage, so the coefficient of  $a_{13}$  increased with the flame size. In other words, it implied that the turbulence was progressively effective as flame developed. The possible reason for coefficients of  $a_{13}$  deviated from the value of 0.88 was the estimation of the turbulent intensities, of which  $u_k'$  was an effective r.m.s velocity dependent on time and the range of turbulence spectrum, so  $u_k' < u'$  accounted for the flame kernel's growing. Regardless of the variation, the value of the power was fixed. This meant the basic trend of this study was in agreement with Eq.5.7, so the experimental results could reasonably approximated by

$$S_t \approx a_{13}u'(K_{as}Le)^{-0.3} \quad 5.8$$

with  $a_{13} = 0.32$  and  $0.35$  for the flame radius of  $r = 46$  mm and 55 mm, respectively.

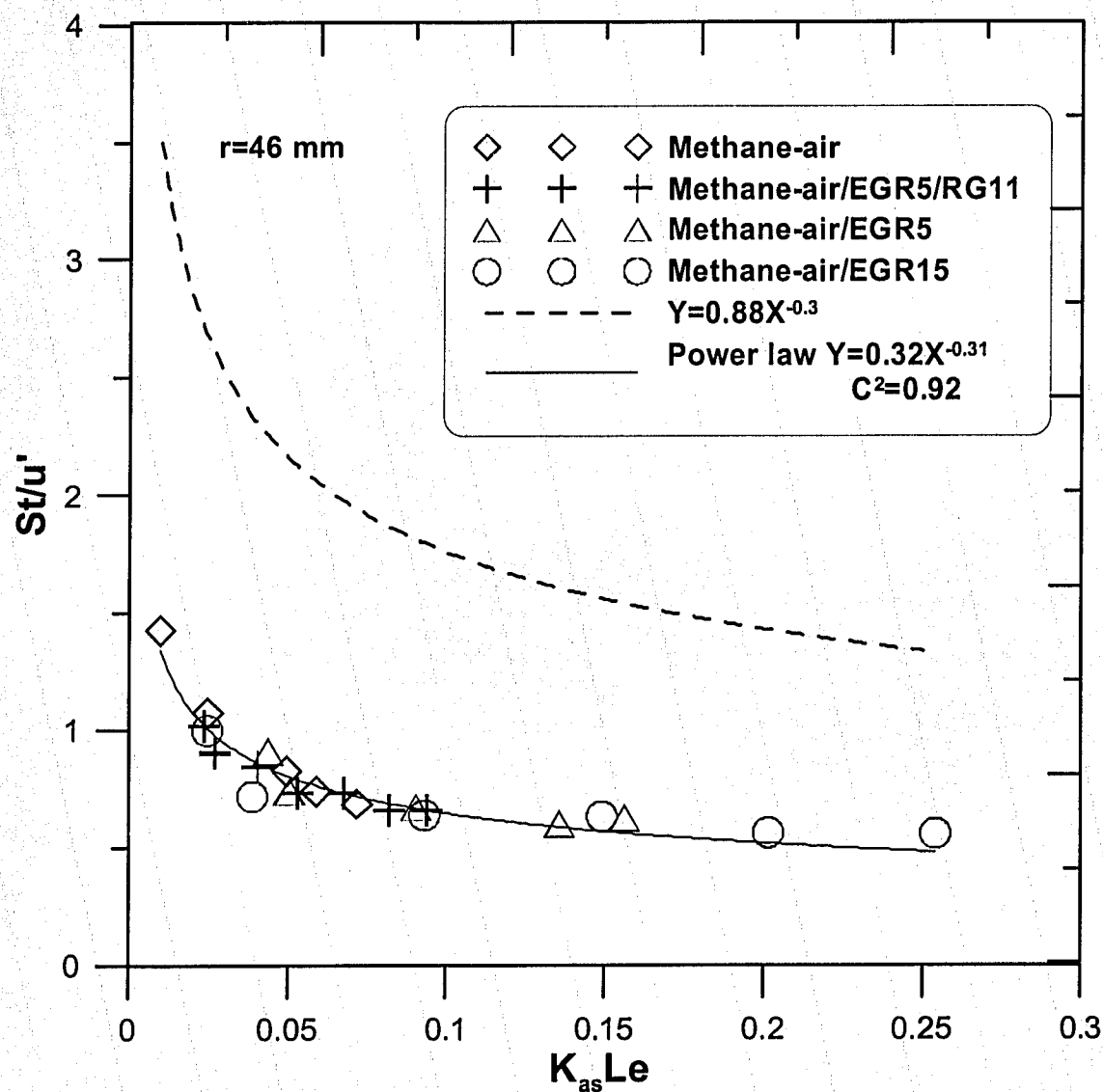


**Figure 5.10 Correlation between  $S_f/u'$  and  $K_{as}Le$  (flame radius  $r = 46$  mm)**

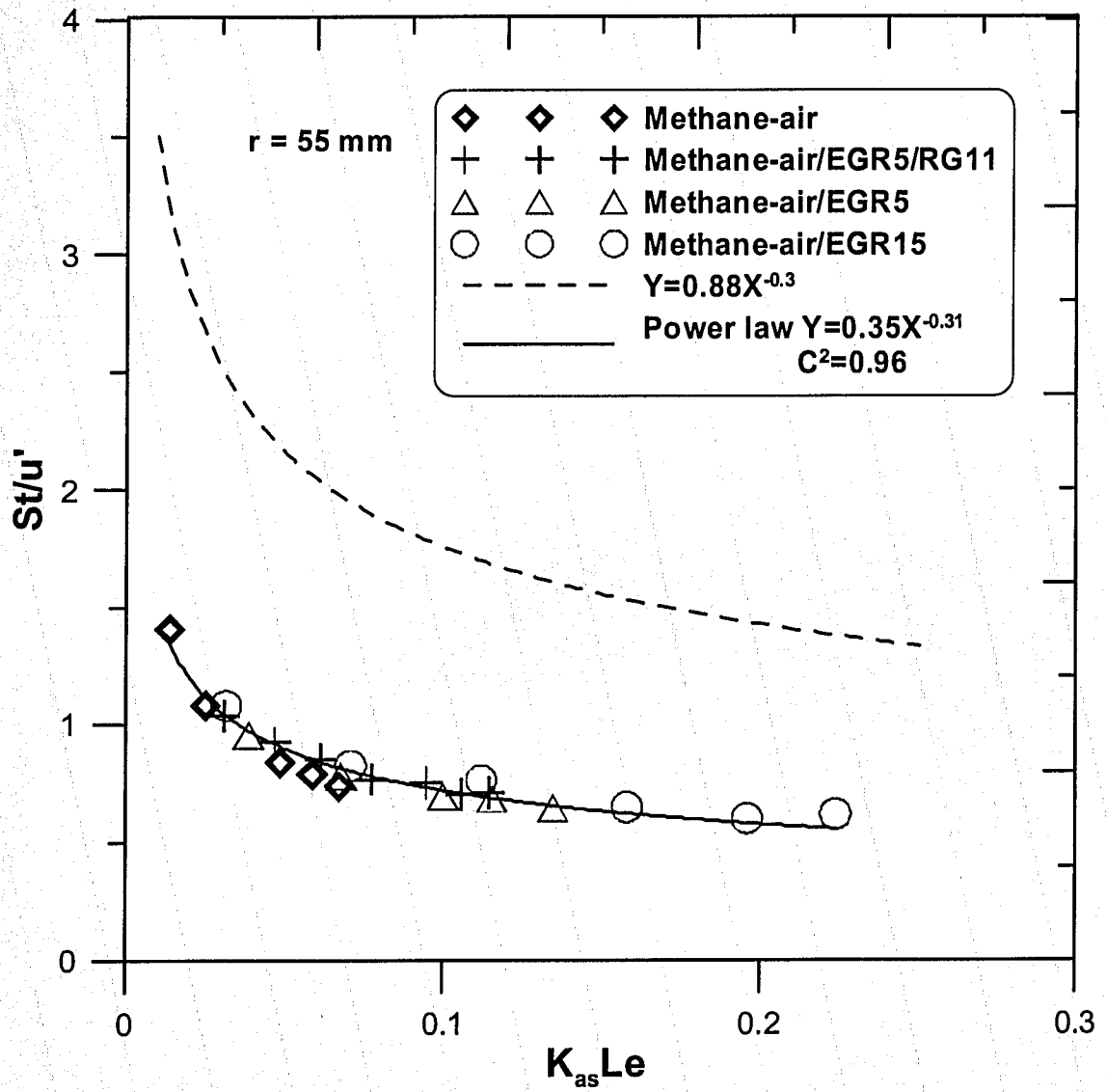


Figure 5.11 Correlation between  $St/u'$  and  $K_{as} Le$  (flame radius  $r = 55 \text{ mm}$ )

#### 5.2.4 With Damköhler Number and Turbulent Karlovitz Number

A further examination of the turbulence effect was to correlate burning velocity with dimensionless timescale of  $Da$  and  $Ka$ .  $Da$  is the ratio of the maximum turbulent time scale ( $\frac{L}{u'}$ ) to the chemical time scale, given by Eq.2.24.  $Ka$  expressed by Eq.2.22 is the ratio of the flame chemical time to the minimum turbulence time ( $\frac{\eta}{u'_\eta}$ ). The detailed data for all the experiments were given in Table 5.3 ~ 5.10.

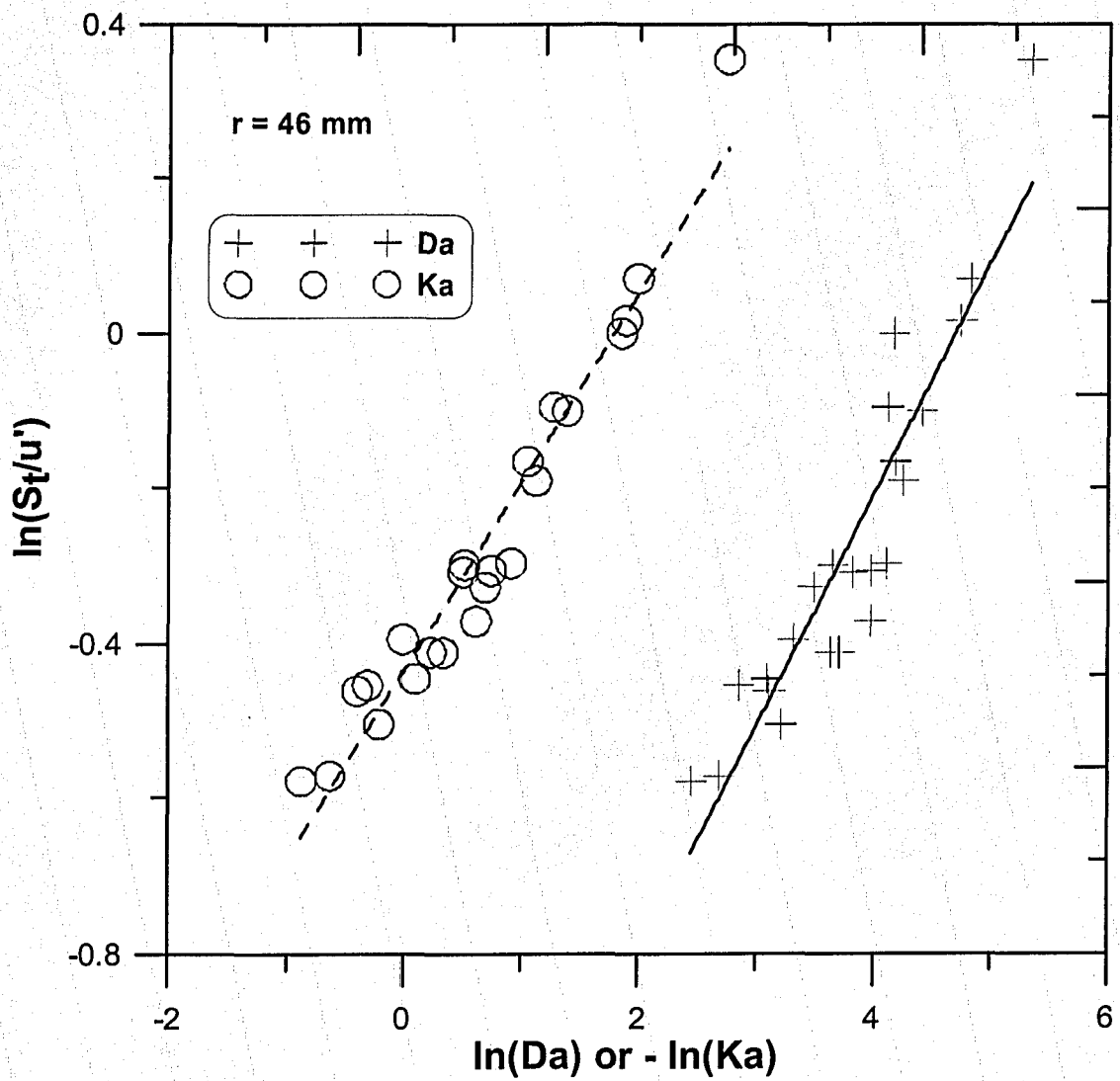
Figures 5.12 and 5.13 showed that the experimental results were reasonably approximated by a function of either  $Da$  or  $Ka$ , particularly  $Ka$ . The lines showed that the least square fitted and the power-law expression was translated from the linear fit of the logarithmic set of data. The slightly more scattered points occurred at the flame size of  $r = 46$  mm. The main reason for this was the uncertainty of the measurements due to the relative high noise-pressure ratio than that of  $r = 55$  mm.

The comparison between Figures 5.12 and 5.13 showed that  $Ka$  was progressively effective as the flame developed, which was reflected by the values of coefficient from 0.65 at  $r = 46$  mm to 0.67 at  $r = 55$  mm, while the effect of  $Da$  was independent of flame size. Lipatnikov et al. [2002] had well processed the experimental database of Karpov and Severin cited therein, and concluded that

$$S_f \sim u' Da^{0.27} \quad \text{and} \quad 5.9$$

$$S_f \sim u' Ka^{-0.37} . \quad 5.10$$

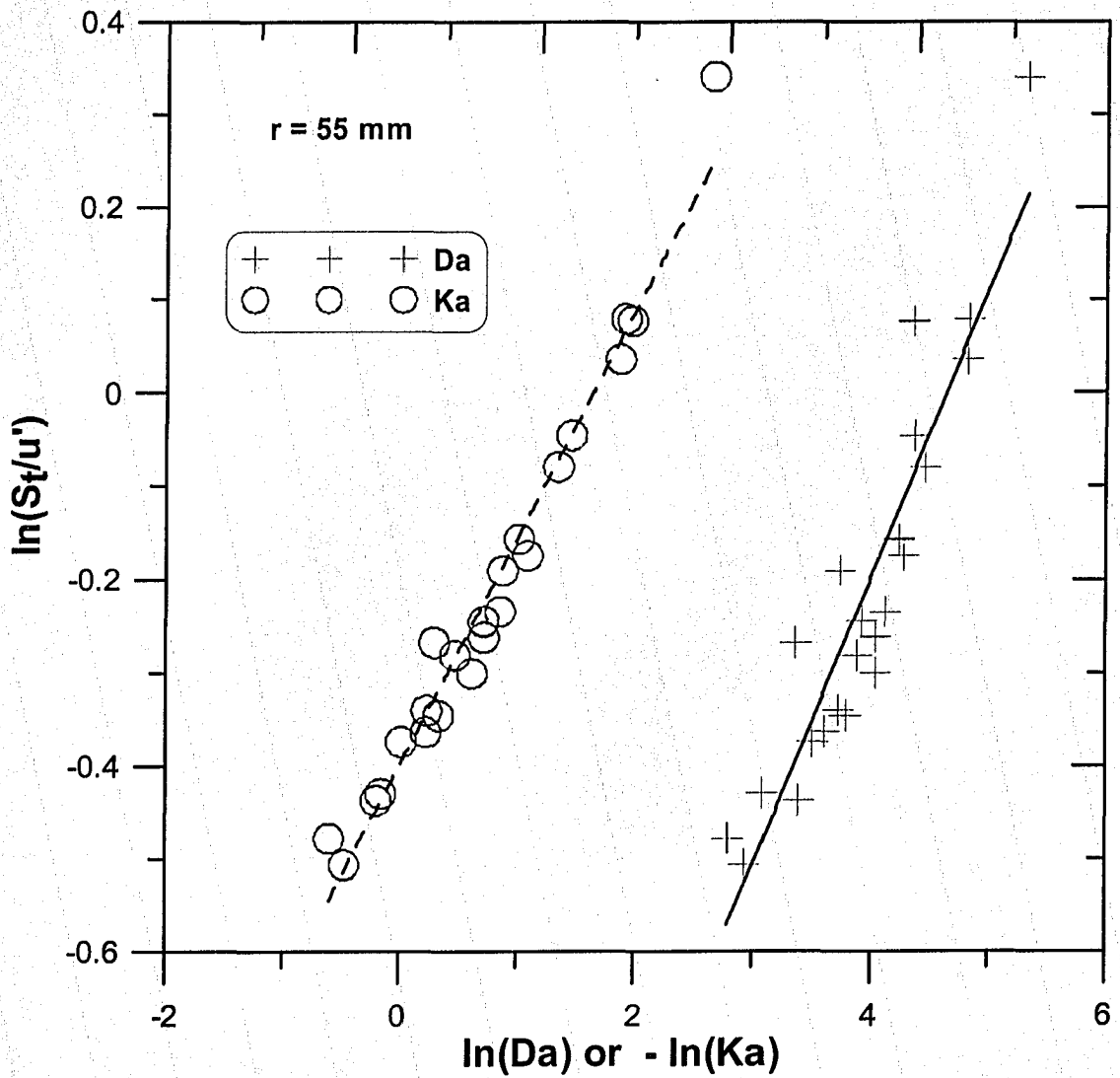
The present experimental results readily yielded a similar empirical expression to the approximation as shown in Figures 5.12 and 5.13.



Solid line expression:  $\frac{S_t}{u'} = 0.24Da^{0.3}$ ,  $C^2=0.86$

Dashed line expression:  $\frac{S_t}{u'} = 0.65Ka^{-0.24}$ ,  $C^2=0.95$

**Figure 5.12 Correlation between  $S_t/u'$  and  $Da$  or  $Ka$  (flame radius  $r = 46 \text{ mm}$ )**



Solid line expression:  $\frac{S_t}{u'} = 0.24 Da^{0.31}$ ,  $C^2 = 0.86$

Dashed line expression:  $\frac{S_t}{u'} = 0.67 Ka^{-0.24}$ ,  $C^2 = 0.97$

**Figure 5.13 Correlation between  $S_t/u'$  and  $Da$  or  $Ka$  (flame radius  $r = 55 \text{ mm}$ )**



### 5.3 Comparison with Peters's Model

As argued by Gülder et al. [2000A], the combustion process in SI engines was within the flamelet regime. This invoked to use a well-defined model in this regimes to examine the present measurements. Peters [1999] derived a model equation of the turbulent to laminar flame surface area ratio ( $\sigma_t$ ) applicable to corrugated and thin zone regimes, namely two sub-regimes of flame flamelet, which were just corresponding to the present turbulent combustion regime as shown in Figure 2.1. This model equation used the level-set approach and took account of the effect of non constant density on the flow field. Also, an empirical expression of  $S_t = 2u'$  for the fully developed turbulent flames were employed. Considering the present test condition that all the flames were still under developing stage beyond the steady state, the expression of  $S_t/u'$  was kept rather than  $\frac{S_t}{u'} = 2$  during the derivation. As a result, the quadratic equation can be expressed as

$$\sigma_t^2 + 0.78 \frac{u'}{S_t} \frac{L}{\delta} \sigma_t - 0.78 \frac{u'}{S_L} \frac{L}{\delta} = 0. \quad 5.11$$

With  $\frac{S_t}{u'} = 2$ , Eq.5.11 was transformed into Peters' model equation:

$$\sigma_t^2 + 0.39 \frac{L}{\delta} \sigma_t - 0.78 \frac{u'}{S_L} \frac{L}{\delta} = 0 \text{ [Peters 1999]}. \quad 5.12$$

The solution for Eq.5.12 is:

$$\sigma_t = -0.39 \frac{u' L}{S_t \delta} + \left[ \left( 0.39 \frac{u' L}{S_t \delta} \right)^2 + 0.78 \frac{u' L}{S_L \delta} \right]^{1/2} . \quad 5.13$$

Fitting the experimental data of  $u'$ ,  $L$ ,  $\delta$  and measured  $S_t$  into Eq.5.13, the model can solve the ratio of turbulent to quiescent burning velocity, that is:

$$\frac{S_t}{S_L} - 1 = -0.39 \frac{u' L}{S_t \delta} + \left[ \left( 0.39 \frac{u' L}{S_t \delta} \right)^2 + 0.78 \frac{u' L}{S_L \delta} \right]^{1/2} . \quad 5.14$$

Based on Eq.5.14, the calculation burning velocity  $S_t$  not only took account of the effect of turbulent intensity and laminar burning velocity, but also the eddy size and laminar flame property.

The comparisons between the experimental values and the function's solutions were plotted in Figure 5.14, where the burning velocity, integral scale, turbulent intensity, the laminar burning velocity and flame thickness were all transient values at  $r = 46$  mm and 55 mm listed in Table 5.3 - 5.10. The solid line was from experimental results and the dashed line was based on model results. Comparing with the experimental results, Peters' model solution was within -7 % deviation from the experimental data over the range of turbulence tested. Also the deviation increased with increasing turbulent intensity. The comparison showed that Peters' model correlated reasonably well with the measured burning velocity at both stages of development being measured. Based on the experiments considered, this model appears to be appropriate for prediction of developing turbulent flames as they exist in engine-like combustion chambers.

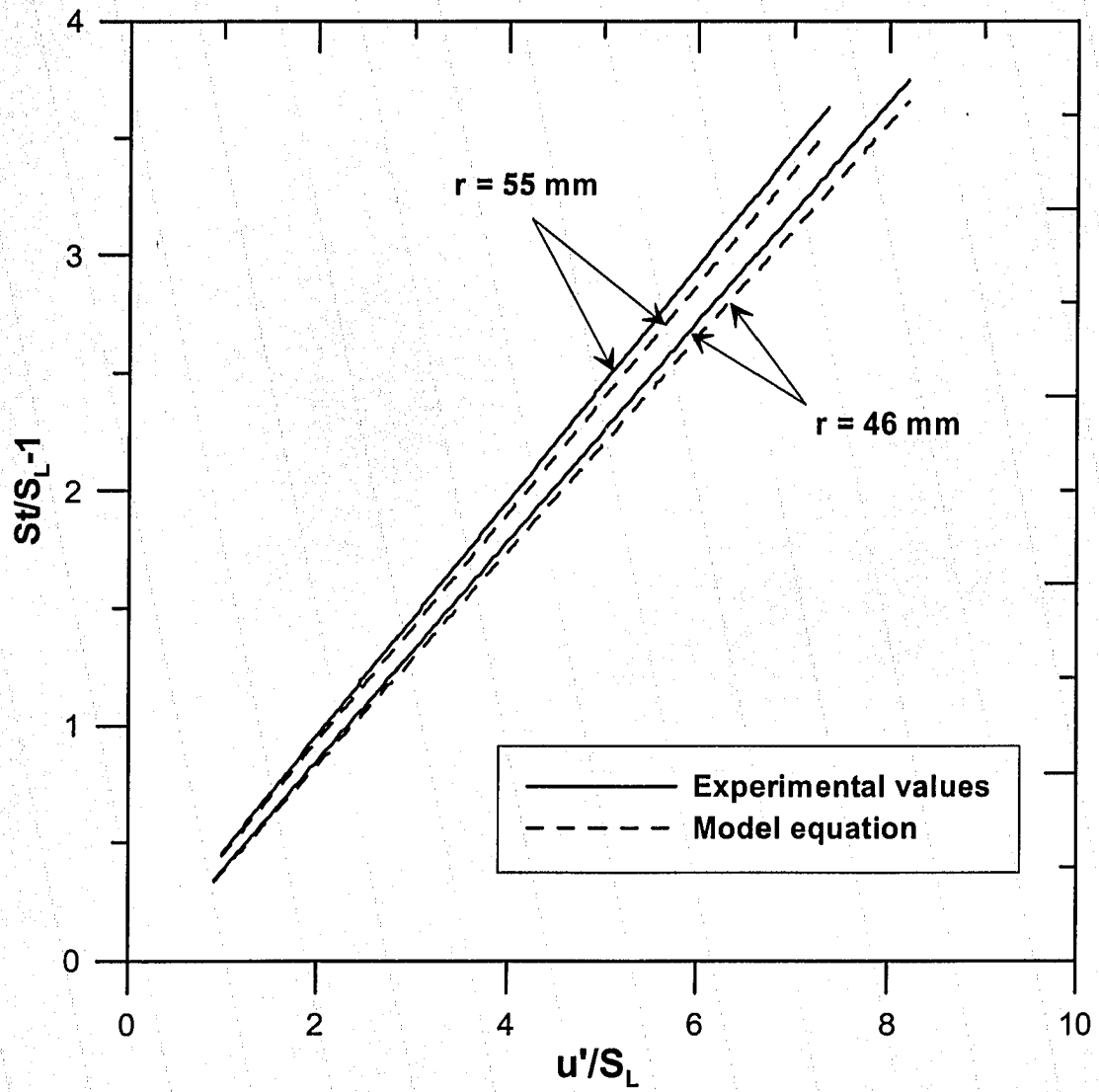


**Figure 5.14 Comparison between Peters's Model Solution and Experimental Results at Flame Radius  $r = 46$  mm and  $r = 55$  mm**

## 5.4 Conclusions

The major conclusions of the study can be summarized as follows:

- 1) Although dilution with simulated exhaust products (EGR) significantly reduced the laminar burning velocity, the turbulence enhancement could effectively bring burning velocity back to the normal level even without fuel enrichment by reformer gas products (RG). For the slower burning (EGR-diluted) mixtures, the turbulence effect on the flame propagation was delayed at very early flame growth stage. However, the turbulent intensification at the later stages of flame growth still determined the combustion time.
- 2) The turbulent burning velocity normalized by the current quiescent burning velocity was linearly dependent on the turbulent intensity relative to the quiescent burning velocity and the effectiveness of turbulence increased as the flame developed. This means that a linear relationship can be demonstrated between  $St/S_L$  and  $u'/S_L$  but the proportional constant increases as the flame grows over the range of flame radius tested. This is attributed to the tendency for the flame to become progressively more wrinkled by distortion of the small turbulence eddy.
- 3) The linear relationship between turbulent burning velocity ratio ( $St/S_L$ ) and turbulence intensity ( $u'/S_L$ ) did not appear to be significantly affected by higher or lower Markstein numbers for the concentrations of EGR and RG tested in this study. For these mixtures, with relatively neutral stable preferential diffusion conditions, the small effects of Markstein number might have been obscured by experimental variability in measurement.

4) The ratio of turbulent to quiescent burning velocity could also be correlated with turbulent strain rate  $u'/\lambda$ , again with a proportional constant that increased as the flame developed. With this relationship, the effect of low or high Markstein number was detectable when shifting from methane-air mixtures to methane-air/EGR15 or methane-air/EGR5/RG11 mixtures. The turbulence enhancement appeared to be more effective for low-Markstein number mixtures diluted by EGR. However, further work would be required to verify the accuracy of this effect.

5) Based on turbulent burning velocity relationships from the literature, several empirical expressions giving turbulent burning velocity as a function of product of Karlovitz number and Lewis number  $K_{as}Le$ , turbulent Damköhler number  $Da$ , and turbulent Karlovitz number were tested for the data reported here. These give  $S_t \sim u'(K_{s}Le)^{-0.3}$ ,  $S_t \sim u'Da^{0.3}$  and  $S_t \sim u'Ka^{-0.24}$ . However, these relationships required different constant for increasing flame radius.

6) The turbulent burning velocity model of Peters [1999] which is based on turbulent/laminar flame area ratios in the flamelet regime was compared with the experimental results. This relationship correlated well with the experimental measurements at both flame radius  $r = 46$  mm and 55 mm, predicting turbulent burning velocity ratios about 7 % less than the measured values.

## **CHAPTER 6: LIMITATIONS AND RECOMMENDATIONS**

One of the challenging points for modeling turbulent combustion is the proper parameters with which the turbulent burning velocity should be correlated. As discussed in developing the major conclusions of Chapter 5, many attempts have been made by various researchers. Due to the dependency of turbulent velocities on their configurations, e.g. the shape of flame, the turbulence generation mechanism and flame growth phase, there is still no comprehensive and sufficient theory for modeling turbulent premixed flames. From this background, in extending these experimental results to applications, attention must be paid to the limitations of this study and future work should be devoted to making improvements.

### **6.1 Turbulence Parameters**

As turbulence intensity and integral scale at ignition time are derived from the established decay model, they are dependent on the control of the plate speed, plate hole diameter and delay time prior to ignition. These factors cause the turbulence parameters to be secondary calculated variables rather than directly measured values. Another possible uncertainty is from the analogy between wind tunnel and constant volume chamber used in developing the present turbulence decay model. The difficulty of measurement conducted in the chamber restricted the comprehensive investigation of various hole size plates. The effect of smaller integral scales than the 8 mm used in this study should be investigated in future work. Instead of hot wire anemometry, the

application of laser anemometry technology has great potential to enable the directly measurement of the turbulence parameters.

The most controversial point lies in the estimation of the turbulent intensity during combustion. This study employed a rapid distortion model to adjust the decayed turbulence. The simplified turbulence and flame interaction resulted in a constant factor as a function of flame radius. The validity of this model must be explored further by experimental approaches. Laser anemometry techniques have potential for this purpose as well.

Moreover, in turbulent micro-structure, the turbulent scales such as Taylor microscale and Kolmogorov scale are dependent on modeling assumptions. So far, it is still doubtful that the macro integral scale influences these microscales.

## **6.2 Range of Turbulent Intensity**

Due to limitations of this apparatus, high turbulence intensity is not available in this study, (maximum of 2.6 m/s at ignition). The weakened effect of turbulence on the burning velocity under intense turbulence condition has been found by other researchers but could not be studied here. This could substantially affect the correlation between turbulence intensity and burning velocity. Therefore, the ideal linear relation obtained in the present investigation is expected to be altered due to turbulence stretch effect with increasing turbulent intensity. In order to simulate the more complete engine operation, future work should include a wide range of turbulence levels, e.g.  $u'$  up to 10 m/s during combustion. According to the investigation as mention in section 2.9.1, the linear relation is expected to be changed as the turbulence intensity increases.

### **6.3 Simulated EGR**

Since the current apparatus made the actual recirculation of the burned gas impractical, the simplified theoretical composition of EGR was adopted and only the major stable species  $\text{CO}_2$  and  $\text{N}_2$  are considered here. This selection ignored the water composition in real EGR. The thermal effect of including water is negligible because the simulated EGR adjusted the amount of carbon dioxide and nitrogen in the simulated EGR to match the specific heat capacity of real exhaust gas [Han 2005]. With respect to the effect of water on the turbulent flame stability, Markstein number and Lewis number are affected by the chosen compositions with water in the EGR. Lewis number tends to increase due to the heat diffusivity increasing, so Markstein number of methane-air-EGR mixtures also increases with water in the EGR. Taking methane-air/EGR5 as an example, with water in the EGR, Lewis number is 0.99, (0.96 for simulated EGR), and Markstein number becomes 2.15, (1.85 for simulated EGR). In other words, it is expected the turbulent flame will become more stable with real exhaust gas recirculation than the current investigation based on simulated EGR that only matched the heat capacity.

On the other hand, due to the dilution of EGR, the initial temperature of the fuel gas deviated from the room temperature. From this viewpoint, future work should consider using water in the mixtures and elevated initial temperature.

### **6.4 Estimation of Markstein Number**

Markstein number is of importance for analyzing the interaction between flame chemistry and turbulence. Although the current experimental results are qualitatively



in accordance with calculated  $Ma$ , the theoretical equation appears to be relatively rough due to the simplified activation energy for multiple reactants. It is expected that future work could measure Markstein number using an experimental approach. By applying the linear relation between the laminar burning velocity with Karlovitz number (Eq.2.39), Markstein number can be measured at very early stage of flame growth with negligible pressure rise in the chamber. Due to the limitation of the pressure trace in measuring burning velocity, measurements could be based on motion picture shadowgraph.

## REFERENCES

- Abdel-Gayed, R. G., Bradley, D., 1977A "Dependence of Turbulence Burning Velocity On Turbulent Reynolds Number And Ratio of Laminar Burning to R.M.S Turbulent Velocity", 16th Symposium (International) on Combustion, 1725-1735
- Abdel-Gayed, R. G., Bradley, D., 1981 "A Two-Eddy Theory of Premixed Turbulent Flame Propagation", D. Phil. Trans. R. Soc. Lond., Vol.A301, pp1457
- Abdel-Gayed, R. G., Bradley, D., Hamid, M. N. and Lawes, M., 1984 "Lewis Number Effects on Turbulent Burning Velocity", 20th Symposium (International) on Combustion, pp.505-512
- Abdel-Gayed, R. G., Bradley, D., and Lawes, M., 1987 "Turbulent Burning Velocities: A General Correlation in Terms of Straining Rates", Proc. R.Soc. Lond. A414, 389-413
- Agrawal, D. D., "Experimental Determination of Burning Velocity Methane-air Mixture in a Constant Volume Vessel", Combustion and Flame 42(1981)243-252
- Allenby, S., Chang, W-C., Megaritis, A. and Wszyński, M. L., "Hydrogen Enrichment: A Way to Maintain Combustion Stability in A Natural Gas Fuelled Engine with Exhaust Gas Recirculation, the Potential of Fuel Reforming", Proc. Instn. Mech. Engrs. Vol 215 Part D
- Andrews, G. E., Bradley, D., 1972 "Determination of Burning Velocities: A Critical Review", combustion and Flame 18, 133-153
- Andrews, G. E., Bradley, D. and Lwakabamba, S. B., 1975 "Turbulence and Turbulent Flame Propagation—A Critical Appraisal", Combustion and Flame 24, 285-304

- Ashurst, W.T., Checkel, M.D. and Ting, D.S.-K., "The Eddy Structure Model of Turbulent Flamelet Propagation, the Expanding Spherical and Steady Planar Cases", Combust. Sci. and Tech.,1994,vol.99.pp51-74
- Aung, K. T. , Tseng, L.-K., Ismail, M. A. and Faeth, G. M., 1995 "Response to Comment by S. C. Taylor and D. B. Smith on "Laminar Burning Velocities and Markstein Numbers of Hydrocarbon/Air Flames", Combustion and Flame102, 526-530
- Aung, K. T., Hassan, M. I. and Faeth, G. M., 1997 "Flame Stretch Interactions of Laminar Premixed Hydrogen/Air Flames at Normal Temperature and Pressure", Combustion and Flame109, 1-24
- Aung, K. T., Hassan, M. I., Kwon, S., Tseng, L.-K., Kwon,O.-C., and Faeth, G. M., "Flame/Stretch Interactions in Laminar and Turbulent Premixed Flames", Combust. Sci. and Tech.,174:61-99,2002
- Batchelor, G. K. and Townsend, A. A., "The Nature of Turbulent Motion at Large Wave-Number", Proceedings. Mathematical, Physical and Engineering Sciences,199(1949) 238
- Bird, R.B., Stewart, W. E. and Lightfoot, E. N., "Transport Phenomena", New York. London, John Wiley & Sons, Inc., 1964
- Bradley, D., Gaskell, P. H. and Gu, X. J., 1996 "Burning Velocities, Markstein Lengths, and Flame Quenching for Spherical Methane-Air Flames: A Computational Study", Combustion and Flame 104, 176-198

- Bradley, D. , Haq, M. Z., Hicks, R. A., Kitagawa, T., Lawes, M., Sheppard, C. G. W. and Woolley, R., 2003A "Turbulent Burning Velocity, Burned Gas Distribution, and Associated Flame Surface Definition ", Combustion and Flame 133, 415-430
- Bradley, D., Gaskell, P.H, Sedaghat, A., Gu, X. J., 2003B "Generation of PDFS for Flame Curvature and for Flame Stretch Rate in Premixed Turbulent Combustion", Combustion and Flame 135, 503-523
- Bray, K. N. C., "Studies of the Turbulent Burning Velocity", Proc. R. Soc. Lond. A431 (1990)315-335
- Checkel, M. D., 1981 "Turbulence-Enhanced Combustion of Lean Mixtures", Ph.D., University of Cambridge
- Checkel , M. D., 1986 "Measurements of Turbulence Generated by 60 Percent Solid Perforated Plates", Journal of fluids engineering , Vol.108/55
- Checkel, M. D. and Ting, D. S-K., 1992 "Measuring Turbulent Flame Growth By Visualization ", SAE TECHNICAL PAPER SERIES 920184
- Checkel, M. D. and Thomas, A., 1994 "Turbulent Combustion of Premixed Flames in Closed Vessels", Combustion and Flame 96, 351-370
- Chen, C. and Veshagh, A., "A Premixed Turbulent Flame Velocity Model Based on Dimensional Reasoning", SAE TECHNICAL PAPER SERIES 910077
- Chen, R., Milovanovic, N., "A Computational Study into the Effect of Exhaust Gas Recycling on Homogeneous Charge Compression Ignition Combustion in Internal Combustion Engines Fuelled with Methane", International Journal of thermal sciences 41 (2002) 805-813

- Chew, T. C. and Britter, R. E., "Effect of Flame-Induced Geometrical Straining on Turbulence Levels in Explosions and Common Burner Configurations", *Int. J. Engng Sci.* Vol.30, No.8. pp.983-1002,1992
- Chomiak, J., "Basic Consideration of the Turbulent Flame Propagation in Premixed Gases", *Prog. Energy Combust. Sci.* Vol.5, 1979, pp207
- Clark, A., Stone, R. and Beckwith, P., "Measuring the Laminar Burning Velocity of Methane/Diluents/Air Mixtures within a Constant-volume Combustion Bomb in a Micro-gravity Environment", *Journal of the Institute of Energy* 68(1995)130-136
- Clavin, P. and Williams, F. A., 1979 "Theory of Premixed-Flame Propagation in Large-Scale Turbulence", *J. Fluid Mech.* 90, 589-604
- Clavin, P., 1985 "Dynamic Behaviour of Premixed Flame Fronts In Laminar and Turbulent Flows ", *Prog. Energy Combust. Sci.* Vol.11, ,pp.1-59
- Corrsin, S., "Turbulent Dissipation Fluctuations", *The Physics of Fluids* 5(1962) 1301
- Dixon-Lewis, G., "Structure of Laminar Flames", 23rd Symposium (International) on Combustion, 1990/pp.305-324
- Gu, X. J., Haq, M. Z., Lawes, M., and Woolley, R., "Laminar Burning Velocity and Markstein Lengths of Methane-Air Mixtures", *Combustion and Flame* 121 (2000) 41-58
- Gülder, Ö. L. and Smallwood, G. J., 2000A, "Do Turbulent Premixed Flame Fronts in Spark-Ignition Engines Behave Like Passive Surfaces?", *SAE TECHNICAL PAPER SERIES* 2000-01-1942

- Gülder, Ö. L., Smallwood, G. J., Wong, R., Snelling, D. R., and Smith, R., 2000B, "Flame Front Surface Characteristics in Turbulent Premixed Propane/Air Combustion", *Combustion and Flame* 120, 407-416
- Han, P., "Burning Velocity of Methane/EGR/Air Mixtures with Reformer Gas Addition", M. Sc., 2005, University of Alberta
- Haq, M. Z., Sheppard, C. G. W., Woolley, R., and Greenhalgh, D. A. and Lockett, R.D., "Wrinkling and Curvature of Laminar and Turbulent Premixed Flames", *Combustion and Flame* 131(2002)1-15
- Heywood, J. B., "Internal Combustion Engine Fundamentals", McGraw-Hill, Inc., 1988
- Kaminski, C. F., Bai, X. S., Hult, J., Dreizler, A., Lindenmaier, S., and Fuchs, L., "Flame Growth and Wrinkling in a Turbulent Flow", *Appl. Phys. B* 71, 711-716 (2000)
- Knaus, D. A. and Gouldin, F. C., "Measurement of Instantaneous Flamelet Surface Normals and the Burning Rate in a SI Engine", SAE TECHNICAL PAPER SERIES 1999-01-3543
- Karpov, V. P. and Severin, E. S., 1978 "Turbulent Burn-Up Rates of Propane-Air Flames Determined in a Bomb with Agitators", *Combustion, Explosion, and Shock Waves* 14, pp319
- Karpov, V. P. and Severin, E. S., 1980 "Effects of Molecular-Transport Coefficient on the Rate of Turbulent Combustion", *Combustion, Explosion, and Shock Waves* 16, pp41

- Kauffman, C. W., "The Effect of Exhaust Gas Recirculation and Turbulence on the Burning Velocity, Dead Space Thickness, and Minimum Ignition Energy in Premixed Methane-Air Combustion", *Combust. Sci. and Tech.*, 1980, vol.23, pp1-15
- Kido, H., Wakuri, Y., Murase, E., 1983 "Measurements of Spatial Scales and a Model for Small-Scale Structure of Turbulence in an Internal Combustion Engine", *Processings of ASME-JSME Thermal Engrg. Joint Conference*, 4:191-199
- Kido, H. , Nakashima, K., Nakahara, M. and Hashimoto, J., 2001 "Experimental Study on the Configuration and Propagation Characteristics of Premixed Turbulent Flame", *JSAE Review* 22, 131-138
- Kwon, S., Wu, M.-S., Driscoil, J.F., and Faeth, G. M., 1992A "Flame Surface Properties of Premixed Flames in Isotropic Turbulence: Measurements and Numerical Simulations", *Combustion and Flame* 88, 221-238
- Kwon, S., Tseng, L.-K. and Faeth, G. M., 1992B "Laminar Burning Velocities and Transition to Unstable Flames in  $H_2/O_2/N_2$  and  $C_3H_8/O_2/N_2$  Mixtures", *Combustion and Flame* 90, 230-246
- Law, C. K., "Dynamics of Stretched Flames", 22nd Symposium (International) on Combustion, 1998/pp.1381-1402
- Lee, G. G. and Huh, K. Y., "Correlation between the Measured Flame Surface Density and Turbulence Parameters in Turbulent Premixed Flames", *SAE TECHNICAL PAPER SERIES* 2000-01-1383
- Lipatnikov, A. N. and Chomiak, J., 1998A "Randomness of Flame Kernel Development in Turbulent Gas Mixture", *SAE TECHNICAL PAPER SERIES* 982617

- Lipatnikov, A. N. and Chomiak, J., 1998B "Lewis Number Effects in Premixed Turbulent Combustion and Highly Perturbed Laminar Flames", *Combust. Sci. and Tech.* 137, pp277-298
- Lipatnikov, A. N. and Chomiak, J., 2002 "Turbulent Flame Speed and Thickness: Phenomenology, Evaluation, and Application in Multi-dimensional Simulations", *Progress in Energy and Combustion Science* 28 (2002)1-74
- Liu, F., Guo, H. and Smallwood, G. J., "The Chemical Effect of CO<sub>2</sub> Replacement of N<sub>2</sub> in Air on the Burning Velocity of CH<sub>4</sub> and H<sub>2</sub> Premixed Flames", *Combustion and Flame* 133 (2003) 495-497
- Mcdonell, B. J., *Turbulent Burning Rates of Propane-Air*", M. Sc. 1988, University of Alberta
- Modien, R. M., "Enhanced Ignition Systems and Turbulence", M. Sc. 1991, University of Alberta
- Ponnusamy, S., "Extending diluent limits in methane/air combustion by adding simulated reformer gases", M. Sc., 2005, University of Alberta
- Peters, N., 1986 "Laminar Flamelet Concepts in Turbulent Combustion", 21st Symposium (International) on Combustion, pp.1231-1250
- Peters, N., 1999 "The Turbulent Burning Velocity for Large-Scale and Small -Scale Turbulence", *J. Fluid Mech.* vol. 384, pp.107-132
- Renou, B., Boukhalfa, A., Puechberty, D., and Trinité, M., "Local Scalar Flame Properties of Freely Propagating Premixed Turbulent Flame at Various Lewis Numbers", *Combustion and Flame* 123 (2000) 507-521



- Ruan, J., Kobayashi, H. and Niiokd, T., "Combined Effects of Nongray Radiation and Pressure on Premixed CH<sub>4</sub>/O<sub>2</sub>/CO<sub>2</sub> Flames", *Combustion and Flame* 124(2001) 225-230
- Shy, S. S., Lin, W. J. and Wei, J. C., "An Experimental Correlation of Turbulent Burning Velocities for Premixed Turbulent Methane-air Combustion", *Proc. R. Soc. Lond.* A456 (2000)1997-2019
- Smallwood, G. J. , Gülder, Ö. L. , Snelling, D. R. , Deschamps, B. M. and Gökalp, I. , "Characterization of Flame Front Surfaces in Turbulent Premixed Methane/Air Combustion ", *Combustion and flame* 101/4(1995) 461:470
- Tanoue, K., "The Effects of CO<sub>2</sub> Dilution on Spherical Premixed Methane Flames", *JSAE* 20030090, (SAE2003-01-1774)
- Taylor, G. I., "Statistical Theory of Turbulence", *Proceedings. Mathematical, Physical and Engineering Sciences*, A151 (1935), pp.421-478
- Tennekes, H., 1968 "Simple Model for the Small-Scale Structure of Turbulence", *The Physics of Fluids* 11, pp669
- Tennekes, H. and Lumley, J. L., 1972 "A First Course in Turbulence ", Cambridge, Mass., MIT Press
- Ting, D. S.-K., 1992 "Turbulent Flame Growth in A Chamber", M. Sc., University of Alberta
- Ting, D. S.-K., 1995 "Modeling Turbulent Flame Growth in A Chamber", Ph.D., University of Alberta
- Ting, D. S.-K. and Checkel, M. D., 1994 "Early Flame Acceleration Measurements in a Turbulent Spark-Ignited Mixture", *SAE TECHNICAL PAPER SERIES* 940687

- Ting, D. S.-K. and Checkel, M. D., 2001 "The Effect of Mean Turbulent Strain Rate on the Flame Speed of Premixed, Growing Flames", *Journal of Engineering for Gas Turbines and Power* Vol. 123/175
- Townsend, A. A., "On the Fine-Scale Structure of Turbulence", *Proceedings. Mathematical, Physical and Engineering Sciences* A208 (1951) 534
- Trouvé, A. and Poinso, T., "The Evolution Equation for the Flame Surface Density in Turbulent Premixed Combustion", *J.Fluid Mech.* 278(1994)1-31
- Tseng, L.-K., Ismail, M. A. and Faeth, G. M., "Laminar Burning Velocities and Markstein Number of Hydrocarbon/Air Flames", *Combustion and Flame* 95 (1993) 410-426
- VKI, Lectures Series 1999-04, "Introduction to Turbulent Combustion"
- Westbrook, C. K. and Dryer, F. L., "Chemical Kinetic Modeling of Hydrocarbon Combustion", *Prog.Energy Combust.* Vol.10, 1984, pp1-57.
- Williams, F. A., "Combustion Theory", The Benjamin/cummings Publishing Company, Inc., 2nd Ed., 1985
- Wu, M. S., Kwon, S., Driscoll, J. F. and Faeth, G. M., 1990 "Turbulent Premixed Hydrogen/Air Flames at High Reynolds Number", *Combust. Sci. and Tech.* 73, 327-350
- Wu, M. S., Kwon, S., Driscoll, J. F. and Faeth, G. M., 1991 "Preferential Diffusion Effects on the Surface Structure of Turbulent Premixed Hydrogen/ Air Flames", *Combust. Sci. and Tech.* 78, 61-96

# APPENDIX A

## TURBULENT EXPERIMENT CONTROL PROGRAM

This appendix gives the detailed program code of turbulent experiment control with LabVIEW 6i.

*turbulent.vi*

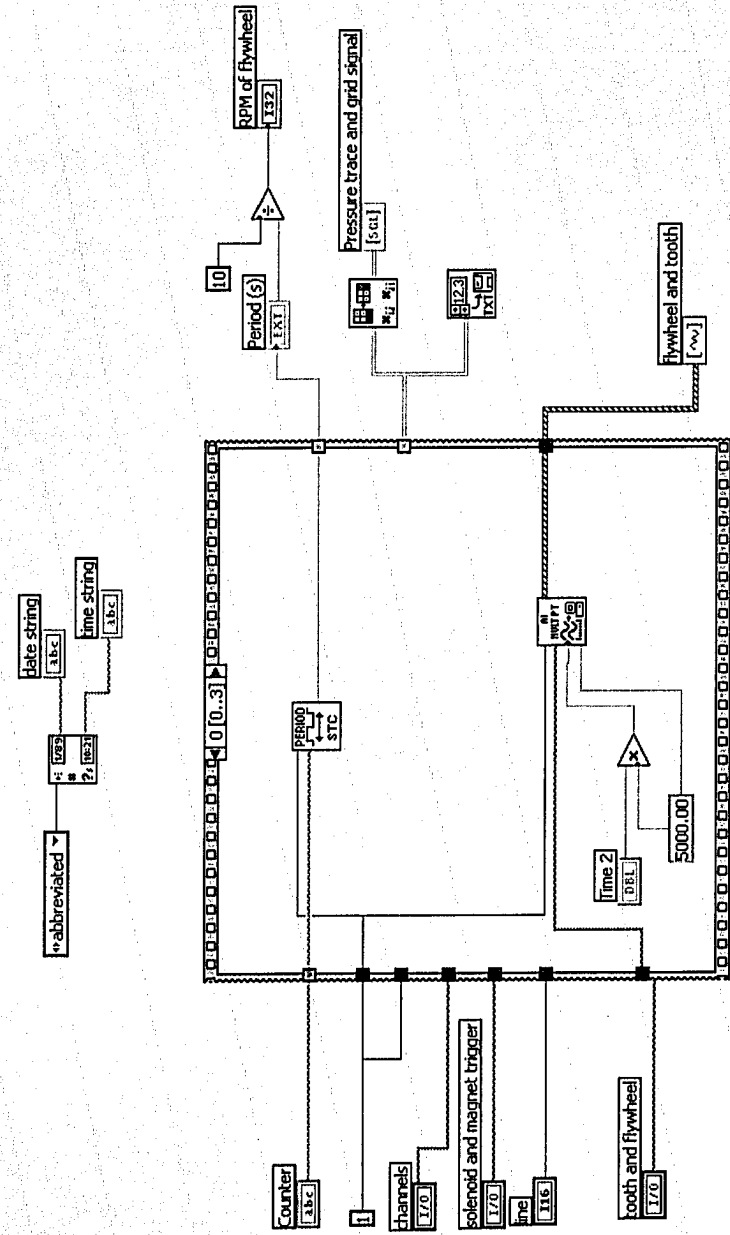


Figure A.1 Sequence Structure Frame 0 of Turbulent Experiment Control Program

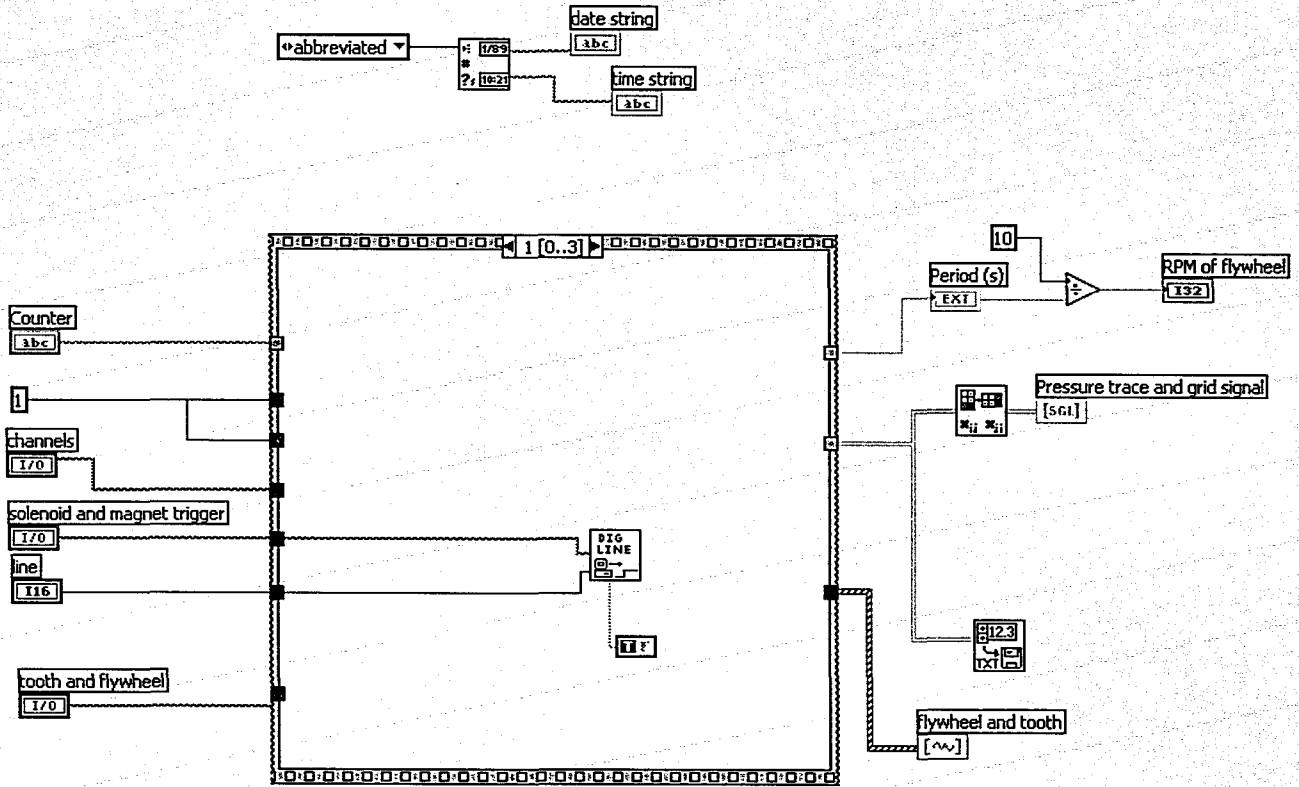


Figure A.2 Sequence Structure Frame 1 of Turbulent Experiment Control Program

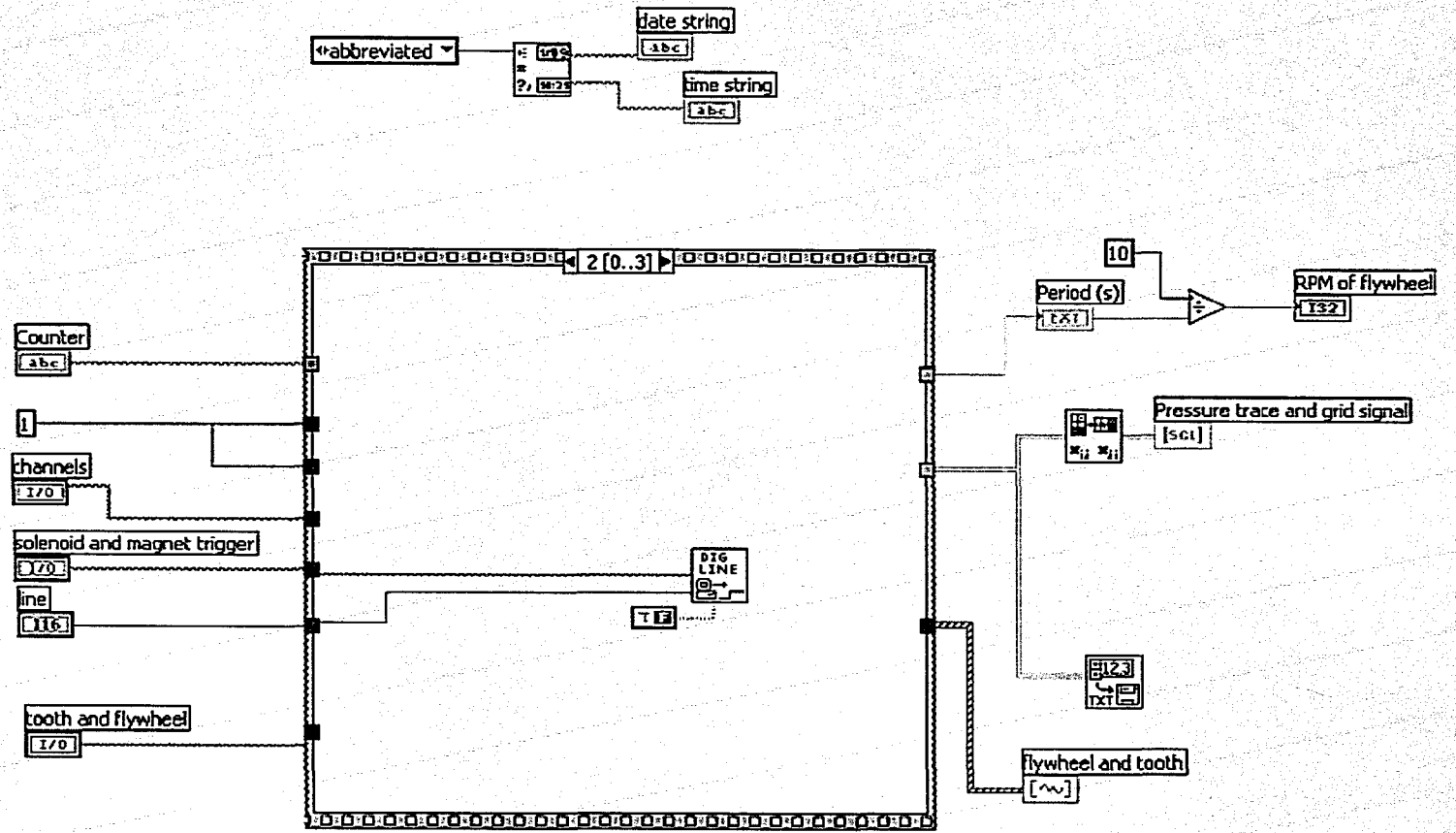


Figure A.3 Sequence Structure Frame 2 of Turbulent Experiment Control Program

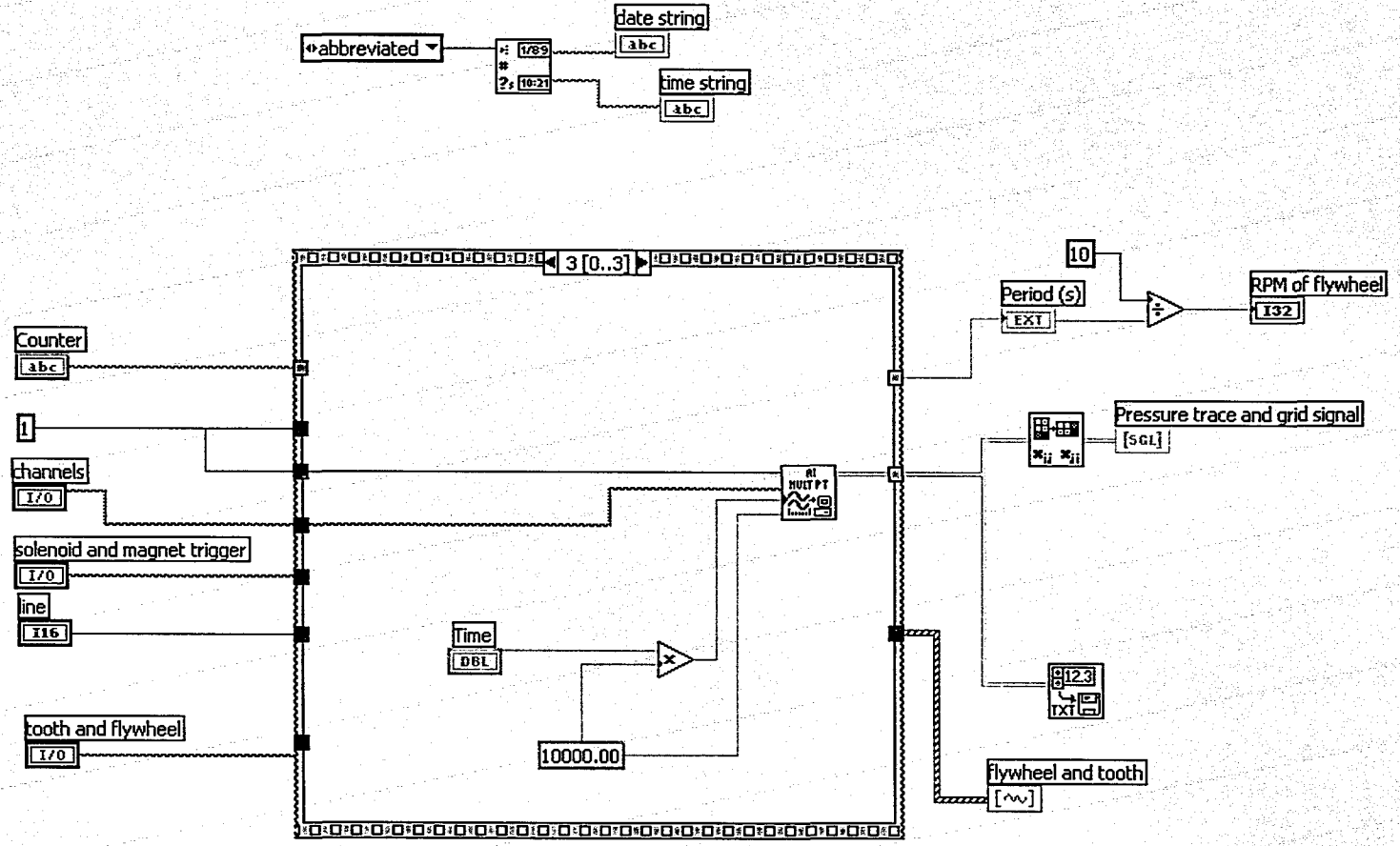


Figure A.4 Sequence Structure Frame 3 of Turbulent Experiment Control Program

## APPENDIX B

### MULTI-ZONE THERMODYNAMIC EQUILIBRIUM MODEL

#### PROGRAM PACKAGE

The details of the multi-zone thermodynamic equilibrium model in Matlab programming language are given in this appendix. The original program in Basic programming language can be consulted in [Ting 1995]. It contains five main programs:

- 1) *BMOB\_A02\_2.m*. generates the theoretical model of a propagating flame in a constant volume chamber.
- 2) *DATA\_labview\_F.m*. processes and transforms LabVIEW output file into Excel file.
- 3) *BP2\_02.m* interpolates the theoretical values into the experimental pressure trace.
- 4) *BV\_02.m* calculates the burning velocity .
- 5) *plot\_relation.m*. solves the laminar burning velocity at standard state. Note this program is used for quiescent combustion only.

The subroutines of the main program *BMOB\_A02\_2.m* are listed as following:

- 1) *EQCONST.m* figures out a set of constants used for calculating chemical equilibrium coefficients.
- 2) *Equiv2.m* calculates equivalence ratio of the given mixtures.
- 3) *REACTPROP2.m* calculates various properties and property coefficients.
- 4) *fngamR1.m* calculates specific ratio of the reactants.







```

[CC, CW, I, W, IC]=EQCONST;
[Equiv]=Equiv2(perc);
%-----
% Set the cell volume.
% Vtot is the bomb volume in m^3. It remains constant.

% RUNTYPE:
Vtot = 0.001882; % volume of cubical chamber
%Vtot = 0.001190867; % volume of cylinder chamber

%-----
% Enter initial conditions to work on.
% Input pressure and temperature in the room
prompt = {'Enter initial PRESSURE:(exp.101325Pa)',...
         'Enter initial TEMPETURE: (exp. 24C)'};
title = 'Input Information';
lines = 1;
def = {'101325','24'};
answer = inputdlg(prompt,title,lines,def);

Pinit = str2double(answer{1}); % pre-combustion pressure in Pa
Tinit = 273.15+str2double(answer{2}); % pre-combustion temperature in K

%-----
% INPUTSECTION:
% Echo back some of the initial parameters for the user

% fprintf('Volume of bomb %2.6f m^3 \n',Vtot);
Rbomb = (0.75 * Vtot / pi) ^ (1 / 3);
fprintf('Initial Temperature is %5.2fK \n', Tinit);
fprintf('Initial Pressure is %5.0f Pa \n', Pinit);
fprintf('Equivalence ratio is %5.3f\n',Equiv);

% GETN:

Ntot = 1500; %1500 elements
Nb = 500; %500 elements to burn
% fprintf('Burn %5.0f of %5.0f elements \n',Nb,Ntot);

%-----
% MAIN LOOP:

% SELECT ELEMENT for PROCESSING - will burn NB elements

% REACTPROP determines the reactant properties
[FCA,FHA,FOA,FMW,mOXY,MF,molR,mN2,MWR,R]=REACTPROP2(Equiv,FUEL,perc);

% MPR = kmol of fuel / element
% MWR = molar mass of reactant mixture (kg/kmol)

[k]=fngamR1(Tinit,FUEL,perc);
GMR = k;
Mass = MWR * Pinit * Vtot / rmol / Tinit;
fprintf('Initial mass is: %5.5f kg, \nMWR=%5.3f kg/kmol \n', Mass,MWR);

totWRK=0; % Initial value of total work done
SUMVBA = 0; % Initial value of the burnt volume
Pe=Pinit;

%-----
% Everything from here until the end of the loop is repeated NB times.

h = waitbar(0,'Calculating Main Loop...');

for I = 1 : Nb

    dVRatio=(I^(3/2)-(I-1)^(3/2))/Ntot^(3/2);

```

```

% MPR = Mass*dVRatio/MWR/(MF+mOXY+mN2);
MPR = Mass*dVRatio/MWR/molR;
% Pressure before burning element I% is set to Pinit if I%=1 or to Pe,
% the pressure after burning the last element, if I% is greater than 1.
% Pi is the initial pressure of the element (not to be confused with Pinit)

Pi=Pe; % instead of IF loop in Qbasic

% Estimate P after next element burns.
% Pe is the end pressure for the element which is just a guess now.

Pe = Pi + Equiv / Ntot^(3/2) * Pinit;

% Flag is set to 0 => that P is only a guess.

ifLP = 0;

% Treactants and GAMMAreactants are evaluated for this Pi.

Tr = Tinit * (Pi / Pinit) ^ ((GMR - 1) / GMR);

[k]=fngamR1(Tr,FUEL,perc);
GMR = k;

%CALCVOLUMES:
CALCVOLUMES=1; % CALCVOLUMES is a flag, 1 continue and 0 stop

while CALCVOLUMES==1
% This section now calculates the volume of the remaining unburnts before and
% after combustion of this element. The work done to compress the unburnts is
% evaluated and then a loop adds the work done to compress each previously
% burned element. if the correct pressure has been selected, the work done on
% all elements will equal the work done by the burning element during its
% combustion and expansion...ie it will match the difference between internal
% energy of that element before and after combustion. When this happens, the
% selected pressure will be the correct pressure after this element burns.

% if the correct pressure is guessed, the sum of the volumes will equal the
% total volume.

% VUB is the total volume of all the unburnt gases in m^3 BEFORE combustion
% of the Ith element (excludes the Ith element).
% VUA is the total volume of all the unburnt gases in m^3 AFTER combustion
% of the Ith element.

VuRatio = 1-(I/Ntot)^(3/2);
VUB = Vtot*VuRatio*(Pinit / Pi) ^ (1 / GMR);
VUA = VUB * (Pi / Pe) ^ (1 / GMR);

% Calculate the work of compression (VUB -> VUA) on unburnt elements in J.
% negative => work done By the burning element
WU = -(Pe * VUA - Pi * VUB) / (1 - GMR);

% Volume sum and work sum are set equal to the volume of unburned gas and
% work done to compress the unburned gas in m^3 and joules respectively.

SUMW = WU;

% if there are previously burned elements, calculate the volume of each before
% and after compression to new pressure, Pe. then calculate the work done to
% compress each one and add it to the work sum done by the burning element.

% VB is the volume of the Jth element before compression.
% VA is the volume of the Jth element after compression.
% WB is the compression work of the Jth element in Joules.
% negative => work done By the burning element
% SUMVBA is the volume of the burnt gases after combustion of element I.

% STORE(J,3) is the volume of the Jth element after combustion.

```

% STORE(J,1) is the pressure of the Jth element after combustion.  
 % STORE(J,9) is the specific heat ratio of products in element J. (=FNGAMP(T))

```

    if I > 1
      SUMVBA = 0;
      for J = 1:(I - 1)
        VB = STORE(J, 4) * (STORE(J, 1) / Pi) ^ (1 / STORE(J, 10));
        VA = STORE(J, 4) * (STORE(J, 1) / Pe) ^ (1 / STORE(J, 10));
        WB = -(Pe * VA - Pi * VB) / (1 - STORE(J, 10));
        % negative => work done by the burning element
        SUMVBA = SUMVBA + VA;
        SUMW = SUMW + WB;
      end
    end
    SUMV = VUA + SUMVBA;
    SUMW2 = SUMW;
  
```

% Use subroutine FLAME to find the temperature of combustion of the burning  
 % element knowing its starting conditions and work output, SUMW.

```
works = SUMW / MPR; % J/(kmol of fuel/element)
```

```
[T, MWR, MWP, molP, M]=FLAME2 (1,0,works,Pe,Tr,Equiv,FUEL,perc);
```

```
% T=abs(T);
```

% Calculate the volume this element would have if it burned to temperature T  
 % at pressure Pe. (MOLP is number of moles of products per mole of fuel, MOLR  
 % is moles of reactants per mole of fuel. Hence VE is in m<sup>3</sup> like V).

```
VE = Vtot*dVRatio* Pinit / Pe * T / Tinit * molP / molR;
```

% Compare this with volume left over from unburned gas and all previous burned  
 % elements at this pressure, Pe.

```
ErV = VE - (Vtot - SUMV);
```

% if the error is greater than .1%, then make a new estimate of pressure  
 % and go back to try again.

```

    ErrLim = VE * 0.0001;
    if Pi < 1.1 * Pinit
      ErrLim = VE * 0.001;
    elseif Pi > 2.5 * Pinit
      ErrLim = VE * 0.0002;
    end
  
```

```
if abs(ErV) > ErrLim
```

% ifLP is a flag which determines whether a previous estimate has been made.  
 % if it has, extrapolate/interpolate to get a new estimate.  
 % Otherwise, simply make a small step in pressure.

```

    if ifLP > 0
      Pe3 = (Pe * ERV1 - Pe1 * ErV) / (ERV1 - ErV);
      Pe1 = Pe;
      Pe = Pe3;
    else
      Pe1 = Pe;
      ifLP = 1;
      if ErV > 0
        Pe = Pi + 1.2 * (Pe - Pi);
      else
        Pe = Pe + (Pe - Pi) / 1.2;
      end
    end
    % Pe=abs(Pe);
  
```

```

% Having established this estimate for pressure after combustion,
% record the current volume error and go back to re-calculate the
% volumes and compression work with the new pressure value.

    ERV1 = ErV;
    CALCVOLUMES=1; % continue to run the while loop
else % if abs(ErV) <= ErrLim
    CALCVOLUMES=0; %stop the while loop
end %end if abs(ErV) > ErrLim
end %end while CALCVOLUMES==1

% Calculation of volumes having converged, enter values for the I%th element
% into the storage arrays STORE.

    STORE(I, 1) = Pe; %pressure of element after combustion
    RR(I) = ((Vtot - VUA) / Vtot) ^ (1 / 3);
    STORE(I, 2) = RR(I); %relative flame radius after element i burns
orR(I)=(I/Ntot); %relative radius before ignition
    STORE(I,3) = (I/Ntot)^(3/2); % mass fraction burnt

STORE(I, 4) = VE; %volume of element after combustion
    STORE(I, 5) = VUB; %volume of unburned before element has burned
    STORE(I, 6) = VUA; %volume of unburned after element has burned
    STORE(I, 7) = Tr; %temperature of the reactants
    STORE(I, 8) = T; %temperature of element after combustion
[k]=fngamR1(Tr,FUEL,perc);
STORE(I, 9) = k;

                                %specific heat ratio of reactants in element #I

    [k]=fngamP(T,M);
STORE(I, 10) = k;

                                %specific heat ratio of products in element I%
    STORE(I, 11) = MWP; %molecular weight of products

% Print out a running listing to let the user know the progress of the
% calculations that are going on.

%fprintf('%2.0f, %2.0f,P=%5.3f Pa, \n Tb=%5.3f K, r/R=%5.3f\n', i, N, Pe, t, RR);

% The total work done is summed in order to compare this program with
% STANJAN. (ie internal energy change = work done)

    totWRK = totWRK + SUMW2;
    % fprintf("TOTAL WORK DONE IS %5.5f, TOTWRK);

waitbar(I/Nb,h);
end % end for I = 1 : Nb

% This is the end of the main loop

%*****
%fprintf("TOTAL WORK DONE IS %5.5f J/kmol \n", totWRK);
fprintf('\n')
%-----
%Prepare the necessary data for writing to data file.
NR=Nb;
DD=zeros(NR,7);
DD(1, 1) = 0;
DD(1, 2) = Pinit / 1000; %Pa to kPa
DD(1, 3) = 0;
DD(1, 4) = 0;
DD(1, 5) = Tinit;
DD(1, 6) = Tinit;
[k]=fngamR1(Tinit,FUEL,perc);
DD(1, 7) = k;

for i = 2 : NR
    DD(i, 1) = i - 1;

```

```

        DD(i, 2) = STORE(i - 1, 1) / 1000; % Pa to kPa pressure of element after combustion
        DD(i, 3) = STORE(i - 1, 2); % relative flame radius after element i burns
        DD(i, 4) = STORE(i - 1, 3); % mass fraction burnt
        DD(i, 5) = STORE(i - 1, 7); % temperature of the reactants
        DD(i, 6) = STORE(i - 1, 8); % temperature of element after combustion
        DD(i, 7) = STORE(i - 1, 9); % specific heat ratio of reactants
    end

% Construct #(NR+1) row to save percentage of mixtures and
% equivalent ratio
    DD(NR+1,1)=Equiv;
    DD(NR+1,2)=Fco;
    DD(NR+1,3)=Fh2;
    DD(NR+1,4)=Fch4;
    DD(NR+1,5)=Fco2;
    DD(NR+1,6)=Fn2;
    DD(NR+1,7)=Fair;
end
% -----
% Save the theoretical data to a file

    cd('H:\combustion model\theory\');

[fname,newpath] = uiputfile('H:\combustion model\theory\'*.csv','Choose Output File Name');

file = fopen(fname,'w'); % creat a new file

% Write the data to the file
[n,m] = size(DD);
for i = 1:n
    for j = 1:m
        if j == m
            fprintf(file,'%5.7f\n',DD(i,j));
        else
            fprintf(file,'%5.7f;',DD(i,j));
        end
    end
end
end

fclose(file); % close the file

cd('H:\combustion model\')
% -----
% End of the program.

function DATA_labview_F

% Sep 2005 Guofang Jiang ( some changes were made)
% July 2002 Panfeng Han
% -----
% Substitute for 4CD16G.BAS & 4CHPLT.BAS
% 1992 & 1993 DSK TING
%
% This program reads data from a EXCEL file obtained from
% Labview program D:\hanfeng\research\program\han1.vi
% and then change it to pressure. AFTER FILTER, save it.
%
% It saves pressure from spark to max
% SAMPLE RATE and STANDARD PRESSURE should be checked before
% the program is run

    %%%%%%%%%%%%%%% File reading %%%%%%%%%%%%%%%

    % File Selection
    cd('H:\combustion model\labview\'); % This folder should be the initial data from Labview
    d = dir('H:\combustion model\labview\');
    str = {d.name};
    [s,g] = listdlg('PromptString','Select a file!');...

```

```

'SelectionMode','single',...
'ListString',str); % Open file

file=str(s);
fid=fopen(file,'r');

if fid==-1
    errordlg(' The file could not be opened!');
end

% Read file
data=xlsread(file);

% Close file
fclose(fid);
cd('H:\combustion model\');

[row,col]=size(data);

% save every column as a variable
colu=data(:,1); % Column 1 is the pressure trace

%%%%%%%%%%%%%%%%%%%%%%%%%%%%%%%%%%%%%%%%%%%%%%%%%%%%%%%%%%%%%%%%%%%%%%%%

f = 10000; %sample rate, from Labview program

dt=1/f; % sec

% Input pressure in the room
prompt = {'Enter room PRESSURE:(exp.708mmHg)'};
title = 'Input Information';
lines = 1;
def = {'692'};
answer = inputdlg(prompt,title,lines,def);

Patm = 101325/760*str2double(answer{1}); % room pressure Pa
% fprintf('the room atmosphere pressure is %5.2f Pa \n',Patm);
p=15*6894.75*colu+Patm; % convert voltage to pressure Pa

Pstand=101325; % 1 Standard Atmosphere Pressure

% Vol=(Pstand-Patm)/15/6894.73 % voltage corresponds to Pinit

% colu=roundn(colu,-3); % round voltage to 10^(-3) digs

% I is a vectore of indictes of beginning elements of colu1
% I=find(colu==roundn(Vol,-3)); % Pinit is NOT room pressure
% I=find(colu1==0); % Pinit is room pressure

% if isempty(I)==1 % voltage corresponding to Pinit cannot be found
% Vol=colu(1); % the 1st value is thought as Pinit
% I=find(colu==Vol);
%end

% indstart=max(1); % Index of the beginning of the spark (indstart)
% indstart=55; % 55 is chosen as roughly present spark point
% indstart =2109;
indstart=2066;

for i=1:row
    if p(i)==max(p);
        indend=i; % Index of the maximum pressure
        break
    end
end

% Pressure from spark to maximum, also is saved later

```







```

'SelectionMode','single',...
'ListString',str); % Open file

file=str(s);
fid=fopen(file,'r');

if fid==1
    error(' The file could not be opened!');
end

% Read file
ED=csvread(file);

% Close file
fclose(fid);
cd('H:\combustion model\');

[NRR,NCC] = size(ED)
%-----

% Set the maximum #points, -- EXPERIMENTAL POINT
NP=NRR;
if NP > 1500
    NP = 1500;
end

%-----
% Set the maximum pressure to analyze THEORETICAL POINT

%INPUTSECTION:
ED(NRR) % experimental maximum pressure
MaxP =0.8* max(DD(1:DNR-1,2)) % factor is an number according to pressure.
% fprintf('Maximum pressure to analyze =%5.3f kPa\n', MaxP);

%-----
% Set up TIME array and determine the #points to analyze

for I = 1: NP-1
    Time(I) = dt*(I-1); %start at time zero

    if ED(I) > MaxP
        IMAXP = I - 1; %end point to analysis
        break
    %GOTO TimeS
end

end

%-----
% This is the start of the main loop where interpolation is done to
% determine various quantities from a data base file based on measured
% pressure.

Res(1, 1) = Time(1); % Time in ms.
Res(1, 2) = DD(1, 2); % Pressure after combustion of element.
Res(1, 3) = 0; % relative radius of flame vs bomb radius
Res(1, 4) = 0; % mass fraction burned
Res(1, 5) = DD(1, 5); % unburned gas temperature after combustion
Res(1, 6) = DD(2, 6); % temperature of element after combustion
Res(1, 7) = DD(1, 7); % specific heat ratio of reactants

for I = 1 : IMAXP

% IMAXP decides the dimension of Res. MaxP decides value of IMAXP.
% IMAXP comes from #row of ED

Res(I, 1) = Time(I);
Res(I, 2) = ED(I);

```



```

% DD(, 1) * Time in ms.
% DD(, 2) * Pressure after combustion of element.
% DD(, 3) * relative radius of flame vs bomb radius
% DD(, 4) * mass fraction burned
% DD(, 5) * unburned gas temperature after combustion
% DD(, 6) * temperature of element after combustion
% DD(i, 7) * specific heat ratio of unburnt mixture

% Open the data file saved by BP2_02_1.m

cd('d:\combustion model\result');
d = dir('d:\combustion model\result\');
str = {d.name};
[s,g] = listdlg('PromptString','Select a file:',...
    'SelectionMode','single',...
    'ListString',str); % Open file

file=str{s};
fid=fopen(file,'r');

% Read file
DD=csvread(file);
% Close file
fclose(fid);
cd('d:\combustion model\');

[Nrow,Ncol]=size(DD);

% -----
% Calculate the burning velocity using geometric methods
%
% Define some initial condition
Pinit = DD(1,2); % pre-combustion pressure in Pa
Tinit = DD(1,5); % pre-combustion temperature in K
% Vtot = 0.001882; %the bomb volume in m^3. It remains constant.
% Vtot = 0.0011717; % volume of past cylinder chamber from (Checkel 1995)
% Vtot = 0.001190867; % volume of current cylinder chamber
Vtot=0.001882 % the cubical chamber total volume
Rcell = (0.75 * Vtot / pi) ^ (1 / 3); % m
TimeL=DD(1,1);

Rlast=0;
for j=2:Nrow-1
    Rb(i)=DD(i,3)*Rcell; % flame radius m

    dVjk=Pinit*DD(i-1,5)*Vtot/Tinit/DD(i-1,2); % flame volume

    dVub=dVjk*(DD(i,4)-DD(i-1,4));
    time(i)=DD(i,1);
    dt=(time(i)-TimeL)*0.001; %convert ms to s

    Rflame=sqrt((Rlast^2+Rb(i)^2)/2);

    deltaV=4/3*pi*Rflame^3+dVub;
    if deltaV < 0
        Ri(i)=0;
    else
        Ri(i)=(0.75/pi*deltaV)^(1/3);
    end

    dRi=Ri(i)-Rflame;
    Su(i)=(dRi/dt)*100; %convert m/s to cm/s

% Flame Growth Rate:
GRate(i)=((Rb(i)-Rlast)/dt)*100; %convert m/s to cm/s
Rlast=Rb(i);
TimeL=time(i);
XRB(i)=Rb(i)*1000; % convert m to mm

```



```

% *****
% %%%SAVE DATA%%
fprintf('\n')
cd('d:\combustion model\burning velocity');

[fname,newpath] = uiputfile('d:\combustion model\burning velocity\*.csv','Choose Output File Name');

% Detect if the filename is '*.csv'
if findstr(fname,'.csv')==isempty(fname)
    errorlg('filename should has csv','wrong file name');
end

file = fopen(fname,'w'); % creat a new file

% Write the data to the file
[n,m] = size(MD);
for i = 1:n
    for j = 1:m
        if j == m
            fprintf(file,'%5.6f,\n',MD(i,j));
        else
            fprintf(file,'%5.6f,',MD(i,j));
        end
    end
end
fclose(file); % close the file

cd('d:\combustion model')

function plot_relation

% Sep 2004 checked and corrected)
%-----Guofang Jiang
%Panfeng Han Feb 2003
% Based on plot_relation
% by Jacob Komar, August 7, 2002
%
% This functin plots the results of curve fitting.
% It calculates curve fit and confidence
% interval.
%
% Su from (1-1.05) is thought as noise and totally deleted
% Su from (1.05-2.2) is fitted, and from (1.05-2.2) is
% curve fitted.
%
% the idea of analysis of data comes from
% Experimental Methods for Engineers
% J.P.Holman, 7th Edition 2001

Patm=101.325;

cd('h:\combustion model\burning velocity');
d=dir('h:\combustion model\burning velocity');
str = {d.name};
[s,g] = listdlg('PromptString','Select a file:',...
    'SelectionMode','single',...
    'ListString',str); % Open file

file=str{s};
fid=fopen(file,'r');

if fid==-1
    errorlg(' The file could not be opened!');
end

```

```

% Read file
DD=csvread(file);

% Close file
fclose(fid);

[Nrow,Ncol]=size(DD);

cd('h:\combustion model');

Perc=[DD(Nrow-3,1:5) DD(Nrow-2,1:5)];
Equiv=Perc(1);
P=DD(1:Nrow-4,1); % pressure
Rb=DD(1:Nrow-4,2); % flame radius
Su=DD(1:Nrow-4,3); % burning velocity
Tu=DD(1:Nrow-4,4); % unburnt temperature
gam=DD(1:Nrow-4,5); % specific heat ratio of reactants

% only burning velocity <= 2.2*Patm is left
r = find(P>(2.2*Patm));
rmin=min(r);
if isempty(rmin)==1
    rmin=length(P);
end

% 1.05-2.2
b=find(P<1.05*Patm);
bmax=max(b);
p1=P(bmax:rmin);
su1=Su(bmax:rmin)
k1=gam(bmax:rmin);
n=length(su1);

% -----
legendN=sprintf('Equivalent Ratio %.1f',Equiv);

plot(p1,su1,'o')
hold on

[suf]=Pfilter(su1,3); % filter the burning velocity
su1=suf;
% *****
% %%% curve fitting %%%
% *****

% Laminar burning velocity (cm/s)
% SL=SL0*(PI/P0)^Pexp*(Tr/T0)^Texp;
% Tr/T0 = (PI/P0)^[(k-1)/k]

% 1.05-2.2

Pexp=-0.16+0.22*(Equiv-1);
Texp=2.18-0.8*(Equiv-1);

exp=Pexp+Texp*(k1-1)/k1;
px1=(p1/Patm).^exp;
h = polyfit(px1,su1,1);
y1 = polyval(h,px1);

size(p1)
size(y1)
% standard deviation is obtained from 1.05-2.2Patm
s=sqrt(sum((su1-y1).^2)/(n-1))
disp('1')

% *****

```

```

% the standard deviation should be less than or equal to 2cm/s
while s > 2
    d=s*1.96 % 95% confidence interval
    j=1;
    for i=1:n
        if su1(i)>=y1(i)-d & su1(i)<=y1(i)+d
            su2(j)=su1(i);
            p2(j)=p1(i);
            k2(j)=gam(i);
            j=j+1;
        end
    end

n=length(su2);

% curve fit again

exp2=Pexp+Texp*(k2-1)./k2;
px2=(p2/Patm).^exp2;
h=polyfit(px2,su2,1);
y2=polyval(h,px2);

s=sqrt(sum((su2-y2).^2)/(n-1))
size(su2)
size(y2)
disp('2')

plot(p2,su2,'o',p2,y2)
ylim([20 60])

% rename the variables
gam=k2'; p1=p2'; su1=su2'; y1=y2';
% plot(px2,su2,'o',px2,y2,'-r')

clear su2 p2 k2 exp2 px2 y2

end % while s > 2

% -----
% confidence interval for the newest standard deviation
% the final error should be less than or equal to 1cm/s

d=s*1 % 68% confidence interval
size(p1)
size(su1)
size(y1)
plot(p1,su1,'+r',p1,y1)
hold on
j=1;
for i=1:n
    if su1(i)>=y1(i)-d & su1(i)<=y1(i)+d
        su2(j)=su1(i);
        p2(j)=p1(i);
        k2(j)=k1(i);
        j=j+1;
    end
end
n=length(su2);

% final curve fit
exp=Pexp+Texp*(k2-1)./k2;
px=(p2/Patm).^exp;
h=polyfit(px,su2,1);
y=polyval(h,px);

% justify if points in(1~1.05) includes or not
% ex is extra

```



```

p_ex=P(1:bmax-1);
k_ex=gam(1:bmax-1);
exp_ex=Pexp+Texp*(k_ex-1)./k_ex;
px_ex=(p_ex/Patm).^exp_ex;
y_ex=h(1)*px_ex+h(2); % 1~1.05 straight line

su_ex=Su(1:bmax-1); % 1~1.05 su
m=length(su_ex);

% justify if there is points between the 1std range
j=1;
for i=1:m
    if su_ex(i)>=y_ex(i)-d & su_ex(i)<=y_ex(i)+d
        su2_ex(j)=su_ex(i);
        p2_ex(j)=p_ex(i);
        k2_ex(j)=k_ex(i);
        j=j+1;
    end
end

Ptrace=[p_ex' p1'];
BV=[su_ex' su1'];

plot(p2,su2,'sk',p2,y,'-k')
hold on
plot(p_ex,su_ex,'>m',p_ex,y_ex,':')
ylim([20 80])
xlabel('pressure (kPa)')
ylabel('burning velocity (cm/s)')
legend('original data','filtered data','1st curve fitting','fitted data','2nd curve fitting','data at 1-1.05Patm','extrapolated line',4);

%*****
% su--value1 @ 101.325 kPa
%
% extrapolate gam @ 101.325 kPa
t=min(find(P>=101.325)); % indicate greater than 101.325
u=max(find(P<101.325)); % indicate less than 101.325
if isempty(u)==1
    u=t+1; % extrapolate
    gam=gam(t)+(gam(u)-gam(t))*(101.325-P(t))/(P(u)-P(t));
else % interpolate
    gam=gam(u)+(gam(t)-gam(u))*(101.325-P(u))/(P(t)-P(u));
end

exp=Pexp+Texp*(gam-1)./gam;
px=1.^exp
v(1)=h(1)*px+h(2)
Equiv;
diluent=Perc(5)+Perc(6);

% su--value2 @ 202.65 kPa
%
% interpolate gam @ 202.65 kPa
t=min(find(p1>=202.65)); % indicate greater than 202.65
u=max(find(p1<202.65)); % indicate less than 202.65

k=k1(u)+(k1(t)-k1(u))*(202.65-p1(u))/(p1(t)-p1(u));

exp=Pexp+Texp*(k-1)./k;
px=2.^exp;
v(2)=h(1)*px+h(2)
%end of program

Function [CC, CW, I, W, IC]=EQCONST

% EQCONST

```

```

% 09-DEC-87 M.D. CHECKEL
% 14-SEP-92 Cleaned up, checked and organized.
% -- D.S-K. Ting
% 28-JUNE-2002 Change to Matlab and combine EQCONST & PROPCOEFF
% -- Panfeng Han
%
% This subroutine EQCONST calculates a set of constants used for calculating
% chemical equilibrium coefficients for CO2 dissociation and the Water-Gas
% reaction. The basic idea is to minimize the gibbs free energy in the
% equilibrium mixture.
%  $\ln(Kp) = -\{ \sum[\nu_i g(T)]_p - \sum[\nu_i g(T)]_r \} - \Delta G_{298} / (R \cdot T)$ 
% where  $\nu_i$  is the stoichiometric coefficient for each reactant and product
% and  $\Delta G_{298}$  is the difference in gibbs energy of formation at 298 k.

% The subroutine also fills an array with coefficients used in
% calculating enthalpy and Gibbs function for CO, CO2, H2, H2O, N2, O2,
% and fuel. It also calculates chemical equilibrium constants used
% for CO2 and CO2-H2O dissociation reactions. The IC() array is used for
% this.
%-----

% the data for the coefficients.
% IC() is the coefficient array.
IC= [3.317 3.7697e-4 -3.2208e-8 -2.1945e-12 0 4.63284 -1.13882e8;... %CO
3.0959 2.73114e-3 -7.88542e-7 8.66002e-11 0 6.58393 -3.93405e8;... %CO2
3.43328 -8.181e-6 9.6699e-8 -1.44392e-11 0 -3.8447 0;... %H2
3.74292 5.65590e-4 4.9524e-8 -1.81802e-11 0 0.96514 -2.39082e8;... %H2O
3.34435 2.9426e-4 1.953e-9 -6.5747e-12 0 3.75863 0;... %N2
3.25304 6.5235e-4 -1.49524e-7 1.53897e-11 0 5.71243 0;... %O2
1.13711 1.45532e-2 -2.95876e-6 0 0 0 0 -0.90510e8;... %C3H8
1.93529 4.96462e-3 -1.24402e-6 1.62497e-10 -8.58611e-15 8.153 -6.69305e7]; %CH4

% CO2 dissociation: CO + (1/2) O2 <-> CO2
%  $K_{co2} = M_{CO2} / (M_{CO} \cdot \sqrt{M_{O2}} \cdot (P/P_n))$ 
%
% CO O2 CO2
CC(1) = IC(1, 1) + IC(6, 1) / 2 - IC(2, 1); % 1st
CC(2) = IC(1, 2) + IC(6, 2) / 2 - IC(2, 2); % 2nd
CC(3) = (IC(1, 3) + IC(6, 3) / 2 - IC(2, 3)) / 2; % 3rd
CC(4) = (IC(1, 4) + IC(6, 4) / 2 - IC(2, 4)) / 3; % 4th
CC(5) = IC(1, 6) + IC(6, 6) / 2 - IC(2, 6); % 5th
CC(6) = IC(1, 7) + 0 - IC(2, 7); % hoR-hoP

%-----
% Water-Gas reaction: CO + H2O <-> CO2 + H2
%  $K_{wg} = M_{CO2} \cdot M_{H2} / (M_{CO} \cdot M_{H2O})$ 
%
% CO2 H2 CO H2O
CW(1) = -IC(2, 1) - IC(3, 1) + IC(1, 1) + IC(4, 1); % 1st
CW(2) = -IC(2, 2) - IC(3, 2) + IC(1, 2) + IC(4, 2); % 2nd
CW(3) = (-IC(2, 3) - IC(3, 3) + IC(1, 3) + IC(4, 3)) / 2; % 3rd
CW(4) = (-IC(2, 4) - IC(3, 4) + IC(1, 4) + IC(4, 4)) / 3; % 4th
CW(5) = -IC(2, 6) - IC(3, 6) + IC(1, 6) + IC(4, 6); % 5th
CW(6) = -IC(2, 7) - 0 + IC(1, 7) + IC(4, 7); % hoR-hoP

%-----

% I() is the alphanumeric name.
% W() is the molecular weight.

% The coefficients and methods of use are described in:
% Rowland S. Benson
% "Advanced Engineering Thermodynamics"
% Pergammon Press, 1977, 2nd Edition
% (eg pg 153, Appendix A)

```

% Propane is per Benson & Baduah, Int J Mech Eng Educ, Vol 4, No 1, p 93

%-----  
I = {'CO', 'CO2', 'H2', 'H2O', 'N2', 'O2', 'C3H8', 'CH4'};  
W = [28.0134 44.00995 2.016 18.016 28.0155 31.9988 44.09 16.04];  
%P = IC; % another coefficient for thermodynamic properties

**function [Equiv]=Equiv2(perc)**

% Equiv.m  
% Mar-2003 -- Panfeng Han  
%  
% Equivalence ratio calculation  
% The method comes from  
% Dr.Checkel "Combustion Engine"  
% handout notes 2002  
% Page 2.11  
% equiv=sum(+V)/sum(-V)  
% V is chemical valence  
% [O -2] [N 0] [H +1] [C +4]  
%  
% as to lean methane-air mixture, if we use this method  
% and include the oxygen & carbon in products which correspond  
% to stoich as there was no free oxygen in our residual, that  
% averages some equiv=1.0 makes it effectively a little less lean  
%  
% For Example: [Equiv]=Equiv(perc)

Fco = perc(1);  
Fh2 = perc(2);  
Fch4 = perc(3);  
Fc3h8 = perc(4);  
Fco2 = perc(5);  
Fn2 = perc(6);  
Fair = perc(7);

% positive valence  
Vp=Fco\*4+Fh2\*2+Fch4\*8+Fc3h8\*20+Fco2\*4;

% negative valence  
Vn=Fco\*2+0.2095\*Fair\*4+Fco2\*4;

% Equivalence ratio  
Equiv=Vp/Vn;

**function**

**[FCA,FHA,FOA,FMW,mOXY,MF,molR,mN2,MWR,R]=REACTPROP2(Equiv,FUEL,perc)**

%-----

% COMPLETED

% REACTPROP

% 09-DEC-87 M.D. CHECKEL  
% 14-SEP-92 Cleaned up, checked and organized.  
% -- D.S-K. Ting  
% JUNE-2002 Change to Matlab  
% -- Panfeng Han  
% NOV-2002 Change to fuel mixtures  
% -- Panfeng Han  
%

% This routine calculates various properties and property coefficients for  
% hydrocarbon fuels + air mixture.  
% Rowland S. Benson  
% "Advanced Engineering Thermodynamics"  
% Pergammon Press, 1977, 2nd Edition  
% (Appendix A)

```

% The fuel is described as FCA=number of carbons per molecule (eg 3 for C3H8)
%           FHA=number of hydrogens per molecule(eg 8 for C3H8)
%           FOA=number of oxygens per molecule (eg 1 for CO)
%           FMW=fuel molar mass kg/kmol (eg 44.09 for C3H8)
%
% The air is assumed to be 21% oxygen and 79% nitrogen (molar ratio 3.76190)
% The mixture strength is described as:
%           Equiv=(F/A)ratio / (F/A)stoich (<1=lean, >1=rich)
%
% The property coefficients of the mixture are calculated from the individual
% element coefficients stored in IC(7,6). IC(7,6) contains coefficients as
% described in EQCONST.
%
% Inputs:   FUEL is a string array with fuel name, eg (CO H2 CH4)
%
% Outputs:  MF = 1 if fuel is present, 0 if it is not
%           mOXY = moles of oxygen per mole of fuel
%           mN2 = moles of nitrogen per mole of fuel
%           MWR = molar mass of reactants in kg/kmol
%           R(I) = mixture property coefficients to calculate mixture
%                 properties in J/kmol and J/kmol.k

```

```

%-----

```

```

[CC, CW, I, W, IC]=EQCONST;

```

```

Fco = perc(1);
Fh2 = perc(2);
Fch4 = perc(3);
Fc3h8 = perc(4);
Fco2 = perc(5);
Fn2 = perc(6);
Fair = perc(7);

```

```

Frac = sum(perc(1:6));
fco = perc(1)/Frac;
fh2 = perc(2)/Frac;
fch4 = perc(3)/Frac;
fc3h8 = perc(4)/Frac;
fco2 = perc(5)/Frac;
fn2 = perc(6)/Frac;

```

```

for i=1:length(FUEL)

```

```

%Judge the fuel and obtain the FCA, FHA and mWR

```

```

switch FUEL {i}
case {'CO'}
    FMW=28.0134;
    F(i)=fco*(1 + 0 / 4 - 1/2);
    FCA(i)=1*fco;
    FHA(i)=0;
    FOA(i)=1*fco;
    MW(i)=FMW*fco;

case {'H2'}
    FMW=2.016;
    F(i)=fh2*(0 + 2 / 4 - 0/2);
    FCA(i)=0;
    FHA(i)=2*fh2;
    FOA(i)=0;
    MW(i)=FMW*fh2;

case {'CH4'}
    FMW=16.043;
    F(i)=fch4*(1 + 4 / 4 - 0/2);

```

```

FCA(i)=1*fch4;
FHA(i)=4*fch4;
FOA(i)=0;
MW(i)=FMW*fch4;

case {'C3H8'}
    FMW=44.09;
    F(i)=fc3h8*(3 + 8 / 4 - 0/2);
    FCA(i)=3*fc3h8;
    FHA(i)=8*fc3h8;
    FOA(i)=0;
    MW(i)=FMW*fc3h8;

case {'CO2'}
    FMW=44.00995;
    F(i)=0;
    FCA(i)=fco2*1;
    FHA(i)=0;
    FOA(i)=2*fco2;
    MW(i)=FMW*fco2;

case {'N2'}
    FMW=28.0155;
    F(i)=0;
    FCA(i)=0;
    FHA(i)=0;
    FOA(i)=0;
    MW(i)=FMW*fn2;

otherwise
    disp('Input correct fuel again')
end

end

if Fco+Fch4+Fc3h8==0 % only Hydrogen exits
    Fair=1-Fh2-Fco2-Fn2; % AIR percentage
    FCA=Fair*0.0314/100; % FCA is the percentage of carbon dioxide
end

FCA=sum(FCA); % number of carbons per molecule FULE mixtures
FHA=sum(FHA); % number of hydrogens per molecule FULE mixtures
FOA=sum(FOA); % number of oxygens per molecule FULE mixtures
FMW=sum(MW); % mixture molar mass
F=sum(F); % stoichiometric oxygen moles

% Determine the number of moles of OXYGEN that per molar fuel
% mixture need theoretically and whether or not fuel is present.
if Equiv > 0

    % positive valence
    Vp=fco*4+fh2*2+fch4*8+fc3h8*20+fco2*4;
    % Oxygen from air on basis of air for 1 mole of fule
    MOXY=(Vp/Equiv-fco*2-fco2*4)/4;
    % Total oxygen
    mOXY=MOXY+FOA/2;
    MF = 1;
else
    mOXY = 0.21;
    MF = 0;
end

%-----
% Based on the number of moles of oxygen, determine the number of moles of
% reactant, number of moles of nitrogen, and molecular weight of reactants.

mN2 = MOXY * 0.7905/0.2095;
molR = MF + MOXY + mN2;
MWR = (MOXY * W(6) + mN2 * W(5) + MF *FMW) / molR;

```

```

%-----
% Calculate the mixture property coefficients.

for i = 1:7
    K(i)=fc3h8*IC(7, i)+fch4*IC(8,i)+fco*IC(1,i)+fh2*IC(3,i);
    R(i) = K(i)+fco2*IC(2,i)+fn2*IC(5,i) + MOXY* IC(6, i) + mN2 * IC(5, i);
end
%-----
% End of Program

function [k]=fngamR1(T,FUEL,perc)

% Program to calculate k
% MD CHECKEL 11 DECEMBER, 1987
% (BASIC)
% SENTHIL PONNUSAMY 4 JULY, 2002
% (MATLAB)
% PANFENG HAN AUGUST, 2002
% ---Correct

% Read in the data for the property coefficients.
% Data statements are at end of the "main" program.
%
%
% Data taken from : R.S Benson, Advanced Engineering Thermodynamics
% 2nd Ed,1977. Appendix A
%

Rmol=8314.3;

[CC, CW, I, W, IC]=EQCONST;

% CO=1, H2=3,C3H8=7, CH4=8 CO2=2 O2=6 N2=5

Fco = perc(1);
Fh2 = perc(2);
Fch4 = perc(3);
Fc3h8 = perc(4);
Fco2 = perc(5);
Fn2 = perc(6);
Fair = perc(7);

sumCp=0;

for j=1:length(FUEL)

    switch FUEL{j}
    case {'CO'}
        i=1;
        Cp = Fco*Rmol * (IC(i,1) + 2 * IC(i,2) * T + 3 * IC(i,3) * T ^ 2 + 4 * IC(i,4) * T ^ 3 + 5 * IC(i,5) * T ^ 4);
    case {'H2'}
        i=3;
        Cp = Fh2*Rmol * (IC(i,1) + 2 * IC(i,2) * T + 3 * IC(i,3) * T ^ 2 + 4 * IC(i,4) * T ^ 3 + 5 * IC(i,5) * T ^ 4);
    case {'C3H8'}
        i=7;
        Cp = Fc3h8*Rmol * (IC(i,1) + 2 * IC(i,2) * T + 3 * IC(i,3) * T ^ 2 + 4 * IC(i,4) * T ^ 3 + 5 * IC(i,5) * T ^ 4);
    case {'CH4'}
        i=8;
        Cp = Fch4*Rmol * (IC(i,1) + 2 * IC(i,2) * T + 3 * IC(i,3) * T ^ 2 + 4 * IC(i,4) * T ^ 3 + 5 * IC(i,5) * T ^ 4);
    case {'CO2'}
        i=2;
        Cp = Fco2*Rmol * (IC(i,1) + 2 * IC(i,2) * T + 3 * IC(i,3) * T ^ 2 + 4 * IC(i,4) * T ^ 3 + 5 * IC(i,5) * T ^ 4);
    end

    sumCp=Cp+sumCp;

end

```

```

% N2 and O2 fraction in Air
F_o2 = Fair*0.2095;
F_n2 = Fair*0.7905;

% N2 -- diluent + fraction in air
Cp_n2=(Fn2+F_n2)*Rmol * (IC(5,1) + 2 * IC(5,2) * T + 3 * IC(5,3) * T ^ 2 + 4 * IC(5,4) * T ^ 3 + 5 * IC(5,5) * T ^ 4);
% O2 -- fraction in air
Cp_o2=F_o2*Rmol * (IC(6,1) + 2 * IC(6,2) * T + 3 * IC(6,3) * T ^ 2 + 4 * IC(6,4) * T ^ 3 + 5 * IC(6,5) * T ^ 4);

sumCp=sumCp+Cp_o2+Cp_n2;

k = sumCp / (sumCp - Rmol);    %GAMMA(reactants)

function [T, MWR, MWP,molP,M]=FLAME2(IND, Q, WORK, PE, TR,Equiv,FUEL,perc)

%   FLAME   Calculating Temperature
%   10-DEC-87   M.D. CHECKEL
%   13-SEP-92   Cleaned up, checked and organized.
%               -- D.S-K. Ting
%   JUNE-2002   Changed to Matlab
%               -- Panfeng Han
% INPUTS:
%   IND = 0 for constant pressure, 1 for varying pressure
%   Q   = heat transfer TO the element during combustion
%   W   = work transfer FROM the gas during combustion (=0 if IND=0) (J/element)
%   - the units of Q and W are ( J/(1 kmol fuel + associated air) )
%   PE = pressure at the end of combustion (Pa)
%   Equiv = stoichiometric ratio (0<S<1) = (F/A)/(F/A)stoic
%   TR  = reactant mixture temperature (K)
%   MPR = kmol of fuel / element
%   FUEL = kind of fuel

% OUTPUTS:
%   T   = flame temperature at equilibrium (K)
%   MWR = molar mass of reactant mixture (kg/kmol)
%   MWP = molar mass of products mixture (kg/kmol)

%-----
% Get the properties and property coefficients of the reactants.

[FCA,FHA,FOA,FMW,mOXY,MF,molR,mN2,MWR,R]=REACTPROP2(Equiv,FUEL,perc);
[CC, CW, I, W, IC]=EQCONST;
rmol = 8314.3;    %ideal gas constant in J/kgmol.k
PN = 101325;     %standard atmosphere (for Go and So)

% calculate enthalpy of reactants in J/kmol at temperature TR

x = R(2) * TR + R(3) * TR ^ 2 + R(4) * TR ^ 3 + R(5) * TR ^ 4;
enthr = rmol * TR * (R(1) + x) + R(7);

% Guess the initial temperature (based on equivalence ratio).

T = TR + 2200 * Equiv;
eri=0; %initial error value

T1 = 0;
T3 = 0;
FLAG = 0;

%-----
% Use subroutine EQCOMP to calculate equilibrium composition at temp T.
% Then calculate the work and energy quantities for first law analysis.

GETCOMP=1;
while GETCOMP==1 % GETCOMP is a flag, 1=continue, 0=stop

```

```

[M,molP,MWP,P]=EQCOMP2(PE,T,Equiv,FUEL,perc);

if T <= 0

    T = 2000;
    T1 = 0;
    T3 = 0;
    FLAG = 0;
    [M,molP,MWP,P]=EQCOMP2(PE,T,Equiv,FUEL,perc);

end

% Calculate enthalpy of products in kJ/kgmol at temperature T
x = P(1) + P(2) * T + P(3) * T ^ 2 + P(4) * T ^ 3 + P(5) * T ^ 4;
enthp = rmol * T * x + P(7);

    if IND == 0 %constant pressure
        eri = enthr + Q - enthp;    % mdc 910712: include HEAT
    else

        intr = enthr - molR * TR * rmol; % internal energy
        intp = enthp - molP * T * rmol;
        eri = intr + Q - WORK - intp;

    end

%-----
% Check the "balance" error in the first law of thermodynamics.
% If error is < 1000 J/(1 kmol.fuel + associated air), then T is OK, end.

    if abs(eri) >= 1000

% try new combustion T.
% For the first iteration, just add or subtract 10 K.

if FLAG == 0

    T1 = T;

        FLAG = 1;

        if eri < 0
            T = T - 10;
        else
            T = T + 10;
        end

% For later estimates, use geometric interpolation.

else

        T3 = (T * ET - T1 * eri) / (ET - eri);
        T1 = T;
        T = T3;
        FLAG = FLAG + 1;

end

    ET = eri;
    GETCOMP=1;

else % if abs(eri) < 1000

    GETCOMP=0;
    break % terminate the program
end % end of if abs(eri) >= 1000

```



```
end % end of while GETCOMP==1
% End of function.
```

```
function [M,molP,MWP,P]=EQCOMP2(PE,T,Equiv,FUEL,perc)
```

```
% EQCOMP1 Equilibrium composition calculation
% *****
% 09-DEC-87 M.D. CHECKEL
% 14-SEP-92 Cleaned up, checked and organized.
% -- D.S-K, Ting
% JUN-2002 Changed to Matlab
% -- Panfeng Han
%
% This subroutine calculates the equilibrium composition of a hydro-carbon
% + air flame given a temperature, T. Additional information is the set of
% coefficients calculated in the main program for the CO2 dissociation and
% the water-gas reactions which are the only two reactions considered.
%
% Information is returned as M(1) which are numbers of moles/mole of fuel.
% M(1)=mCO, M(2)=mCO2, M(3)=mH2, M(4)=mH2O, M(5)=mN2, M(6)=mO2
% equation 1*FUEL+a*O2+3.76*a*N2=M(1)*CO+M(2)*CO2+M(3)*H2+M(4)*H2O+M(5)*N2+M(6)*O2
% INPUT PE: pressure
% MF: moles fuel
% MWR: mole weight(reactants)
% FCA: fuel carbon atoms
% FHA: fuel hydrogen atoms
%
% OUTPUT M: mole number of products
% molP: total mole number of products
% MWP: mole mass of products
% P: coefficients of products
%
% The 6 constants (A1-A6 per Benson and Hfo) are also calculated for the
% equilibrium product mixture and returned as P(1) through P(7).
%
[FCA,FHA,FOA,FMW,mOXY,MF,molR,mN2,MWR,R]=REACTPROP2(Equiv,FUEL,perc);
[CC, CW, I, W, IC]=EQCONST;

rmol = 8314.3; %ideal gas constant in J/kgmol.k
PN = 101325; %standard atmosphere (for Go and So)

M(5) = mN2;

quit = 1; % flag to jump out the loop
K1=1e-10;

if (MF > 0)&(quit == 1)

% L is a flag to sense failure to converge iterative solution starts by
% assuming no CO2 dissociates.

L = 0;
M(2) = FCA;

% IFLAG=0 indicates this is first guess.

IFLAG = 0;
if (T > 500) &(quit == 1)

%-----
% Calculate equilibrium constants at the current temperature, T.

Fco2 = CC(1) * (1 - log(T)) - CC(2) * T - CC(3) * T ^ 2;
KCO2 = exp(-(Fco2 - CC(4) * T ^ 3 - CC(5) + CC(6) / T / rmol));
Fwg = CW(1) * (1 - log(T)) - CW(2) * T - CW(3) * T ^ 2;
KWG = exp(-(Fwg - CW(4) * T ^ 3 - CW(5) + CW(6) / T / rmol));
```

```

%-----
% Calculate the kgmol of H2O,CO,H2,O2 and the total kgmol based on the
% assumed CO2.
INCL=1;
  while (INCL==1)&(quit == 1)

  L = L + 1;

  M(4) = FHA / 2 * M(2) / ((FCA - M(2)) / KWG + M(2));
  M(1) = FCA - M(2);
  M(3) = FHA / 2 - M(4);

%-----
% Calculate CO2 "equilibrium constant" of this composition and see how it
% compares with that already calculated above.

M(6) = mOXY - M(2) - M(1) / 2 - M(4) / 2;

molP = sum(M);
  %KPwg = M(2) * M(3)/(M(1)+realmin)/M(4);
% M(1) * sqrt(M(6) * PE /(molP*PN)) /M(2)
  KPCO2 = M(1) * sqrt(M(6) * PE /(molP*PN)) /M(2);
  %ER = KWG - KPwg;
  ER = KCO2 - KPCO2;

% If error is small, calculate property coefficients.
% Otherwise, make a new estimate of moles CO2.

if (abs(ER) > 0.00001 *KCO2) & (quit == 1)

% First iteration is to assume 1/2 of the CO2 dissociates.

  if IFLAG == 0
    EL = ER;
    ML = M(2);
    M(2) = 0.5 * FCA;
    IFLAG = 1;

% Subsequent iterations use geometric interpolation.

  else

    M1 = (M(2) * EL - ML * ER) / (EL - ER+realmin);

    if M1 < 0
      M1 = 0.01; % must have some CO2
    end
    if M1 > FCA
      M1 = FCA; % but not more than FCA
    end
    ML = M(2);
    EL = ER;
    M(2) = M1;

  end % IFLAG == 0

% Failure printout message for subroutine.

  if L < 601

    INCL=1;

  else
    % EFAIL to converge again

    INCL=0; % jump out while INCL==1
    quit=1; % continue run if abs(ER) > KCO2 * 0.00001
  end
end

```

```

end
else % abs(ER) <= 0.00001 *KCO2

    quit = 0; % jump out the if loop and run PROP
    break
end % if abs(ER) > KCO2 * 0.00001

end % while INCL==1

elseif T <= 500
% EFAIL

    fprintf('EQCOMP failure: T= %5.2f, T);
    fprintf('\n iterations L= %5.0f\n',L);
        M(1) = 0;          %mCO
        M(2) = FCA;       %mCO2
        M(3) = 0;         %mH2
        M(4) = FHA / 2;   %mH2O
        M(6) = mOXY - FCA - FHA/4; %mO2
        T = -T;
    quit=0; % jump out the if loop and immediately run PROP

end % if T < 500

else % if MF <= 0, i.e. no fuel
    M(1) = 0;
        M(2) = 0;
        M(3) = 0;
        M(4) = 0;
        M(6) = mOXY + FOA;

end % end of if MF <= 0

M=real(M);
if M(6) < 0
    M(6)=1e-6; % rich mixtue, there must have some oxygen
end

%-----
% Evaluate property coefficients for this equilibrium mixture.
% PROP

P=zeros(1,7);
    for I = 1: 7
        for J = 1: 6
            P(I) = P(I) + M(J) * IC(J, I);
        end
    end

%-----
% Calculate the number of moles of product, molP, and the molecular weight
% of the product, MWP.
% W is the molecular weight.

    molP = sum(M);

    MWP = 0;

    for J = 1:6
        MWP = MWP + M(J) * W(J);
    end

    MWP = MWP / molP;

%-----
% End of subroutine.

```

## APPENDIX C

### TURBULENCE PARAMETERS CALCULATION PROGRAM

This appendix gives the detailed program code, *Turb\_para.m*, calculating turbulence parameters during combustion.

#### function Turb\_para

```
% Nov 2004 Gufoang Jiang
% This subroutine generates turbulence parameters (rms turbulence intensity,
% integral scale etc) as a function of combustion time, the plate hole diameter, D,
% the plate speed U, the normalized downstream distance XDi at ignition
%INPUT: D    = plate holediameter(m)

%    ri= radius of the element at spark time
%-----

cd('H:\combustion model\turbulence\');
d = dir('H:\combustion model\turbulence\');
str = {d.name};
[s,g] = listdlg('PromptString','Select a file:',...
               'SelectionMode','single',...
               'ListString',str); % Open file

file=str{s};
fid=fopen(file,'r');

if fid==-1
    errordlg(' The file could not be opened!');
end

% Read file
para=xlsread(file);

% Close file
fclose(fid);
cd('H:\combustion model\');

[r,c]=size(para);

XDI= para(:,2); % X/D at ignition time
U= para(:,1); % plate speed U
Time=para(:,3); %time duration from ignition to certain flame radius

% Enter the plate hole diameter
prompt = {'Enter the plate hole diameter(mm) '};
title = 'hole diameter';
lines = 1;
def = {'20'};
answer = inputdlg(prompt,title,lines,def);

D = str2double(answer); % hole diameter

% Enter ROR
prompt = {'Enter the radius of this element at spark time '};
title = 'ROR';
lines = 1;
def = {'25.5'};
answer = inputdlg(prompt,title,lines,def);

ri= str2double(answer); %radius of the element at spark time
```

```

% Rapid Distortion Effects.

z = (101.325 / 167) * (336/ 296); % unburned gas density ratio as a function of flame radius
c = (ri/ 55) ^ 2; % expansion ratio dependent on flame radius

% Mui = ratio of turbulent kinetic energy after distortion to that
% before in direction i
% i=1 is radial direction to flame front
% i=2, 3 are transverse direction to flame front
%%consider compression and geometric distortion together
b = sqrt(1 / (z ^ 2) / (c ^ 3) - 1);
mu1 = 0.75 * ((b * b - 1) / b ^ 3 * atan(b) + 1 / b / b) / z ^ 3 / c / c;
mu2 = 0.75 * c / z;
mu2 = mu2 + 0.375 * (atan(b) / b ^ 3 - 1 / b / b / (b * b + 1)) / z ^ 5 / c ^ 5;
mu3 = mu2;

Uratio = sqrt((mu1 + mu2 + mu3) / 3);

%%consider distortion only, z=1
b_d=sqrt(1 / (c ^ 3) - 1);
mu1_d = 0.75 * ((b_d * b_d - 1) / b_d ^ 3 * atan(b_d) + 1 / b_d / b_d) / c / c;
mu2_d = 0.75 * c;
mu2_d = mu2_d + 0.375 * (atan(b_d) / b_d ^ 3 - 1 / b_d / b_d / (b_d * b_d + 1)) / c ^ 5;
mu3_d=mu2_d;
Uratio_d = sqrt((mu1_d + mu2_d + mu3_d) / 3);

%%consider compression only,c=1
b_c = sqrt(1 / (z ^ 2) - 1);
mu1_c = 0.75 * ((b_c * b_c - 1) / b_c ^ 3 * atan(b_c) + 1 / b_c / b_c) / z ^ 3;
mu2_c = 0.75 / z;
mu2_c = mu2_c + 0.375 * (atan(b_c) / b_c ^ 3 - 1 / b_c / b_c / (b_c * b_c + 1)) / z ^ 5;
mu3_c = mu2_c;

Uratio_c = sqrt((mu1_c + mu2_c + mu3_c) / 3);

for i=1:r
XD(i)=XDI(i)+U(i)*Time(i)/D;
% First calculate Iscale and Urms assuming normal decay Only.
Iscale(i) = 0.38 * D; % integral scale in mm
if XD(i) > 14.3
Iscale(i) = 0.1 * D * sqrt(XD(i));
end
if XD(i) <= 10
Urms(i) = U(i) * 10.96 / (XD(i) ^ 1.812);
end
if 10<XD(i) & XD(i)<=20
Urms(i) = U(i) * 2.627 / (XD(i) ^ 1.191);
end
if XD(i) > 20
Urms (i)= U(i) * 0.773 / (XD(i) ^ 0.783);
end

Urms_rd(i) = Uratio * Urms(i);
Iscale(i) = sqrt(z) * Iscale(i)
Urms_d(i) = Uratio_d * Urms(i);
Urms_c = Uratio_c * Urms;
end
% print the results
%write the data to a file
for i=1:r
DD(i,1)=U(i);
DD(i,2)=XDI(i);
DD(i,3)=Urms_rd(i);
DD(i,4)=Urms_d(i);
DD(i,5)=Urms_c(i);
DD(i,6)=Urms(i);

```

```

DD(i,7)=XD(i);
DD(i,8)=Time(i);
DD(i,9)=Iscal(i);
end
%save data
cd('H:\combustion model\turbulence')
[fname,newpath] = uinputfile('H:\combustion model\turbulence\*.csv','Choose Output File Name');

file = fopen(fname,'w'); % creat a new file

% Write the data to the file
[n,m] = size(DD);
for i = 1:n
    for j = 1:m
        if j == m
            fprintf(file,'%5.7f\n',DD(i,j));
        else
            fprintf(file,'%5.7f,',DD(i,j));
        end
    end
end
fclose(file); % close the file

cd('H:\combustion model\')

% end of the program

```